Doctorate Program in Molecular Oncology and Endocrinology
Doctorate School in Molecular Medicine

XXVI cycle - 2010–2013
Coordinator: Prof. Massimo Santoro

"Study of anti-tumoral activity of HIV-Protease Inhibitor nelfinavir and identification of new nelfinavir-derivative compounds"

Maria Soprano

University of Naples Federico II
Dipartimento di Medicina Molecolare e Biotecnologie Mediche

Administrative Location

Dipartimento di Medicina Molecolare e Biotecnologie Mediche
Università degli Studi di Napoli Federico II

Partner Institutions

Italian Institutions
Università degli Studi di Napoli "Federico II", Naples, Italy
Istituto di Endocrinologia ed Oncologia Sperimentale "G. Salvatore", CNR, Naples, Italy
Seconda Università di Napoli, Naples, Italy
Università degli Studi di Napoli "Parthenope", Naples, Italy
Università degli Studi del Sannio, Benevento, Italy
Università degli Studi di Genova, Genova, Italy
Università degli Studi di Padova, Padova, Italy
Università degli Studi "Magna Graecia", Catanzaro, Italy
Università degli Studi di Udine, Udine, Italy

Foreign Institutions
Université Libre de Bruxelles, Bruxelles, Belgium
Universidade Federal de Sao Paulo, Brazil
University of Turku, Turku, Finland
Université Paris Sud XI, Paris, France
University of Madras, Chennai, India
University Pavol Jozef Šafàrik, Kosice, Slovakia
Universidad Autonoma de Madrid, Centro de Investigaciones Oncologicas (CNIO), Spain
Johns Hopkins School of Medicine, Baltimore, MD, USA
Johns Hopkins Krieger School of Arts and Sciences, Baltimore, MD, USA
National Institutes of Health, Bethesda, MD, USA
Ohio State University, Columbus, OH, USA
Albert Einstein College of Medicine of Yeshiwa University, N.Y., USA

Supporting Institutions
Dipartimento di Medicina Molecolare e Biotecnologie Mediche, Università degli Studi di Napoli "Federico II", Naples, Italy
Istituto di Endocrinologia ed Oncologia Sperimentale "G. Salvatore", CNR, Naples, Italy
Istituto Superiore di Oncologia, Italy

Italian Faculty

Salvatore Maria Aloj
Vittorio Enrico Avvedimento
Francesco Beguinot
Maria Teresa Berlingieri
Roberto Bianco
Bernadette Biondi
Francesca Carlomagno
Maria Domenica Castellone
Gabriella Castoria
Angela Celetti
Annamaria Cirafici
Annamaria Colao
Gerolama Condorelli
Vittorio De Franciscis
Sabino De Placido
Gabriella De Vita
Monica Fedele
Pietro Formisano
Alfredo Fusco
Fabrizio Gentile
Domenico Grieco
Michele Grieco
Maddalena Illario
Paolo Laccetti
Antonio Leonardi
Paolo Emidio Macchia
Rosa Marina Melillo
Claudia Miele
Nunzia Montuori
Roberto Pacelli
Giuseppe Palumbo
Maria Giovanna Pierantoni
Rosario Pivonello
Giuseppe Portella
Maria Fiammetta Romano
Giuliana Salvatore
Massimo Santoro
Donatella Tramontano
Giancarlo Troncone
Giancarlo Vecchio
Giuseppe Viglietto
Mario Vitale

If at first the idea is not absurd,
then there is no hope for it

Albert Einstein

“Study of anti-tumoral activity of HIV-Protease Inhibitor nelfinavir and identification of new nelfinavir-derivative compounds”

TABLE OF CONTENTS

LIST OF PUBLICATIONS

This dissertation is based upon the following publications:

1. Monaco S, Rusciano MR, Maione AS, **Soprano M**, Gomathinayagam R, Todd LR, Campiglia P, Salzano S, Pastore L, Leggiero E, Wilkerson DC, Rocco M, Selleri C, Sankar U, Illario I. A novel crosstalk between Calcium/ Calmodulin Kinases II and IV regulates cell proliferation (Manuscript in submission).

2. Bertamino A, **Soprano M,** Musella S, Rusciano MR, Sala M, Vernieri E, Di Sarno V, Limatola A, Carotenuto A, Cosconati S, Grieco P, Novellino E, Illario M, Campiglia P, Gomez-Monterrey I. Synthesis, in Vitro, and in Cell Studies of a New Series of [Indoline-3,2'-thiazolidine]-Based p53 Modulators. J Med Chem. 2013 Jul 11; 56(13):5407-21 (Attached at the end of the dissertation).

LIST OF ABBREVIATIONS

AIDS Acquired ImmunoDeficiency Syndrome
AP-1 Activator Protein 1
ATM Ataxia Telangiectasia Mutated
BRCA BReast CAncer
CDK Cyclin-Dependent Kinase
ECM Extracellular Matrix
EGFR Epidermal Growth Factor Receptor
ER Endoplasmatic Reticulum
FDA Food and Drug Administration
GLUT Glucose Transporter
GR Glutathione Reductase
HAART Highly Active AntiRetroviral Therapy
HIF-1α Hypoxia Inducible Factor-1α
HIV Human Immunodeficiency Virus
HSP90 Heat Shock Protein 90 kDa
IRS Insulin Receptor Substrate
Mdm2 Mouse double minute 2 homolog
MMPs Matrix Metalloproteinases
mTORC mammalian Target of Rapamycin Complex
NFkB Nuclear Factor kappa B
NO Nitric Oxide
NOS Nitric Oxide Synthase
NRTIs Reverse Transcriptase-Nucleoside Inhibitors
NSCLC Non-Small-Cell Lung Carcinoma
PDK 1 Phosphoinositide-Dependent kinase1
PI3K Phosphatidylinositol 3-kinase
PIs Protease Inhibitors
PRAS40 Proline-rich Akt Substrate 40 kDa
PTEN Phosphatase and tensin homolog
ROS Reactive Oxygen Species
SAPK Stress-Activated Protein Kinase
SOD Superoxide Dismutase
UPR Unfolded-Protein Response
VEGF Vascular Endothelial Growth Factor

ABSTRACT

Human Immunodeficiency Virus-Protease Inhibitors (HIV-PIs) are peptidomimetic drugs used in AIDS therapy to inhibit HIV infection by blocking viral protease. The advent of these drugs has led to a reduced incidence of HIV-associated tumors, particularly Kaposi's sarcoma, non-Hodgkin's lymphoma and cervical cancer. Many studies have also reported an anti-proliferative non-virological action of HIV-PIs in HIV-free models leading them to be further investigated as anti-cancer drugs. In particular HIV-PIs affect several pathways involved in tumor-cell proliferation and survival, angiogenesis, invasion, inflammation, and antitumor immunity in HIV-free models.

The most effective anti-cancer HIV-PIs is nelfinavir, that is in clinical trial for several tumor types, thus encouraging the study of the intracellular pathways at the basis of their anti-tumor activity. The anti-tumoral effects of nelfinavir have been related to inhibition of Akt activation, but to date the molecular mechanism at the basis of anti-cancer activity in breast cancer is poorly understood.

My results suggest an anti-proliferative activity of nelfinavir in a panel of cancer cell lines. In particular, nelfinavir induces apoptosis and necrosis in breast cancer cell lines such as MDA-MB231 and MCF-7 cells by affecting cell cycle in a cell line dependent way. The anti-tumor activity of nelfinavir is linked to the perturbation of cellular redox state; resulting in an increase of intracellular reactive oxygen species (ROS) production in breast cancer cells but not in normal breast epithelial cells. Nelfinavir treated tumor cells show also a downregulation of akt pathway due to the disruption of akt-Heat Shock Protein 90 kDa (HSP90) complex that is induced by nelfinavir and subsequent degradation of akt via proteasome. These effects result to be ROS dependent. Since treatment with anti-oxidant free radical scavenger tocopherol restores akt expression levels as well as viability of nelfinavir-untrated cells, the increase of ROS production represents the main and necessary molecular mechanism to induce cell death in breast cancer cell lines. The anti-cancer effectiveness of nelfinavir has motivated its use as lead compound in this study to design novel anti-tumoral compounds. Primary screening has led to the identification of novel nelfinavir-derivative (4n) with a high anti-cancer efficacy (IC_{50} 50nM), that is a promising molecule to further evaluate for cancer therapy.

1. INTRODUCTION

1.1 HIV-PIs AND IMMUNODEFICIENCY SYNDROME

HIV is a lentivirus responsible for acquired immunodeficiency syndrome (AIDS), a condition that in humans determines progressive failure of the immune system and allows life-threatening opportunistic infections and cancers to thrive (Munoz et al. 1993; Weiss 1993; Monini et al. 2004). HIV-Protease Inhibitors (HIV-PIs) have been rationally designed to block HIV aspartyl protease, a viral enzyme that cleaves the HIV gag and gag-pol polyprotein backbone at nine specific cleavage sites to produce shorter and functional protein (Deeks et al. 1997). Three of the nine cleavage reactions occur between a phenylalanine or a tyrosine and a proline. Since none of the known mammalian endopeptidases cleaves before a proline, HIV-PIs have been designed to mimic the phenylalanine-proline peptide bond thus determinig tolerable toxicity and mild side effects (Monini et al. 2003).

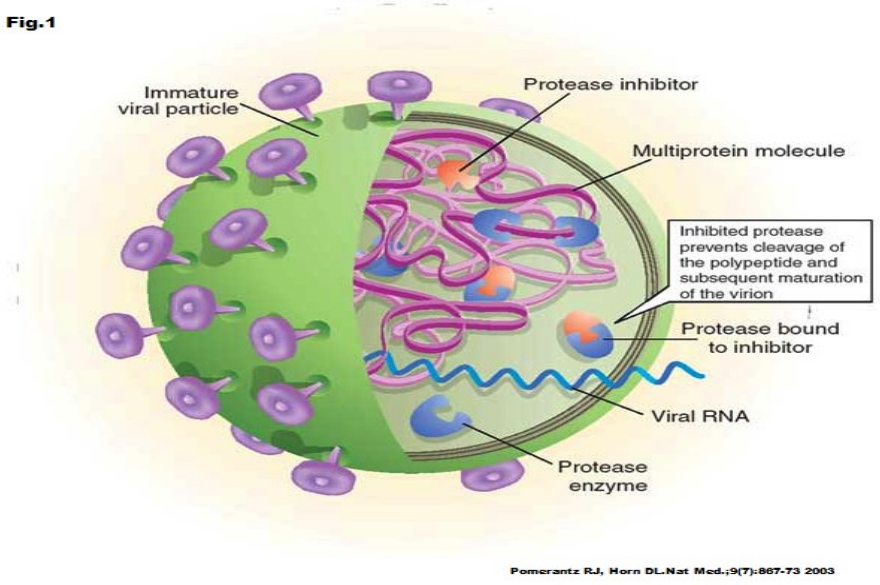

Figure 1. Protease inhibitors: mechanisms of action
Core proteins of HIV-1 are produced as part of long polypeptides that are cut into smaller pieces by protease to create functional and mature proteins. Protease inhibitors bind to the active site, where protein cleavage occurs. With the inhibition of protease, new viral particles cannot mature and do not become infectious.

HIV-PIs, combined with reverse transcriptase-nucleoside inhibitors (NRTIs) are included in the highly active antiretroviral therapy (HAART) that significantly improved the clinical management of HIV-1 infected patients and currently makes the acquired immunodeficiency syndrome a chronic,

manageable disease. The rationale for these combination therapies is to inhibit several steps of the viral life cycle. Combination regimens based on HIV-PIs and NNRTIs are more effective than single or dual combination of NRTIs in suppressing HIV replication, and in preserving or reconstituting both naive and memory T-lymphocytes repertories. Indeed, HAART suppresses HIV replication and can lead to a large reduction in HIV plasma viremia, restoration of normal numbers of CD4-positive T lymphocytes, immunological recovery, and reduction of morbidity and mortality related to HIV and opportunistic infections (Sgadari et al. 2003; Monini et al. 2004). The first HIV-PIs approved by FDA, is saquinavir, a peptidomimetic hydroxyethylamine. It is a transition state analogue of a native substrate of the HIV protease and It has a decahydroisoquinoline (DIQ) important substituent that improves aqueous solubility and potency by limiting the conformational freedom of the inhibitor (Wlodawer 2002).

Ritonavir, a peptidomimetic HIV protease inhibitor (Flexner 2007), was designed by removing terminal phenyl residues and laying pyridyl groups instead to add water solubility (Wlodawer 2002). As it is a strong inhibitor of the cytochrome P450 enzyme mediated metabolism, it is used in a combination therapy with other protease inhibitors, increasing plasma concentrations of agents that are primarily metabolized by cytochrome P450 (Wlodawer 2002).

Indinavir, is a peptidomimetic hydroxyethylene HIV protease inhibitor (Flexner 2007), designed by molecular modeling and the X-ray crystal structure analysis of the inhibited enzyme complex. The terminal phenyl constituents contribute hydrophobic binding to increase potency (Wlodawer 2002).

Nelfinavir was the first protease inhibitor that was not peptidomimetic. In the design process of nelfinavir, iterative protein cocrystal structure analysis of peptidic inhibitors was used and parts of the inhibitors were replaced by nonpeptidic substituents (Wlodawer 2002). Nelfinavir contains a novel 2-methyl-3-hydroxybenzamide group, whereas its carboxyl terminal contains the same DIQ group as saquinavir. Nelfinavir was the first protease inhibitor to be indicated for pediatric AIDS (Wlodawer 2002).

Amprenavir is an N,N-disubstituded amino-sulfonamide nonpeptide HIV protease inhibitor. It has a core similar to that of saquinavir but with different functional groups on both ends that make its structure easier to synthesize and gives better oral bioavailability (Wlodawer 2002).

Lopinavir was originally designed to diminish the interactions of the inhibitor with Val82 of the HIV-1 protease, a residue that is often mutated in the drug resistant strains of the virus (Wlodawer 2002). Fosamprenavir is a phosphoester prodrug that is rapidly and extensively metabolized to amprenavir (Luber et al. 2007). Its solubility and bioavailability are better than amprenavir resulting in reduced daily pill burden (Chapman et al. 2004).

Atazanavir is an azapeptide protease inhibitor (Flexner 2007) that shows

better resistant profiles than previous HIV protease inhibitors (Yanchunas et al. 2005).

Tipranavir is a nonpeptidic HIV-1 protease inhibitor developed from a nonpeptidic coumarin template and its antiprotease activity was discovered by high-throughput screening (Larder et al. 2000). It possesses broad antiviral activity against multiple protease inhibitor resistant HIV-1 (Doyon et al. 2005).

Darunavir reached the market in 2006 (Flexner 2007) and is a non-peptidic analogue of amprenavir, with a critical change at the terminal tetrahydrofuran (THF) group. Instead of a single THF group, darunavir contains two THF groups fused in the compound, to form a bis-THF moiety which makes it more effective than amprenavir. With this structural change, the stereochemistry around the bis-THF moiety confers orientational changes, that allows for continued binding with the protease which has developed a resistance for amprenavir (McCoy 2007). Therefore, darunavir has been designed to form robust interactions with the protease enzyme from many strains of HIV, including strains from patients with multiple resistance mutations to HIV-PIs (Chow et al. 2009). All the HIV protease inhibitors on the market contain a central core motif consisting of a hydroxyethylen scaffold, with the only exception being the central core of tipranavir, which is based on a coumarin scaffold (De Clercq 2009). A very important group on the HIV protease inhibitors is a hydroxyl group on the core motif which forms a hydrogen bond with the carboxylic acid on the Asp-25 and Asp-25´ residues in the binding site (Mimoto et al. 2000; Liu et al. 2008). Hydrogen bonds between the water molecule, which is linked to Ile50 and Ile50', and carbonyl groups of the peptidomimetic inhibitors seem to connect them with the flap regions (Wlodawer 2002). On the other hand, on the nonpeptidic inhibitors, there is a proton acceptor which replaces the tetracoordinated water molecule and interacts directly with the two Ile50 residues on the flap of the enzyme (Lebon and Ledecq 2000).

CTP-518 is a novel HIV protease inhibitor developed by replacing certain key hydrogen atoms of atazanavir with deuterium. Pre-clinical studies demonstrated that this modification fully retains the antiviral potency but can evidently slow hepatic metabolism and thereby increase the half life and plasma levels. CTP-518, therefore, has the potential to be the first HIV protease inhibitor to eliminate the need to co-dose with a boosting agent, such as ritonavir (*http://www.concertpharma.com/CTP518Ph1bStudy.htm*).

On the other hand, the clinical employment of these drugs is limited by many side effects such as diabetes, atherosclerosis, and cardiovascular complications (Carr et al. 1998; Ben-Romano et al. 2004; Chai et al. 2005), and the more recent HIV-PIs have only slightly reduced the toxic effects in clinical use.

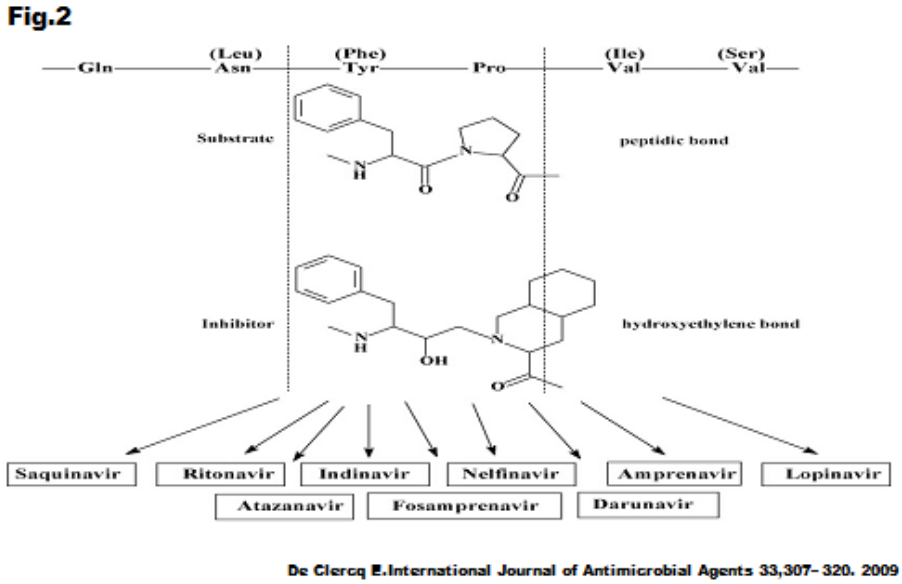

Figure 2. HIV-PIs structure Mechanism of action of protease inhibitors based on a hydroxyethylene scaffold, which mimics the normal peptide linkage cleaved by the HIV protease.

1.2 HIV-PIs AND CANCER

HIV infection is associated with an increased risk of certain AIDS-defining tumors: Kaposi's sarcoma, non-Hodgkin's lymphoma, and invasive cervical cancer (Monini et al. 2004). However, other types of cancer, such as Hodgkin's disease, anal cancer, lung cancer, and testicular germ cell tumors are more common among HIV-infected subjects compared to the general population. These malignancies have been referred to as AIDS-associated malignancies. Although it remains unclear whether HIV acts directly as an oncogenic agent, it may contribute to the development of malignancies through several mechanisms such as infection by oncogenic viruses, failure of immune surveillance, and imbalance between cell proliferation and differentiation (Barbaro and Barbarini 2007). The advent of the HAART has led to a reduced incidence and/or regression of AIDS-defining tumors. This effect cannot be explained by the ability of these drugs to suppress HIV replication and thereby reconstitute the immune system: indeed tumor development is not correlated with a patient's viral load or level of immune reconstitution (Monini et al. 2004). These have been the earliest clinical indications that HIV-PIs antitumor activity has a non immune mediated mechanism. Many studies attempted to evaluate anti-cancer activity of the most widely used HIV-PIs, including ritonavir, saquinavir, indinavir and nelfinavir in HIV-free models. HIV-PIs directly affect many steps of tumor cell progression that lead from carcinoma in situ to invasive cancer and metastasis formation. At concentrations similar or

above therapeutic peak levels, HIV-PIs promote apoptosis and inhibit proliferation of tumor cells with little or no effects on survival and proliferation of normal cells (Gaedicke et al. 2002; Pati et al. 2002), furthermore inhibiting tumor angiogenesis and cancer-cell invasion (Pomerantz and Horn 2003). The HIV-PIs affected steps of tumor progression are described in Figure 3.

Fig.3

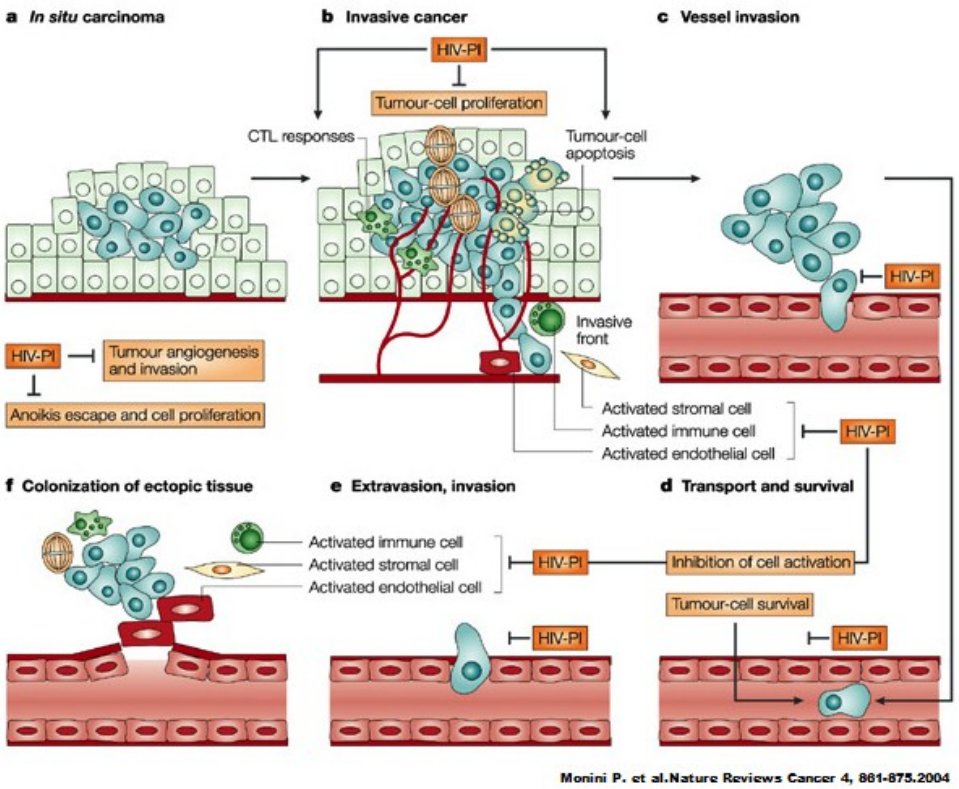

Figure 3. Steps in tumor progression and metastasis affected by HIV-PIs Tumor pathways that underlie the various steps of cancer development can be disrupted by HIV-PIs. These steps usually lead to progression of *in situ* carcinoma (**a**) to invasive cancer (**b**) and to metastasis formation and dissemination (**c**–**f**). These processes are all affected by HIV-PIs through their ability to inhibit cytokine and chemokine production, cell activation, and basal membrane and ECM degradation and remodelling.

First, these drugs influence tumor cell proliferation, thus limiting tumor growth and invasion. As metastatic cell clones emerge, tumor cells loosen their contact with surrounding cells and the extracellular matrix (ECM), leading to invasion of blood or lymphatic vessels, and to extravasation of tumor cells at distant sites. These steps require the degradation of basement membranes and, at the same time, inhibition of apoptosis following loss of cell anchorage (anoikis), processes that are also inhibited by HIV-PIs. To invade neighboring tissue and metastasize, tumor cells require the presence of other cells such as

activated endothelial cells, stromal and immune cells. These cells are able to destroy basement membrane and ECM, modify the ECM composition, release ECM-bound growth and angiogenic factors, produce cytokines and chemokines that stimulate tumor-cell growth and migration. All these processes sustain tumor growth and invasion, regulating local immunity. In this context, HIV-PIs exert remarkable immunomodulatory effects through their ability to inhibit cytokine and chemokine production, cell activation, basal membrane and ECM degradation and remodeling. In particular, it has been demonstrated that ritonavir and saquinavir inhibit the production and/or release of TNF-alpha, IL-6 and IL-8 by peripheral-blood mononuclear cells and endothelial cells (Pati et al. 2002). Furthermore, ritonavir inhibits the expression by endothelial cells of adhesion molecules, including Vascular Cell Adhesion Molecule (VCAM), Intercellular Adhesion Molecule 1 (ICAM1), and selectin E, which mediate leukocyte recruitment at sites of inflammation (Pati et al. 2002). HIV-PIs also regulate tumor immunity directly by modulating antigen processing, T-cell survival and dendritic cell maturation and function. In particular, differentiation of human circulating monocytes in the presence of these drugs leads to the generation of dendritic cell that fail to terminally differentiate and sustain the inflammatory process (Sloand et al. 1999; Lu and Andrieu 2000; Giardino Torchia et al. 2010). The most prominent mechanism underlying these HIV-PIs antitumoral effects is likely to be matrix metalloproteinases (MMP) inhibition, that is not only responsible for the blockage of cell invasion but is also involved in several crucial immunomodulatory functions as well as in cancer mediated immune suppression (Barillari et al. 2012). Evidences indicate that MMPs participate in antigen processing and modulate inflammatory cytokines and chemokines (Lopez et al. 2000). In summary, HIV-PIs block angiogenesis and tumor cell invasion, inhibit endothelial and tumor cell growth by inducing tumor cell apoptosis, thus modulating cell-mediated cytotoxic responses (Toschi et al. 2011). Many other molecular mechanisms have been suggested to explain the anticancer activity of these drugs but the primary targets are still unknown. To date, some HIV-PIs are in phase I/phaseII clinical trials for several tumor types, thus encouraging the study of the intracellular pathways at the basis of their anti-tumoral activity and of novel, more effective derivatives.

The identification of new activity for approved drugs is termed “repositioning”. It takes advantage of avaiable pharmacokinetic and toxicity data on existing drugs, limits risk and costs to pharmaceutical companies, and expedites the sustainable evaluation and movement of new cancer therapies to the clinic (Gills et al. 2007).

Molecular mechanisms at the basis of anti-tumoral activity of nelfinavir

HIV protease inhibitors include quite distinct compounds with many cell effects that account for their broad antitumor activity. The molecular mechanisms underlying anticancer activity of different HIV-PIs are summarized

in table 1.

Table 1

	Low concentration (<10 µmol/L)	High concentration (>10 µmol/L)
Saquinavir	Inhibition of MMP2 proteolysis Synergism with tyrosine kinase inhibitors	Inhibition of proteasome Inhibition of p-Akt
Indinavir	Inhibition of MMP2 proteolysis	Inhibition of proteasome
Ritonavir	Inhibition of cytokine production Inhibition of NFκB activation Downregulate endoplasmic reticulum expression Inhibition of cdk 2,4,6, and cyclin D1 Inhibition of phospho-Akt Inhibition of Hsp90 Radiosenitisation Upregulation of Bax and inhibition of Bcl-2 Inhibition of CYP3A4 and synergism with docetaxel Inhibition of CYP24 and synergism with 1,25(OH)$_2$D$_3$ Inhibition of MRP-1	Inhibition of proteasome
Nelfinavir	Inhibition of p-Akt Inhibition of STAT3 signalling Downregulation of androgen receptor Synergism with docetaxel Radiosensitization Decrease HIF-1α and VEGF* Inhibition of CDK2 and Rb dephosphorylation Inhibition of SREBP-1 processing Upregulation of P21, Fas and Bax	Upregulation of P53 Upregulation of P21 and P27 Downregulation of Bcl-2 Downregulation of MMP2 Synergism with temozolomide Induce endoplasmic-reticulum stress–unfolded-protein response pathway Induce autophagy
Amprenavir	Inhibition of phospho-Akt	

Chow W.A. et al. The Lancet Oncology Volume 10, Issue 1, Pages 61–71.2009

Table 1. HIV-protease inhibitors and their proposed mechanisms of action CDK: Cyclin-dependent kinases; HIF-1α: Hypoxia-inducible factor 1-alpha; MMP: Matrix metallo-proteinases; MRP-1: Multidrug resistance- associated protein-1; NFkB: Nuclear Factor-KappaB; VEGF: Vascular endothelial growth factor.

Among these drugs, nelfinavir is considered the most potent antitumor HIV-PIs (Chow et al. 2006; Yang et al. 2006b; Gills et al. 2007), although its toxicity and side effects limit its use as antitumoral drug (Carr et al. 1998; Hui 2003; Koster et al. 2003; Ben-Romano et al. 2004; Reyskens and Essop 2014). The antitumoral effects of nelfinavir have been related to several mechanisms of action: inhibition of matrix metalloproteinase (MMP)-2; induction of endoplasmatic reticulum (ER) stress; inhibition of proteasome function and Nuclear factor kappa B (NfkB) activity; inhibition of Akt phosphorylation; and induction of autophagy (Pajonk et al. 2002; Monini et al. 2003; Yang et al. 2006b; Toschi et al. 2011). As the downregulation of akt pathway represents the main molecular mechanism underlying nelfinavir anti-proliferative activity, it will be discussed in a dedicated chapter.

One of the most analysed antitumor mechanism of action for nelfinavir is the induction of ER stress (Gills et al. 2007; Pyrko et al. 2007). ER has a fundamental role in the synthesis of surface and secreted proteins, their

assembly and folding; thanks to its oxidative environment that is critical for formation of disulfide bonds (Schroder and Kaufman 2005). Alterations of ER functions can determine ER stress, that elicits the activation of the unfolded-protein response (UPR), a cell protective mechanism, resulting in transient induction of cell cycle arrest and accumulation of molecular chaperons to bind and recover unfolded proteins. Prolonged exposure of cells to ER stress or cell cycle arrest can induce a switch from cell survival to caspase dependent apoptosis (Kaufman 2002; Xu et al. 2005). Nelfinavir activates the endoplasmic reticulum stress–UPR pathway in different tumor types such as breast cancer, ovarian cancer, non-small-cell lung carcinoma and glioma cells (Pyrko et al. 2007; Bruning et al. 2009; Bruning et al. 2010; Thomas et al. 2012). As part of UPR, global protein synthesis decreases and DNA damage inducible protein (GADD34) are induced by acting as a phosphatase in complex with protein phosphatase 1. This complex can dephosphorilate akt, determining double anti-cancer effect of nelfinavir in tumoral cells (Gupta et al. 2007).

The induction of ER stress coud be dependent by inibition of proteasome activity. The proteasome controls protein turnover, clearance of misfolded proteins, apoptosis, degradation of tumor-suppressor gene products, the function of cyclin-dependent kinase (CDK) inhibitors, and the proteolytic maturation and activation of the transcription factor NF-kB. The inhibition of the proteasome leads to excessive accumulation of misfolded proteins in the endoplasmic reticulum and activates UPR. It has been demonstrated that nelfinavir inhibits 26S chymotrypsin-like proteasome activity and promotes apoptosis in myeloma cell lines by inducing UPR pathway (Bono et al. 2012). Moreover, nelfinavir used in combination with a proteasome inhibitor bortezomib enhances proteotoxicity in non-small-cell-lung carcinoma (NSCLC) and multiple myeloma (Kawabata et al. 2012). Nevertheless, the hypotesys of nelfinavir mediated inhibition of proteasome activity was not supported in all studied tumor types: indeed, in the original report of 1998 (Andre et al. 1998) and in more recent work (Jiang et al. 2007b), nelfinavir does not affect the chymotrypsin-like activity of 20S proteasome even at a high concentration (100μM).

Autophagy is a process in which intracellular membrane structures sequester proteins and organelles to degrade and turn over these materials under conditions of stress, starvation, or inhibition of the phosphatidylinositol-3-kinase (PI3K)–Akt-mammalian target of rapamycin pathway (Pyrko et al. 2007; Levine and Kroemer 2008). The role of autophagy has been investigated in nelfinavir-mediated cell effects and it has been demonstrated that this drug can induce autophagy. The induction of autophagy counteracts the cytotoxicity of nelfinavir, because inhibition of autophagy with 3-methyladenine (a small-molecule inhibitor of autophagy) increased nelfinavir-induced death (Gills et al. 2007).

Nelfinavir regulation of AKT pathway

Akt or Protein Kinase B (PKB) is a serine/threonine protein kinase that functions as a critical regulator of cell survival and proliferation. In mammals three akt isoforms (akt1,akt2,akt3) have been identified with the same conserved domain structure: an amino terminal pleckstrin homology (PH) domain, a central kinase domain and a carboxyl-terminal regulatory domain with hydrophobic motif. All akt isoforms except akt3 contain two regulatory phosphorylation sites, Thr-308 in the activation loop within the kinase domain and Ser-473 in the C-terminal regulatory domain (Song et al. 2005). Akt signaling cascade starts with the activation of PI3K following cross-linking of a growth factor with its surface tyrosine kinase receptor. Active PI3K phosphorylates membrane bound phosphoinositidies, thus converting phosphatidylinositol (4,5)-bisphosphate (PIP2) to phosphatidylinositol (3,4,5)-trisphosphate (PIP3) (Coffer et al. 1998; Chan et al. 1999; Yuan and Cantley 2008). Akt interacts with PIP3 through PH domain, and moves to the inner cell surface where it can be phosphorilated on Thr-308 by the phosphoinositide-dependent kinase1 (PDK1). Although phosphorylation at Thr-308 partially activates akt, full activation requires Ser-437 phosphorylation by mammalian target of rapamycin complex 2 (mTORC2) (Shiota et al. 2006; Yang et al. 2006a) or by akt autophosphorylation (Chan and Tsichlis 2001). PIP3 levels are tightly regulated by the action of phosphatases PTEN, an important negative regulator of PI3K/akt signaling (Cantley and Neel 1999; Di Cristofano and Pandolfi 2000). Other negative regulators of akt signaling include phosphatases PP2A that preferentially dephosphorylate akt on the Thr-308 but also on the Ser-473 and phosphatases PHLPP that specifically dephosphorylate on Ser-473 (Liao and Hung 2004; Brognard et al. 2007).

Following phosphorylation, activated akt phosphorylates many substrates, which control important cell processes such as cell cycle progression, apoptosis, transcription and translation, summarized in figure 4 (Ahmed and Davies 2011).

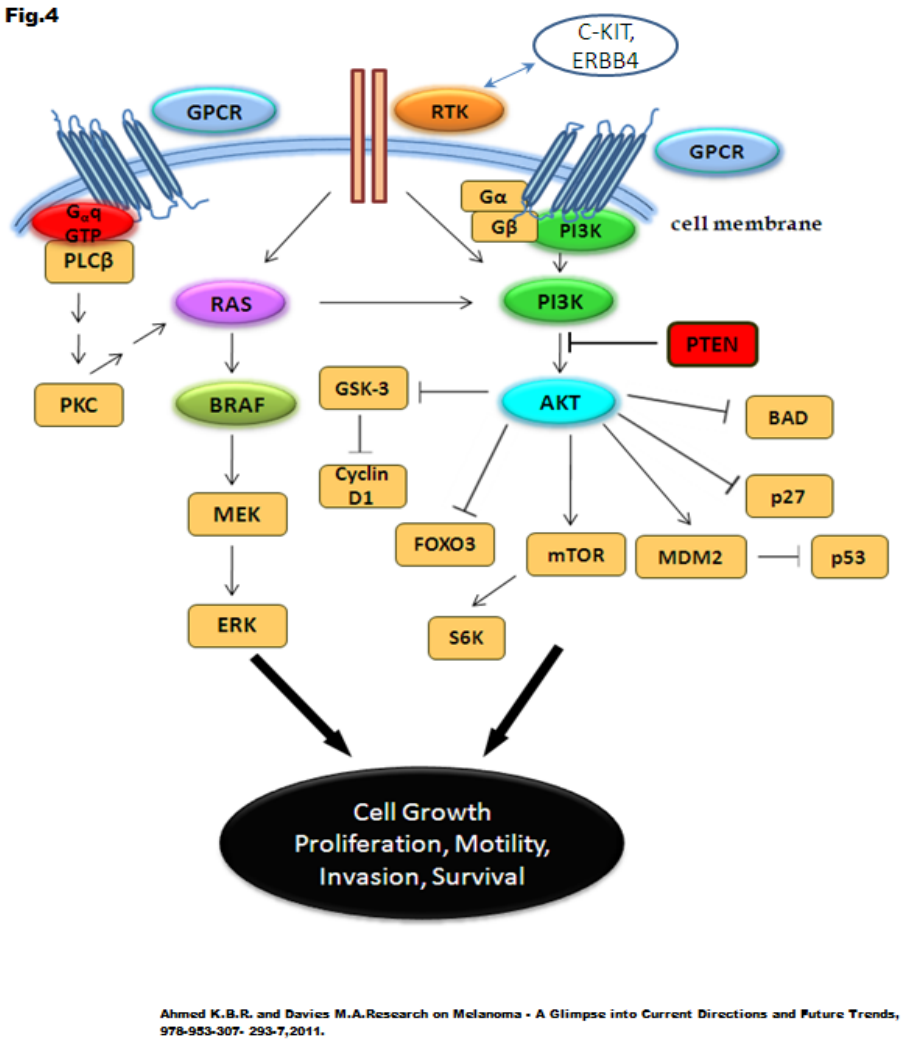

Figure 4. Akt regulates many intracellular processes through phosphorylation of different targets Following surface receptors activation, PI3k induces akt activation. phosphorylation of akt promotes cell proliferation by activation of mTOR and cyclin D by GSK-3 inhibition and blocks apoptosis through MDM2/p53 and Bad regulation.

Akt activation affects cell cycle progression, through regulation of cyclin D stability (Muise-Helmericks et al. 1998) and inhibition of cell cycle negative regulators such as p27 (Collado et al. 2000) and p21 (Zhou et al. 2001). Akt can also regulate nucleo-cytoplasmic localization of critical substrates involved in cell cycle and apoptosis. In particular, phosphorylation by akt is necessary for nuclear translocation of Mouse double minute 2 homolog (Mdm2). It has been reported that when Mdm2 is restricted to the cytoplasm it is degraded (Mayo et al. 2002). After growth factor stimulation, Mdm2 is phosphorylated by akt and enters the nucleus, leading to reduction of both p53 levels and transactivation (Mayo and Donner 2001). To prevent apoptosis, akt phosphorylates and inactivates the pro-apoptotic factors BAD and pro-caspase 9, inhibing the

release of cytochrome c from mitochondria (Datta et al. 1997; Cardone et al. 1998). Akt also phosphorylates and inactives different kinases upstream stress-activated protein kinase (SAPK) leading to inhibition of SAPK-mediated apoptosis (Kim et al. 2001). Moreover, akt activates Ikb kinase, a positive regulator of NF-kB, and increases transcriptional activation of CREB which results in transcription of anti-apoptotic genes such as Bcl-2 (Wang et al. 1999; Burgering and Medema 2003). However, the major physiological function of akt is the regulation of cell metabolism. In particular, Akt phosphorylates and inactivates glycogen synthase kinase 3, thus stimulating glucose utilization (Cross et al. 1995). Akt also regulates protein synthesis through mammalian target of rapamycin complex 1 (mTORC1), a protein complex that functions as a nutrient/energy/redox sensor. mTORC1 activates transcription and translation through its interactions with p70-S6 Kinase 1(S6K1) and 4E-BP1, the eukaryotic initiation factor 4E (eIF4E) binding protein 1 (Hay and Sonenberg 2004). Akt regulates mTORC1 through direct phosphorylation of tuberous sclerosis complex-2 (TSC2) and proline-rich akt substrate 40 kDa (PRAS40), proteins that suppress mTORC1 kinase activity and thereby activate mTORC1 (Dunlop and Tee 2009; Huang and Manning 2009). Under certain physiological or pathophysiological conditions, akt protein can be degraded by the ubiquitin proteasome-dependent pathway, caspase-mediated cleavage, and caspase-dependent ubiquitination (Liao and Hung 2010). Akt stability are regulated by Hsp90, an important molecule chaperone which acts in cooperation with cdc37 to stabilize akt and prevent akt from PP2A-mediated inactivation (Hanada et al. 2004). Among molecule chaperones, Hsp90 is of prime importance to the survival of cancer cells, since the list of Hsp90 client proteins includes key components of multiple signaling pathways utilized by cancer cells for growth and/or survival (Neckers and Ivy 2003; Neckers and Neckers 2005). Detachment of akt from the Hsp90/cdc37 complex increases akt sensivity to PP2A-mediated dephosphorylation and results in ubiquitination and degradation of akt via proteasome. It is not yet clear under what patho-physiological conditions will the ubiquitin proteasome pathway recycle or degrade Hsp90-bound akt (Sato et al. 2000; Georgakis and Younes 2005; Powers and Workman 2006). Another mechanism to regulate akt folding and stability is the phosphorylation of particular Thr-Pro motifs on Thr-92 and Thr-450 which in turn promotes the interaction of akt with Pin1, a peptidyl-prolyl cis/trans isomerase required for the maintenance of akt stability and activation phosphorylation (Liao and Hung 2010).

The signaling crosstalks involving akt determine its role in the development of cancers possibly through effects on cell proliferation, adhesion, migration, invasion, apoptosis, and angiogenesis. Cancer genomic analyses have revealed that multiple components of the PI3K/akt pathway are frequently mutated or altered in common human cancers (Wood et al. 2007), underscoring the importance of this pathway in cancer. In addition, akt activation promotes resistance to chemotherapy as well as radiation therapy (Tsurutani et al. 2007).

For these reasons the inhibition of akt pathway should offer some selectivity in the treatment of many cancers.

Several groups (Gupta et al. 2005; Yang et al. 2006b; Cuneo et al. 2007) suggested that inhibition of PI3K-induced activation of akt by HIV-PIs is an important mechanism by which these drugs exert anti-tumor effect. Moreover, PIs-mediated decreased phosphorylation of akt correlates with increased sensitivity to ionizing radiation and chemotherapy (Gupta et al. 2005; Yang et al. 2006b; Cuneo et al. 2007). Yang and colleagues (2006) demonstrated that nelfinavir inhibits growth and induces apoptosis in cell lines of prostate cancer, via disrupted signal transducer and activator of transcription 3 (STAT3) signalling. The same investigators also showed similar proapoptotic effects in NSCLC via upregulation of p53 and the cyclin-dependent kinase inhibitors p21 and p27 and downregulation of Bcl-2 and MMP2. All these effects might be mediated through inhibition of Akt phosphorylation, as forced expression of constitutively active Akt partly reverses the nelfinavir-mediated growth inhibition. It has been suggested that akt inactivation could be related to block of akt translocation to plasma membrane, where it is phosphorylated by PDK1 and mTORC2 kinases (Ben-Romano et al. 2004). Nelfinavir could also act upstream of the akt signaling pathway by inhibition of tyrosine kinase receptor activation (Gills et al. 2007). However, Nelfinavir-mediated inhibition of Akt phosphorylation reduce in vitro tumoral cell proliferation and sensityzed tumor cells to chemotherapy and radiotherapy. Indeed, nelfinavir can be used in combination with chemoradiation for locally advanced rectal cancer (Buijsen et al. 2013), glioblastoma (Jiang et al. 2007c), head and neck carcinoma and non-small-cell lung carcinoma (Pore et al. 2006; Rengan et al. 2012). Another possible explanation for the efficacy of combinatorial approach in cancer therapy has been given by Fukuda et al. (2013). In this study, they demonstrated that nelfinavir interacts with multidrug resistance protein 4/ATP binding cassette transporter 4 (MRP4/ABCC4) and regulates its substrate-stimulated ATPase activity, thus increasing its own antitumor efficacy as well as cancer chemotherapeutics (Fukuda et al. 2013). It has been reported that also saquinavir and amprenavir but not indinavir or ritonavir inhibit akt phosphorylation in different tumor types: H-ras mutated bladder cancer, epidermal growth factor receptor mutated head and neck cancer, and K-ras mutated pancreatic cancer and lung cancer cell lines (Gupta et al. 2005). This resulted in radiosensitisation of these tumors in vitro and in vivo in a nude-mouse model.

Nelfinavir does not decrease phosphorylation of Akt in normal cells and/or radiosensitise them, thus suggesting drug selectivity for malignant cells (Jiang et al. 2007c). In addition, the kinetics of akt inhibition are cell line specific and do not correlate with other nelfinavir biological effects such as ER stress and autophagy (Gills et al. 2007).

Therefore, akt inactivation is not a general molecular mechanism at the basis of nelfinavir anti-tumoral activity, since this phenomenon has not been

confirmed in all tumor types. Indeed, nelfinavir does not affect akt activity in particular breast carcinoma cell lines (Bruning et al. 2010) and in melanoma cells (Jiang et al. 2007b). Although there are exceptions, the inhibition of Akt signaling remains one of the main antitumor mechanisms of nelfinavir.

Nelfinavir in Breast Cancer

Breast cancer is the most frequent cancer in the female population. It comprises 22,9% of invasive cancers in women and 16% of all female cancers (http://*www.who.int/cancer/detection/breastcancer/en*). Despite recent advances in chemotherapy, recurrent or metastatic breast cancer patients have a median survival of 20 months. There are many risk factors known to increase the occurrence of breast cancer: female sex, older age, genetics, lack of childbearing or lack of breastfeeding, higher levels of some hormones, specific dietary patterns, and obesity (McPherson et al. 2000; Reeder and Vogel 2008).

How these risk factors contribute to the transformation of normal cells into cancer cells remains incompletely understood. Many evidence suggests that genetic alterations, including both inherited and acquired mutations of specific tumor suppressors and oncogenes, represent the primary cause of 5-10% of all cases (Gage et al. 2012). For example, inherited mutations in Breast Cancer (BRCA) tumor suppressors confer more than 50% higher risk for women to develop breast cancer. Women with inherited BRCA1 or BRCA2 gene mutations also have an increased risk of ovarian cancer (Chen and Parmigiani 2007). More than 70% of breast cancer cases with BRCA mutations have also mutated p53 gene resulting in a doubling of breast cancer occurrence. However, mutations in BRCA genes account for only 2 to 3 percent of all breast cancers (Wooster and Weber 2003). The specific characteristics of the cancer determine the treatment, which may include surgery, hormonal therapy, chemotherapy, radiation and/or immunotherapy (Florescu et al. 2011).

Breast cancer is usually classified primarily by its histological appearance. Most breast cancers are derived from the epithelium lining the ducts or lobules, and these cancers are classified as ductal or lobular carcinoma. Breast cancers are classified also by grade of differentiation, stage, receptor status and genetic alterations (Yerushalmi et al. 2009). Receptor status is defined by the presence of three important receptors: estrogen receptor (ER), progesterone receptor (PR), and HER2.

ER positive cancer cells depend on estrogen for their growth, so they can be treated with endocrine therapy that blocks estrogen effects by affecting receptor binding with antagonists such as tamoxifen or by depriving the tumor from estrogen by aromatase inhibitors. Older endocrine therapies are based on high dose of estrogens and androgens, and work by less well-known mechanisms, although it has been proposed that high-dose estrogen can induce apoptosis by activationing intrinsic and exstrinsic pathways (Lewis-Wambi and Jordan 2009). Endocrine therapy is the most effective treatment for ER-positive breast

cancer, but its effectiveness is limited by high rates of de novo resistance and resistance acquired during treatment. The mechanisms responsible for endocrine resistance include the loss of ER expression and activation of escape pathways such as HER2 pathway, that can provide tumors with alternative proliferative and survival stimuli (Osborne and Schiff 2011).

Approximately 25%-30% of human breast cancers overexpress HER2 and tend to be more aggressive and less responsive to hormone treatments than other types of breast cancer. This type of cancer is treated with trastuzumab, a monoclonal antibody that interferes with HER2, and lapatinib, a dual inhibitor of HER2 and EGFR tyrosine kinases that is used in combination with chemotherapeutic agent capecitabine (Goldenberg 1999; Geyer et al. 2006). Cells that do not have any of these three receptor types (estrogen receptors, progesterone receptors, or HER2) are called triple-negative, and can be treated only with chemotherapy which destroys fast-growing cancer cells with serious side effects on normal cells. Even within these major types of breast cancer, individual tumors appear to be driven by their own sets of genetic changes, that affect anticancer treatment efficiency. To overcome this problem, many other drugs that inhibit different targets could be useful for therapy. An important target in breast cancer research is represented by PI3K/akt pathway, as it is frequently aberrantly activated in breast cancer occurring in up to one quarter of breast cancers (Baselga 2011). The majority of mutations are in PIK3CA, encoding the catalytic p110α subunit of PI3K, and the proportion of breast tumors exhibiting mutations in PI3K is in the range of 20%–25%, depending on the breast cancer subtype. For example, in ER–positive tumors, these mutations occur in >30% of cases. Also, in HER2 positive disease, mutations are evident in about one quarter of tumors. Meanwhile, it seems that mutations in triple-negative breast cancer may be less frequent (Stemke-Hale et al. 2008). It has been demonstrated that PI3K mutations play a role in resistance to some of the therapies that block upstream tyrosine kinase receptors such as anti-HER2 agents. Current PI3K inhibitors under development are grouped by their specificity, ranging from pure PI3K inhibitors, to compounds that block both PI3K and mTOR (dual inhibitors), to pure catalytic mTOR inhibitors, and to inhibitors that block Akt. Among these, anti-mTOR agents have clinical activity against breast cancer, but activation of feedback loops may result in decreased efficacy (Baselga 2011). In this context, novel inhibitors directed to different cell targets and affecting breast cancer cell growth and survival, may potentially improve the efficacy of therapy and the survival rate. There are few evidences that nelfinavir exerts an anti-proliferative effect in breast cancer, but the mechanisms by which nelfinavir may be involved in cancer inhibition are not well understood.

It has been demonstrated that nelfinavir affects breast cancer cell viability by inducing endoplasmic reticulum stress and autophagy (Bruning et al. 2010). ER stress and autophagy are related: many agents that cause ER stress lead to increased autophagic activity; conversely, there are indications that blockage of

autophagy increases ER stress. There are evidences that induction of ER stress with simultaneous inhibition of autophagy lead to efficient killing of triple negative breast cancer in vitro and in vivo. For this reason, when nelfinavir is used in combination with inhibitors of autophagy, the killing of cancer cells is potentiated (Thomas et al. 2012).

The involvement of akt signalling and proteasome activity in nelfinavir-mediated effects has been questioned and could be related to the analyzed cell lines. Several studies have shown that ER stress induces activation of akt signaling, which primarily represents a short-term effect whereas prolonged exposure of cells to ER stress induces akt inactivation (Hosoi et al. 2007; Dai et al. 2009). This indicates that the downregulation of akt phosphorylation is a secondary event. As above mentioned, the downregulation of akt phosphorylation is an important mechanism of nelfinavir to inhibit cell growth in several tumor types such as advanced pancreatic cancer, malignant glioma, head and neck carcinoma, and advanced rectal cancer, leading to increased sensitivity to radiation (Gupta et al. 2007; Pyrko et al. 2007; Brunner et al. 2008; Buijsen et al. 2013). In breast cancer there are contrasting data regarding the nelfinavir-mediated inhibition of akt pathway. A recent study demonstrated that nelfinavir affects not only akt phosphorylation but also reduces akt total protein expression levels (Shim et al. 2012). The authors suggested that akt downregulation is mediated by the inhibition of HSP90 chaperon activity resulting in degradation of HSP90 client proteins. These proteins are HER2, akt, Epidermal Growth Factor Receptor **(**EGFR), Hypoxia Inducible Factor-1α (HIF-1α), androgen receptor, Bcr-Abl, and CDKs, that are key players of cancer cell survival and proliferation. Therefore the indirect inhibition of HSP90 function by nelfinavir can cause simultaneous inhibitory effects on multiple pathways of cancer cell signaling. Because of the large number of signaling proteins affected, nelfinavir could overcome the drug resistance which can occur during treatment with trastuzumab and lapatinib (Berns et al. 2007) that is generally due to mutation in PI3K gene. However, the modality of interaction between nelfinavir and HSP90 remains to be further elucidated using such techniques as x-ray crystallography.

Another molecular mechanism analyzed in nelfinavir treated breast cancer is the proteasome inhibition. This mechanism seems to be cell line specific, since nelfinavir exerts no significant effect on the chymotryptic proteasome activity in HER2 negative breast cancer cell models (Bruning et al. 2010) while it inhibit 20S proteasome chymotrypsin-like activity in HER2 positive breast cancer cells (Shim et al. 2012). However, the inhibition of proteasome in HER2 positive breast cancer cells does not explain the effects of nelfinavir on akt pathway, since classical proteasome inhibitors do not reduce akt protein levels. Furthermore, proteasome inhibitors prevent certain nelfinavir effects thus suggesting that proteasome is not the relevant target for nelfinavir.

In conclusion, nelfinavir exerted pleiotropic biochemical and cell effects that included induction of endoplasmic reticulum stress, autophagy, and

apoptosis but the molecular mechanism at the basis of these anti-tumoral effects as well as akt downregulation is still unknown.

To date nelfinavir is in clinical trial for several cancers such as rectal cancer, solid tumors, multiple myeloma, cervical cancer, pancreatic cancer, non small cell lung carcinoma, glioblastoma, renal cell cancer, cancers of the head and neck, liposarcomas (*http://www.cancer.gov/clinicaltrials*) further investigations are necessary to identify all molecular targets and to exend the treatment to breast cancer.

It was established that the nelfinavir maximum plasma concentration of 3-4mg/l in HIV-infected patients patients (Tebas and Powderly 2000) is also able to inhibit tumoral cell growth. However, it has been reported that in HIV-positive patients, long-term treatment with nelfinavir at therapeutic concentrations can trigger metabolic side-effects that resemble the metabolic syndrome, a combination of risk factors that predispose to future onset of type 2 diabetes mellitus and cardiovascular disease (Reyskens and Essop 2014). For this reason also the use of HIV-PIs as anticancer agents could be limited by these side effects. There are several mechanisms whereby HIV-PIs can exert their detrimental effects, however, it has been proposed that drug-induced generation of oxidative stress and associated downstream targets play a central role in this process. Indeed, the link between HIV-PIs usage and increased reactive oxygen species (ROS) production is well established by several cell studies, including macrophages (Wang et al. 2007), cardiomyocytes (Deng et al. 2010), beta cells (Chandra et al. 2009); endothelial cells (Mondal et al. 2004), skeletal muscle cells (Touzet and Philips 2010), adipocytes (Ben-Romano et al. 2006), porcine arteries and aortas in an atherogenic mouse model (Conklin et al. 2004; Chai et al. 2005).

To date, It has not been reported a PIs-mediated induction of ROS in tumor cells and the role of ROS as players in the molecular mechanism underlying anti-cancer effects of these drugs has not been investigated.

1.3 INVOLVEMENT OF ROS IN CANCER THERAPY

ROS

ROS consist of radical and non-radical oxygen species formed by the partial reduction of oxygen (Halliwell 1996; Fridovich 1999). Some of the most common ROS are superoxide anion, hydrogen peroxide and the higher reactive hydrogen radical. Superoxide radical anion derives from molecular oxygen by the addition of an electron, and has a short lifetimes in the cell as it quickly reacts with antioxidants or transform to hydrogen peroxide through spontaneous or enzyme catalysed reaction. Different from superoxide anion, hydrogen peroxide can penetrate biological membranes. It plays a radical forming role as an intermediate in the production of more reactive ROS molecules such as hydroxyl radical via oxidation of transition metals. Due to its

strong reactivity with biomolecules, hydroxyl radical is capable of doing more damage to biological systems than any other ROS (Betteridge 2000). ROS production is a natural process of normal cells. The formation of superoxide takes place spontaneously, especially in the mitochondria through the oxidative phosphorylation process that occur during aerobic respiration. Superoxide is also produced endogenously by lipoxygenase, cyclooxygenase, and flavoenzymes such as NADPH-oxidase and xantine-oxidase (Nordberg and Arner 2001). Although the majority of ROS production originates from mitochondria, generated by respiratory chain complex I and III, matrix dehydrogenases and mono-amine oxidase (Muller et al. 2004; Zorov et al. 2006), NADPH-oxidases represent key modulators that generate highly regulated amounts of superoxide anion by electron transfer from NADPH to molecular oxygen (Meitzler et al. 2013). Hydrogen peroxide can be generated directly by some oxidoreductases, but most hydrogen peroxide production results from the dismutation of superoxide anion (Forman 2007). Nitric oxide (NO) is considered another member of the free radical family for its capability to easily react with other free radicals, generating less or more reactive molecules. It has been demonstrated that NO acts both as anti-oxidant and oxidant molecule, because it can inhibit lipid peroxidation in cell membranes (Hogg and Kalyanaraman 1998; Rubbo et al. 2000) but it can react with anion superoxide to produce peroxynitrite, which is highly cytotoxic (Beckman and Koppenol 1996). Peroxynitrite may react directly with different biomolecules in one- or two-electron reactions, readly react with CO2 to form highly reactive nitroso peroxocarboxylate, or protonated as peroxonitrous acid undergo homolysis to form either hydroxyl radical and nitrogen dioxide or rearrange to nitrate. NO is synthesized enzymatically from L-arginine by NO synthase (NOS)(Beck et al. 1999; Bredt 1999). The complex enzymatic catalysis of NOS involves the transfer of electrons from NADPH, via the flavin FAD and FMN in the carboxy-terminal reductase domain, to the heme in the amino-terminal oxygenase domain, where L-arginine is oxidized to L-citrulline and NO. There are three main isoforms of the enzyme which differ in their expression and activities: neuronal NOS (nNOS), inducible NOS (iNOS), and endothelial NOS (eNOS)(Beck et al. 1999; Bredt 1999).

A common feature among the different ROS types is their capacity to cause oxidative damage to DNA, lipids, and proteins (Marnett 2000; Stadtman and Levine 2000). In particular, ROS can react with DNA leading to oxidation of purines, DNA-protein cross links, and cleavage of DNA. If these alterations are not rapidly repaired, cells can accumulate DNA mutations promoting cancerogenesis or cell-death. Polyunsaturated fatty acids as well as several amino acid residues are other targets for free radical attacks. The oxidative modification of proteins results in changes in structure and/or function of the protein, and has been recognized as playing a role in the progression of several pathophysiologic processes (Dean et al. 1997). These cytotoxic effects of ROS explain the evolution of complex arrays of nonenzymatic and enzymatic

detoxification mechanism (Decker and Muller 2002). The antioxidant enzyme systems include superoxide dismutase (SOD), superoxide reductase (SOR), catalase, peroxiredoxin, thioredoxin, and glutathione peroxidase. SOD was the first ROS-metabolizing enzyme discovered (McCord and Fridovich 1969) and consist of three forms with different intracellular localization: cytosolic (SOD1), mitochondrial (SOD2) and extracellular (SOD3) (Nordberg and Arner 2001). These isoforms differ also in metal co-factor; SOD1 and SOD3 use copper and zinc while SOD2 uses manganese to fulfill to their functions. The role of all three forms of SOD is to catalyze the formation of hydrogen peroxide from superoxide. Although not as reactive as superoxide, hydrogen peroxide induces cell damage by conversion into hydroxyl radical via the Fenton-reaction catalyzed by copper or iron ions (Fridovich 1999; Halliwell 1999). Thus, another enzyme, catalase, transforms hydrogen peroxide into molecular oxygen and water, lowering the risk of hydroxyl radical formation. However, it is likely that the major hydrogen peroxide-removing enzymes in mammalian cells are the glutathione peroxidase, which contain selenium in their active site and are involved not only in hydrogen peroxide removal, but also in the metabolism of lipid peroxides. Reduced glutathione, the substrate of glutathione peroxidase, may additionally exert direct antioxidant effects. ROS formation and metabolism can be summarized as shown in figure 5. The oxidative status of the cell is the primary factor regulating gene expression and activity of these enzymes (Rodriguez et al. 2004).

A large number of low molecular weight compounds are considered to be antioxidants of biological importance, including vitamins C and E, different selenium compounds, lipoic acid, and ubiquinones (Nordberg and Arner 2001).

Therefore the role of cellular antioxidant systems is to protect cells and organisms from the lethal effects of excessive ROS formation. When ROS overcome cell antioxidant defense system, through both an increase in ROS levels and a decrease in the cellular antioxidant capacity, oxidative stress occurs (Ray et al. 2012). Cells often tolerate mild oxidative stress by upregulating synthesis or activity of antioxidant defense systems in an attempt to restore the balance (Veal et al. 2007). However, severe oxidative stress produces DNA damage, rises in intracellular free Ca^{2+} and iron, proteins damage (including membrane ion transporters), and lipid peroxidation, leading to cell injury (Alfadda and Sallam 2012).

Fig.5

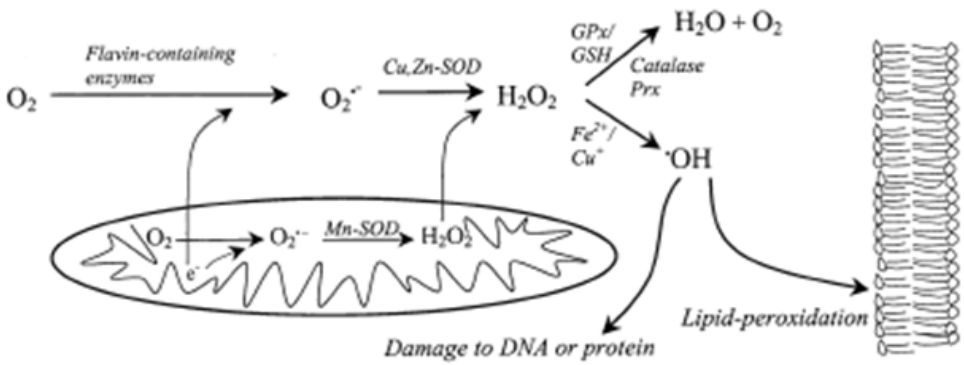

Nordberg J, Arnér ES. Free Radic Biol Med;31(11):1287-312.2001

Figure 5. ROS formation and metabolism Molecular sources of superoxide anion (O_2), are represented by flavin-containing enzymes and mitochondrial oxidative phosphorylation. Hydrogen peroxide (H_2O_2) and hydroxyl radicals ($^{\cdot}OH$) are generated through superoxide anion and H_2O_2 reduction/oxidation reactions by anti-oxidant enzymes such as SOD, glutathione peroxidase (GSH), catalase and peroxiredoxin (Prx). A massive ROS production determines lipid peroxidation and DNA and protein damages.

ROS have not only a negative role in cell. While an excessive production of ROS leads to cell-damage, regulated ROS production is indispensable for several biological function such as cell growth (Foreman et al. 2003), differentiation (Li et al. 2006), apoptosis (Cai 2005) by regulating different intracellular pathways. Indeed, ROS are involved in immune defense, antibacterial action, vascular tone (Alfadda and Sallam 2012). Moreover, ROS are used as secondary messengers in the intracellular signal transduction by several cytokines, growth factors, hormones, and neurotransmitters (Thannickal and Fanburg 2000). Indeed, ROS show the essential characteristics of second messenger: increases in their concentration occur through enzymatic generation; decreases in their concentration occur through enzymatic degradation catalyzed by catalase, glutathione peroxidase and peroxiredoxins; their intracellular concentration rises and falls within a short period; and they are specific in action (Forman 2007).

Cellular ROS sensing and metabolism are tightly regulated by a variety of proteins involved in the reduction/oxidation mechanism. The main molecular mechanism through which ROS and NO directly interact with critical signaling molecules consists of redox regulation of redox-reactive cysteine residues on proteins. Generally, any protein containing a deprotonated cysteine residue is susceptible to oxidation by ROS. The cysteine residues of most cytosolic proteins are protonated, due to the low pH of the cytosol, and therefore unable to react with sense hydrogen peroxide. It is thus an essential feature of most hydrogen peroxide sensor proteins that they contain cysteine residues with a

low pKa that make more susceptible to oxidation (Veal et al. 2007).

Oxidation of these residues forms reactive sulfenic acid that can form disulfide bonds with nearby cysteines or undergo further oxidation to sulfinic or sulfonic acid. The attachment of nitrosonium ion (NO^+) to cysteine sulfhydryls defined protein *S*-nitrosylation, emerged recently as a prototype of redox-dependent post-translational modifications (Stamler et al. 2001), which mediate a number of actions of the NO group in various biological processes (Stamler et al. 2001; Gow et al. 2002). Recently, protein *S*-nitrosylation/denitrosylation has been recognized as a regulatory component of signal transduction comparable with phosphorylation/ dephosphorylation (Mannick and Schonhoff 2002; Liu et al. 2004).

ROS, especially hydrogen peroxide, can also interfere with other post-transcriptional modifications such as sumoylation, thus regulating localization, activity and stability of many proteins. It has been demonstrated that hydrogen peroxide at lower concentration inhibits conjugation of SUMO to proteins, while at higher concentrations causes an increase of sumoylation levels in proteins (Manza et al. 2004; Zhou et al. 2004). Therefore, exposure to ROS leads to reversible oxidation of thiol groups of key cysteine residues in many proteins, including transcriptional regulators, kinases, phosphatases, structural proteins, metabolic enzymes, and SUMO ligases (Veal et al. 2007). These oxidative modifications result in changes in structure and/or function of proteins and enzymes (Ray et al. 2012).

Through oxidative modification, ROS production promotes the activation of many intracellular pathways involved in cell survival and proliferation. In particular ROS activates Mitogen-activated protein kinases (MAPK) cascade by direct activating-oxidation of several kinases, or by inhibiting-oxidation of related phosphatases. In the same way, ROS regulate PI3K pathway, thus playing a key role in cell proliferation. Hydrogen peroxide oxidizes and inactivates PTEN phosphatase through disulfite bond formation, leading to activation of the PI3K pathway. Furthermore, through upregulation of tyrosine kinases activity, low levels of hydrogen peroxide can regulate the activity of antioxidant enzyme. High levels of ROS can directly oxidize these enzyme thus modulating their activity or inducing their degradation (Veal et al. 2007).

ROS are also able to modulate transcription factor activity via decreased binding to promoter regions through different mechanisms: via oxidative damage to the DNA (Ghosh and Mitchell 1999), or more directly by redox regulation of transcription factor activation (Allen and Tresini 2000) and/or altered DNA binding due to redox-induced modification of the transcription factor protein (Abate et al. 1990; Marshall et al. 2000). Redox regulation of transcription factors is important in determining gene expression profile and cell response to oxidative stress. Some of the most important transcription factors involved in the response to oxidative stress are activator protein 1(AP-1), p53, NFkB, hypoxia inducible factor-1 (HIF-1α) and nuclear factor (erythroid-derived 2)-like 2 (Nrf2), that are all modulated by redox regulation

of redox factor-1(Ref-1). The transcriptional regulatory function of Ref-1 is mediated through its redox activity on above mentioned transcription factors. A particular cysteine residue in N terminus region of Ref-1 is required for the reduction and increased DNA binding of targeted transcription factors. Ref-1 was shown to be upregulated by genotoxic agents and oxidants, and protect cells from DNA and oxidative damage inducing the transcription of antioxidant detoxification genes. ROS are also involved in DNA damage response through ataxia-telangiectasia mutated (ATM) pathway. Indeed, hydrogen peroxyde is able to activate ATM not through DNA damage but through formation of active ATM dimers via intermolecular disulfite bond (Ray et al. 2012).

In conclusion, "oxidative regulation" better describes the action of ROS, since ROS modulate physiological processes but are also involved in many pathological situations. Therefore, according to their nature, quantity, source, and production kinetics in the cell, ROS differently affect cell regulation.

ROS as pro-tumoral or anti-cancer factors

It has been demonstrated that ROS promote a number of cancers. This phenomenon can be explained primarily by the ROS ability to induce DNA damage enhancing the rate of tumor-causing mutations and genetic instability, and by their pro-inflammatory effects (Alfadda and Sallam 2012). Another aspect of ROS protumoral effects is that they are able to provoke uncontrolled cell growth by overstimulation of Mitogen-activated protein kinases (MAPK) signal transduction pathways (Kulisz et al. 2002). Furthermore, ROS can activate hypoxia induced factor 1 (HIF-1) that stimulates the cells to gain energy from glucose under hypoxic conditions. HIF-1 increases the expression of glycolysis enzymes and additionally stimulates the development of new blood vessels by increasing the expression of angiogenic factors such as Vascular Endothelial Growth Factor (VEGF) to enhance oxygen supply (Gao et al. 2007). Therefore, ROS promote cell damage that may be advantageous to cancer cell growth. Indeed, ROS can induce both genomic instability and alterations in cell signaling processes related to survival, proliferation, resistance to apoptosis, angiogenesis and metastasis, thus contributing to cancer initiation, promotion and progression. Accordingly, antioxidants could be able to decrease tumorigenesis by neutralizing the deleterious effects of ROS (Sablina et al. 2005; Reliene and Schiestl 2006). Many studies have shown a different point of view regarding the link between ROS and cancer, pointing out ROS production as an effect of tumoral transformation. Indeed, it has been well established that cancer have a greater concentration of endogenous ROS than normal cells (McEligot et al. 2005; Lu et al. 2007; Hoyt et al. 2011). Several works have reported a presence of markers of constitutive oxidative stress in samples from in vivo breast carcinoma (Toyokuni et al. 1995; Portakal et al. 2000; Brown and Bicknell 2001).

One explanation is that cancer cells are more metabolically active than

normal cells, thus they accumulate more superoxide anion by electron transport chain in mitochondria as respiration byproducts. The resulting oxidative stress may cause further damage to both mitochondrial DNA and the respiratory chain, amplifying ROS generation (Zorov et al. 2006). In particular, generated ROS can be released into cytosol and trigger "ROS-induced ROS release" (RIRR) in neighbouring mitochondria. Tumor cells may also overproduce ROS for the upregulation of an important ROS-producer enzyme such as NADPH-oxidase (Meitzler et al. 2013). Another possible mechanism underlying the overproduction of ROS that has been demonstrated in breast cancer is the overexpression of thymidine phosphorylase, an enzyme that catabolizes thymidine to thymine and 2-deoxy-D-ribose1-phosphate, that is able at last to generate ROS (Brown et al. 2000). Oxidative stress within breast carcinoma may also be caused by a breast specific mechanism, that implicates the oxidation of one-electron of 17b-estradiol to a reactive phenoxyl radical (Sipe et al. 1994). There are a number of reports, establishing a strong correlation between oxidative stress and estrogen presence (Han and Liehr 1994; Yager and Liehr 1996; Cavalieri et al. 2000) or estrogen receptor status (Musarrat et al. 1996). In addition to metabolism of estrogen there is an ER mediated pathway capable of inducing ROS production through the regulation of antioxidant genes. It has been demonstrated that estrogen treatment causes a decrease in catalase activity followed by an increase in glutathione peroxidase activity, thus increasing the sensitivity to peroxide-induced cell damage in ER positive breast cancer cells, but not in ER negative breast cancer cells (Mobley and Brueggemeier 2004).

The higher oxidative stress observed in cancer cells can also result from a decrease or inactivation of antioxidants (Oberley and Buettner 1979; Oberley et al. 2004; Ridnour et al. 2004; Senthil et al. 2004; Sinha et al. 2009). Tumor cells usually present very few antioxidative enzymes, such as catalase, SOD and glutathione peroxidase, making these cells very vulnerable to oxidative stress. A high percentage of tumors show low catalase activity, which means an advantageous adaptation for the tumor, that continues to benefit from the high levels of ROS. There are conflicting data in the results obtained by different researchers regarding the levels of antioxidant, especially SOD, in tumor tissue and in blood from cancer patients. In breast cancer, for example, several studies describe an increase of lipid peroxidation and a decrease of antioxidants (Khanzode et al. 2004; Sener et al. 2007). The decrease of SOD activity could be related to the generation of free radicals that cause direct damage to the enzyme (Manoharan et al. 2004). However, other studies performed in neoplastic tissues have shown a greater presence of ROS and a high expression of SOD2 (Oberley and Buettner 1979; Cullen et al. 2003; Oberley et al. 2004; Ridnour et al. 2004), probably as a consequence of selective pressure towards stress adaptation. ROS can induce the up-regulation of SOD2 and other antioxidant enzyme through the modulation of the redox states of the transcription factors such as AP-1 and NFkB. The increase of ROS in tumor

cells may induce an increase of endogenous antioxidants in order to avoid intracellular lesions. Redox adaptation may be crucial also for drug resistance (Sullivan and Graham 2008). Redox adaptation, through the increase of endogenous antioxidants, may confer greater capacity to tolerate the action of exogenous stress, with capacity for increasing DNA repair and decreased apoptosis. As illustrated in figure 6, the high basal level of ROS in cancer cells make them more vulnerable to the increase of ROS that cause cell cycle arrest, apoptotic or necrotic cell death, depending on the degree of oxidative damage. In contrast, in normal cells, the ROS detoxifying capacity can protect cells from the increase of ROS levels maintaining redox homeostasis (De Miguel and Cordero 2012). Since tumor and normal cells show different redox balance, one therapeutic strategy might be the induction of cytotoxic oxidative stress.

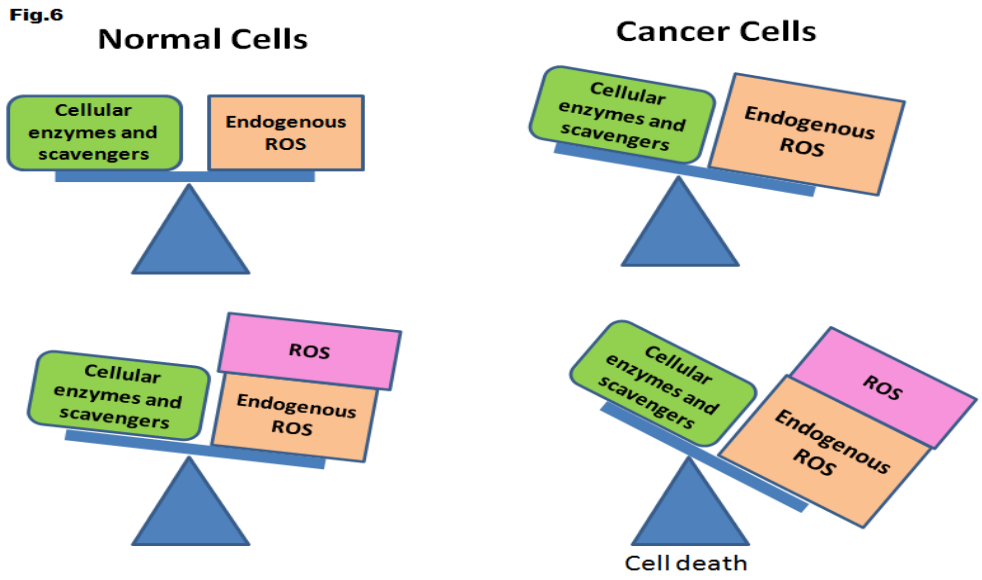

Figure 6. Different balance of redox status in normal and cancer cells In normal cells, the redox detoxifying capability is capable to control exogenous oxidative stress from a ROS producer. In cancer cells, the load of endogenous ROS is already straining the buffering capacity of the cell, causing redox imbalance and cell death when an exogenous source of ROS is added.

This "oxidative therapy" could be achieved by two different methods: inducing the generation of cytotoxic levels of ROS, and inhibiting the antioxidant system of tumor cells (De Miguel and Cordero 2012). Since the antioxidant system is compromised in many tumors, one alternative approach could be to replace the antioxidant activity. In particular, the overexpression of SOD2 in human melanoma, fibrosarcoma, breast carcinoma, oral squamous carcinoma and prostatic carcinoma has determined a reduction of in vitro and in vivo tumor cell growth (Li et al. 1995; Oberley et al. 2004; Ridnour et al. 2004). Overexpression of SOD2 leads to an accumulation of intracellular

peroxides that cannot be reduced, since catalase is downregulated in tumor cells. Indeed, it has been reported that the overexpression of either glutathione peroxidase or catalase reversed the growth inhibitory effects of SOD2 by altering the intracellular redox status (Li et al. 2000; Rodriguez et al. 2000). Ridnour and Oberley (2004) hypotized that the tumor suppressive effect for both the over- and under-expression of SOD2 may be explained by alterations in antioxidant balance characterized by the ratios of hydrogen peroxide generating to hydrogen peroxide-metabolizing enzyme activities. Their results reflect the dual nature of SOD2, acting as an antioxidant by removing superoxide, but also functioning as a pro-oxidant by producing hydrogen peroxide (Ridnour et al. 2004).

Chemical agents, medical, diagnostic ionizing and non-ionizing radiations ROS are able to induce oxidative stress. The excessive production of ROS induce tumor cell death by macromolecules damage and mitochondrial injury that causes the permeabilization of the mitochondrial membrane with release of cytochrome c, and activating caspase dependent apoptosis. In the same cases, the high levels of ROS that are generated may inhibit apoptosis at caspase level, and divert the process toward necrosis (Chandra et al. 2000; Conklin 2004). The change from apoptosis to necrosis is critical in solid tumors, and requires considerable amounts of ROS, a decrease of ATP and alterations in mitochondrial electron-transport chain (Lee et al. 2000) (Lee Y.J. 1999). In tumor cells, also the induction of small amount of ROS could induce cell death by causing downstream signalling for the pro-apoptotic molecules. One example is p53, that detects oxidative damage in nuclear and mitochondrial DNA and regulates the expression of genes involved in redox status, cell-cycle regulation and apoptosis (Achanta and Huang 2004).

Reciprocal regulation of AKT and ROS

Akt pathway is involved in cell proliferation, differentiation, survival, and/or migration. Alterations of akt pathway lead uncontrolled cell signaling which promotes the acquisition of a cancerous phenotype. Although Akt gene mutations are rare in human cancer, several studies have shown Akt amplifications in human ovarian, pancreas, breast, and gastric malignant tumors (Staal 1987; Bellacosa et al. 1995; Cheng et al. 1996; Knobbe and Reifenberger 2003). Akt signaling exerts a direct influence on glycolysis in cancer cells by several mechanisms. Akt is able to regulate the localization of the glucose transporter GLUT1 to the plasma membrane (Clarke et al. 1994; Kim et al. 2007) and regulates hexokinase expression, activity, and mitochondrial interaction (Vander Heiden et al. 2001; Miyamoto et al. 2008). In addition, Akt may indirectly activate the glycolysis rate-controlling enzyme phosphofructokinase-1 (PFK1) by directly phosphorylating phosphofructokinase-2 (PFK2) (Deprez et al. 1997). Furthermore, the activity

of Akt correlated to the degree of glycolysis in many cancer cells (Elstrom et al. 2004; Pelicano et al. 2006). Glucose metabolism plays an important role in hydroperoxide detoxification and the inhibition of glucose metabolism increases prooxidant production and cytotoxicity in cancer cells. If increased Akt pathway signaling is correlated with increased rates of glucose metabolism observed in cancer cells versus normal cells, then the inhibition of Akt pathway signaling would be expected to inhibit glycolysis and increase hydroperoxide production which would preferentially kill tumor cells versus normal cells via oxidative stress. Inhibiting glucose metabolism with Akt pathway inhibitors in cancer cells is hypothesized to limit the production of pyruvate and the regeneration of NADPH leading to increased steady-state levels of hydrogen peroxides from metabolic sources resulting in cytotoxicity.

On the other hand, intracellular redox status plays a vital role in the reversible activation and inactivation of Akt pathway (Leslie et al. 2003; Yasukawa et al. 2005; Leslie 2006; Pelicano et al. 2006; Kaneki et al. 2007). For example, moderate levels of ROS activate Akt pathway signaling and promote cell survival, but high or chronic oxidative stress inhibits this pathway resulting in apoptosis. Activation of the Akt pathway occurs mainly through the oxidative inactivation of Cys-dependent phosphatases (CDPs) or the direct activating oxidation of pathway kinases (Leslie et al. 2003; Leslie 2006). For example, the phosphatase PTEN, the main phosphatase involved in the negative regulation of the Akt pathway, is inactivated by oxidation by both hydrogen peroxide and nitrosylation, posttranslational modifications which would hyper-activate the Akt signaling pathway. Akt can be also directly activated by oxidative stimuli such as hydrogen peroxide and peroxynitrite via posttranslational modification of Akt (Leslie 2006; Clerkin et al. 2008; Nogueira et al. 2008). ROS-mediated posttranslational modification can also block akt function such as S-nitrosylation, a covalent attachment of NO moiety to thiol sulfhydryls that reversibly block akt activation (Yasukawa et al. 2005; Leslie 2006; Kaneki et al. 2007). Many antitumoral compounds such as resveratrol, jacarone, 15d-PGJ2, curcumin, and quercetin downregulate phosphorilated and total levels of Akt via ROS generation (Woo et al. 2003; Granado-Serrano et al. 2006; Shin et al. 2009; Hussain et al. 2011; Massaoka et al. 2012; Okoh et al. 2013). Pre-treatment with scavenger of ROS or detoxifying enzymes prevented drug-induced inactivation of akt. However, the exact mechanism by which ROS release leads to inactivation of akt is not known. Shin S.W. and colleagues (2009) suggest that 15d-PGJ2 induced akt inactivation might represent a consequence of engagement of the ROS induced caspase cascade, even if they demonstrated that caspase inhibitors did not completely restore normal levels of akt. A possible mechanism that may contribute to akt inactivation by ROS generation is the activation of stress-induced MAPKs, such as c-Jun N-terminal kinases (JNKs) but this cannot explain the downregulation of total protein form of akt (Shin et al. 2009).

Another ROS mediated mechanism to block akt activity is the oxidation

of its chaperone HSP90. A recent study demonstrated that oxidative stress can inhibit HSP90 function by disruption the super-chaperone complex. Indeed, High ROS production can oxidize thiol groups of HSP90 protein, leading to protein aggregation and dysfunction. Consequently, akt and other client protein of HSP90 are degradated via proteasome (Sarkar et al. 2013). Alternatively, HSP90 can be cleaved by ROS at its amino-terminal aminoacid motiv determinig HSP90 and its client protein degradation (Beck et al. 2012).

Since cancer cells are under increased metabolic oxidative stress compared to normal cells and the Akt pathway may be activated for survival under these oxidizing conditions, the therapeutical approach may take into account also inhibition of akt pathway and/or induction of ROS production, taking advantage of their multiple involvement in the control of cell proliferation.

1.4 ROS AS SIDE EFFECT OF HIV-PIs

Despite the clinical successes of HIV-PIs, accumulating clinical evidence suggests that treatment with PIs is implicated in the pathogenesis of metabolic syndrome (Carr et al. 1998; Ben-Romano et al. 2004; Chai et al. 2005). Most patients on PIs therapy develop a metabolic syndrome associated with partial lipodystrophy, hyperlipidemia, insulin resistance, premature atherosclerosis and myocardial infarction (Carr et al. 1998; Hui 2003; Koster et al. 2003). Supporting these evidences are human, animal, and cell-based studies, demonstrating that increased plasma cholesterol and triglyceride levels, and the development of lipodystrophy and insulin resistance, are the most common metabolic perturbations found with HIV-PIs treatment (Reyskens and Essop 2014).

Table 2

Name	Trade name	Manufacturer	Side Effects
Indinavir	Crixivan	Merck & Co.	ER stress [129,131], mitochondrial toxicity [113], inhibition of GLUT4 [207]
Nelfinavir	Viracept	Agouron Pharmaceuticals	↑UCP3, IR, ↑ROS [93,95]
Lopinavir/Ritonavir	Kaletra	Abbott	Hyperlipidemia, LD, dyslipidemia, MetS, CVD, IR, DM [21,22,131], ER stress [53,141–143], ↑ROS, ECG abnormalities [182,183]
Atazanavir	Reyataz	Bristol-Myers Squibb	ECG abnormalities [182,183], Crystalluria [208]
Darunavir	Prezista	Tibotec	Crystalluria [208]
Saquinavir	Invirase/Fortovase	Hoffman-La/Roche	Alterations to mitochondrial metabolism, ER stress [209]
Amprenavir	Agenerase	GlaxoSmithKline	Dyslipidemia [210]
Fosamprenavir	Lexiva/Telzir	GlaxoSmithKline	↑ Liver enzymes [211]
Tipranavir	Aptivus	Boehringer-Ingelheim	Mild hepatic side-effects [212]

Symbols: ↑–increase. Abbreviations: CVD–cardiovascular diseases, DM–diabetes mellitus, ER–endoplasmic reticulum, ECG–electrocardiogram, GLUT4–glucose transporter 4, IR–insulin resistance, LD–lipodystrophy, MetS–metabolic syndrome, ROS–reactive oxygen species.

Reyskens, K.M.S.E.; Essop, M.F. BBA - Molecular Basis of Disease vol. 1842 issue 2, p. 256-268.2014

Table 2. HIV-PIs and associated-complications

Cell and molecular mechanisms underlying PIs associated metabolic diseases seem to be related to overproduction of ROS (Mondal et al. 2004; Gills et al. 2007; Pyrko et al. 2007). Clinical studies suggested that PIs may induce oxidative stress in HIV positive patients (Jareno et al. 2002; Hulgan et al. 2003).

Oxidative stress has been shown to induce insulin resistance, at least in culture cells (Bloch-Damti and Bashan 2005). The insulin signalling defect induced by exposure of adipocytes to hydrogen peroxide shares striking similarities to that observed with chronic exposure to nelfinavir, as both conditions induce a defect in signal propagation between PI3-kinase and Akt (Ben-Romano, Rudich et al. 2004). Although insulin-stimulated phosphorylation of insulin receptor substrate (IRS) proteins and their association with PI3kinase, as well as PI3kinase activity, are all maintained following nelfinavir treatment, the phosphorylation of downstream PI3K effector such as akt is impaired. The reduction in Akt phosphorylation may be due to a failure of insulin to promote its translocation to the plasma membrane, a process required for its phosphorylation and activation. Indeed, it has been observed that nelfinavir treatment or other oxidant agents impair capacity of signalling molecules to be normally relocated in response to insulin, and to be activated in a specific cell site (Ben-Romano et al. 2004). One important example is the block ROS-mediated of translocation of glucose transporter GLUT4 which leads to impaired glucose uptake (Rudich et al. 2001; Ben-Romano et al. 2004; Bloch-Damti and Bashan 2005; Rudich et al. 2005). The increase of intracellular ROS may also directly inhibit insulin action by activating stress kinases involved in insulin signalling cascade such as MAPKs and NFkB and/or by inducing protein oxidative modifications (Evans et al. 2003). One of the oxidative modification involved in insulin pathway is nitrosylation of insulin receptor, akt and IRS1 which determine an impaired insulin signaling to different levels (Carvalho-Filho et al. 2005; Yasukawa et al. 2005). Oxidative modification can affect also several transcription factors such as NFkB and AP1 involved in the insulin pathway. These transcriptional factors, activated for direct oxidation or indirectly in response to oxidative stress (Ammendola et al. 1994), mediate GLUT1 transcriptional activation, thus increasing basal glucose uptake and mitochondrial ROS production. On the contrary, a massive ROS production reduces both mRNA and protein expression of GLUT4 by decreasing DNA-binding of nuclear protein to GLUT4 promoter (Pessler et al. 2001).

Therefore, whereas short-term exposure to millimolar ROS concentrations results in the activation of insulin pathway by increased basal tyrosine phosphorylation and activation of glucose transport, high levels of ROS inhibit insulin-stimulated glucose uptake by activation of cellular stress kinases, impaired insulin-signaling cascade and changes in gene regulation and protein stability (Bloch-Damti and Bashan 2005).

The exposure to nelfinavir not only induces peripheral insulin resistance

but also impairs glucose-stimulated insulin secretion from beta (Chandra et al. 2009). Study conducted by Chandra et al (2009) revealed that nelfinavir is the most potent HIV-PI to suppress glucose stimulated insulin secretion and simultaneously increase oxidative stress to a significant level. Nelfinavir-induced ROS production is associated with redox status perturbation with low protein levels but greater enzyme activity of antioxidant SOD1 and decrease in the intracellular levels of GSH. These conditions can represent both cause and effect of ROS production, since a reduction of ROS-detoxifying enzyme increases ROS production and, at the same time, oxidative stress can lead to inactivation or downregulation of these enzymes. The implication of oxidative stress in PIs-induced cell damages is demonstrated by co-treatment with antioxidants. In rat pancreatic insulinoma cells, nelfinavir dependent inhibition of glucose-stimulated insulin secretion is prevented by thymoquinone (Chandra et al. 2009), a potent antioxidant. Moreover, in adipocytes, the SOD-mimetic antioxidant MnTBAP protects against nelfinavir-induced insulin resistance and apoptosis (Ben-Romano et al. 2006). Thus, nelfinavir alters glucose metabolism, and can impair glucose tolerance as well as whole-body glucose disposal, uptake, transport and phosphorylation, at the same time contributing to insulin resistance at peripheral sites.

ROS production are well known triggers of ER stress (Hetz 2012), another molecular mechanism involved in HIV-PIs-induced side effects such as insulin resistance, dislipidemia, and lypodistrophy. Indeed, the production of ROS interferes with protein disulphide bonding and results in misfolding of proteins that accumulate in endoplasmic reticulum lumen (Gotoh and Mori 2006). One of the most important protein affected by ROS-induced ER stess is sterol regulatory element binding protein SREBP, a lipid-status regulator that increase its intracellular levels after HIV-PIs treatment, causing cholesterol and sterol components production (Hirano et al. 2001; Riddle et al. 2001). Many studies reported that nelfinavir long-time treatment can affect adipose tissue by several mechanisms, including: induction of adipocyte necrosis (Vincent et al. 2004); interference with terminal adipocyte differentiation (Zhang et al. 1999); interference with intracellular insulin signalling leading to the deregulation of glucose and lipid metabolism (Ben-Romano et al. 2004); accumulation of intracellular free cholesterol in hepatocytes (Zhou et al. 2006; Cao et al. 2010); activation of the expression of inflammatory cytokines in macrophage (Zhou et al. 2007). The subsequent increase of free fatty acids levels can affect endothelial function and survival, and contribute to cardiovascular morbidity in PIs therapy treated patients.

It has been reported that HIV-PIs treatment determines an increase of the incidence of cardiovascular diseases probably through ROS production. Increased production of ROS is associated with coronary atherosclerosis, ischemia, reperfusion injury, and progression of chronic congestive heart failure (Moskowitz and Kukin 1999). In particular, oxidative stress is one of the important mechanisms of vascular injury and endothelial dysfunction, both

recognized as critical initiating factors in atherogenesis and other cardiovascular diseases. Indeed, it has been proposed that an increased extracellular or intracellular production of ROS induces vascular smooth muscle cells apoptosis in atherosclerotic plaque (Irani 2000). Using this cell model, it has been demonstrated that nelfinavir induces an increase of ROS production leading to apoptotic cell death (Rudich et al. 2005).

PIs increase ROS production also in human aortic endothelial cells, and increase the endothelial properties of leukocyte recruitment leading to vascular dysfunction (Mondal et al. 2004).

It has been demonstrated that ritonavir significantly impairs vasomotor activities through the increase of oxidative stress and the decrease of endothelial nitric oxide synthase (eNOS) in porcine coronary artery and endothelial cells. A decrease of eNOS expression leads to a decrease of NO production, which may contribute to the pathophysiology of several major disease of the cardiovascular system. In addition, decreased eNOS expression is always accompanied by the overproduction of ROS, a known risk factor for cardiovascular disease (Fu et al. 2005). In the model of porcine coronary artery cultures, ritonavir, amprenavir and saquinavir have more detrimental effects than indinavir and nelfinavir, resulting in vasomotor dysfunction, eNOS downregulation, and superoxide anion overproduction. In particular, ritonavir induces smooth muscle cell and endothelial cell injury while indinavir and nelfinavir have very limited effects on vasomotor function in this model (Zhong et al. 2002; Chai et al. 2005). The source of PIs-induced ROS is not clear but fluorescence microscopy analysis of ROS and cellular mitochondria co-localizion in endothelial cells have suggested that mitochondrial ROS are involved (Jiang et al. 2007a). In these cells, the increase of ROS determines a decrease in the mitochondrial transmembrane potential and mitochondrial dysfunction, thus promoting endothelial dysfunction but not endothelial cell death. PIs-induced ROS production results in lipid peroxidation, that is abrogated by overexpression of mitochondria-targeted catalase (Jiang et al. 2007a). Moreover, high ROS intracellular levels determine calcium overload by oxidation of sulfhydryl groups of several receptor, ionic channels and pumps, leading to mitochondrial damage, ATP-generating capacity impairment, and dysfunction of electrical signaling in the myocardium (Reyskens and Essop 2014).

Although the specific cell mechanism of ROS production has not been elucidated, PIs-induced ROS may prove to be an important common cell mechanism in HIV-PIs-induced side effects. The identification of novel nelfinavir-derived molecules with anti-proliferative activity might determine lower side effects and improve the therapeutic range.

1.5 NELFINAVIR CHEMICAL DERIVATIZATION

The use of nelfinavir in HAART protocols for AIDS therapy as well as its strong anti-tumoral potentiality is undermined by its many side effects. To improve therapeutic efficacy in AIDS therapy, limit side effects and/or generate effective drugs against new HIV-mutants, several pharmaceutical companies have developed, an increasing number of second-generation protease inhibitors, either with or without a flexible structure (Rusconi and La Seta Catamancio 2002). Nelfinavir has attracted the attention of synthetic chemists due to its huge market, unique structural features comprising five stereogenic centers and a core four carbon backbone in which each carbon is attached to a heteroatom.

To data no Nelfinavir-analogues is side effects-free, or more effective than nelfinavir or other FDA-approved HIV-PIs. A strategy for the synthesis of thiophene containing nelfinavir analogues has been developed by Bonini et al. (2004), with the preparation of key-chiral compounds, which can be utilized for the synthesis of different potential HIV-PIs. Data deriving from biological experimental strategies and theoretical data revealed a low activity of derivative compounds compared to the Nelfinavir unmodified molecule (Bonini et al. 2004, Bonini et al. 2005). Zhou and Yang (2008) designed a series of hybrid molecules as non-peptidic HIV-PIs by incorporating methyl sulfonamide moiety of amprenavir into hydroxyethyl decahydroisoquinoline backbone of nelfinavir. Although derivatives exhibit moderate to significant HIV-protease-inhibitory activities, to date the best revealed inhibitory activity is essentially equipotent to classical HIV-PIs (Zhou et al. 2008).

While chemical design based on HIV-protease/substrate interaction is important to synthesize novel protease inhibitors capable to improve clinical trend in HIV-infected subjects (Bonini et al. 2010), the absence of defined molecular target at the basis of anti-cancer activity of nelfinavir, makes the development of novel anti-cancer compounds very difficult. However, the characterization of the functional groups of nelfinavir responsible for its biological activities are relevant to support the design of novel, more effective anti-tumoral compounds compared to actual chemotherapeutic agents.

2. AIMS OF THE STUDY

The advent of HIV-PIs has led to a reduced incidence and/or regression of AIDS-associated tumors by a non-immune mediated mechanism. Indeed, the anti-cancer effect cannot be explained by the ability of these drugs to suppress HIV replication and thereby reconstitute the immune system (Monini et al. 2004). Based on these evidences, many researchers attempted to evaluate the anti-cancer activity of the most used HIV-PIs including amprenavir, indinavir, lopinavir, nelfinavir, ritonavir, and saquinavir in HIV-free models. Nelfinavir represents the most potent anti-tumor HIV-PIs. Although the molecular mechanisms at the basis of its anticancer activity has not been elucidated yet, many studies suggested that inhibition of akt pathway is a relevant mechanism by which nelfinavir exerts anti-tumor effect in different cancer types. Controversial and few informations have been generated by studies on nelfinavir activity in breast cancer, that established its anti-proliferative effect in this tumor. However, the development of many side-effects in HIV-patients treated with nelfinavir has reduced the interest versus nelfinavir as anti-tumoral drug. Recent evidences demonstrated that the alteration of redox state is responsible for the side effects observed in HIV-positive patients treated with this drug, but the involvement of ROS in the molecular mechanism underlying its anti-cancer effects has not been investigated .

Aim of the present thesis is to study the mechanisms at the basis of anticancer activity of nelfinavir in breast cancer, and to identify novel nelfinavir-derivatives with increased efficacy and reduced cell toxicity.

To this purpose, I analyzed:

a) the anti-proliferative effects and specificity of nelfinavir in breast cancer cell lines
b) the effect of nelfinavir on akt pathway
c) the role of redox status in nelfinavir anti-cancer activity.
d) the chemical nelfinavir structure in order to design and synthesize novel anti-tumor compounds.

3. MATERIAL AND METHODS

3.1 Cell Culture

Human breast cancer (MCF-7; MDA-MB231), human thyroid tumor (TPC), human lung adenocarcinoma (Calu), human hepatoma (HepG2), and colon adenocarcinoma (HT-29) were grown at 37 °C in Dulbecco's modified Eagle's medium (DMEM) (Life Technologies) containing 10 mM glucose supplemented with 10% fetal calf serum (GIBCO) and 100 units/mL each of penicillin and streptomycin and 2 mmol/L glutamine and incubated in standard culture conditions (95% air and 5% CO_2 at 37 °C).

3.2 Culture of human primary mammary epithelial cells

Human mammary epithelial cells (HMEC) were derived from surgical specimens from normal women who had undergone reduction mammoplasty, after informed censent. Epithelial cells were culled and grown by the method of Stampfer (Labarge et al. 2013). Briefly, upon receipt, tissue was washed extensively in phosphate-buffered saline (PBS) supplemented with 200 U of penicillin, 200 μg/ ml streptomycin and 5 μg/ml fungizone (all from SIGMA), then minced finely and disaggregated for 18-20 min in 0.1% collagenase type III (Life Technologies). Digested tissue was removed from the incubator, the fat supernatant tissue was removed and the tube was shaken vigorously by hand to disaggregate any remaining large clumps. Three cell populations (epithelial breast cells, stromal breast cells and organoid substance) were then isolated using differential centrifugation. For the first 24 h, cells from the organoid and epithelial fractions were plated in 75% organoid medium (OM) to promote cell attachment. OM consisted of DMEM/F12 supplemented with 100 U/ml penicillin, 100 μg/ml streptomycin, 2 mM glutamine, 10 mM Hepes, 0.075% bovine serum albumin (BSA), 10ng/ml cholera toxin, 0.5μg/ml hydrocortisone, 5μg/ml insulin and 5ng/ml epidermal growth factor (EGF) (all from SIGMA). After 24 h media was removed and replaced with OM. Cells were maintained in this way for the duration of the culture. To remove the fibroblasts from HMEC, it was performed Differential Trypsinization (DT), based on the rapid detachment of fibroblasts from the surface plastic (Olumi et al. 1999). The predominance of epithelial cells and the absence of fibroblasts was confirmed by immunofluorescence staining with the broad spectrum, cytokeratin antibody AE1/AE3 and the lack of staining for vimentin (Santa Cruz).

3.3 Reagents and inhibitors

Nelfinavir mesylate hydrate was dissolved in DMSO to a final concentration of 50 mM and stored at -20°C. It was obtained through the NIH

AIDS Research and Reference Reagent Program, Division af AIDS, NIAID, NIH. It was used at indicated concentration and added in colture medium each 48 hours. Nelfinavir-derivatives were designed and producted by University of Salerno, Department of Pharmacy. Intracellular translation inhibitor cycloheximide (Sigma), proteasome inhibitor MG-132 (Sigma), HSP-90 inhibitor 17-AAG (Calbiochem), PI3K inhibitor LY294002 (Sigma), ROS scavenger tocopherol (Sigma) were used at indicated concentrations.

3.4 Cell Viability Assay

Cells were seeded into 96-well plates to a density of 5x 10^4 cells/well. After 24 hours of growth to allow attachment to the wells, nelfinavir or nelfinavir-derivatives were added at different concentrations for indicated time points. At the end of incubation times, PrestoBlue™ Reagent (Invitrogen) were added directly to cells in culture medium for 2 hours at 37°C in the dark. PrestoBlue® reagent is a resazurin-based solution that functions as a cell viability indicator and it is modified by the reducing environment of the viable cell. This change was detected using absorbance measurements at 570 nm and the values normalized to the 600 nm values for the experimental wells. Results were expressed as percentage relative to vehicle-treated control (0.5% DMSO was added to untreated cells).

3.5 Growth Curve

Cells were seeded in 12-well culture plates at density of 1x10^4 cells/well and allowed to attach for 24h. Cells were then treated with indicated reagents. Attached cells were harvested and a cell count performed using a Bürker chamber, until 6th day.

3.6 Cell cycle analysis

For FACS analysis cells were seeded in 6-well plates at density of 3x10^5 cells/dish and treated as indicated. Attached MDA-MB231 and MCF-7 cells were collected and fixed over-night in ice-cold 70% ethanol at -20°C. Washed pellets were resuspended in PBS containing 250µg/ml RNAseA (Roche) and 10µg/ml Propidium Iodide (PI) (Sigma), incubated for 30' at room temperature, and analyzed for emission in PE-Texas Red channel. The samples were acquired with a CYAN flow cytometer (DAKO Corporation, San Jose, CA, USA). To remove artifacts such as doublets and aggregates from the analysis, an electronic doublet discrimination was performed using the area and width of the fluorescence PE-texas red pulse.

The cell cycle distribution, expressed as percentage of cells in the G0/G1, S, and G2/M phases, was calculated using SUMMIT software.

3.7 Annexin V/PI staining

MDA-MB231 and MCF-7 cells were plated at $1x10^5$ in 6-well plates and washed with PBS1X and then with Annexin V Binding Buffer. After centrifugation at 2000 rpm for 3 min, the cells were resuspended in 100µl of Annexin V Binding Buffer (Biolegend) and incubated with 5 µl of FITC-conjugated Annexin V (Biolegend) for 15 min at 25°C in the dark. Finally, 400 µl of Annexin V Binding Buffer and 2 µl of 500 µg/ml PI was added to each sample just before analysis. PI can penetrate only in non-vital cells, whereas Annexin V binds to living cells with exposed phospholipid phosphatidylserine, an early marker of apoptosis. PI single positivity represents necrosis, single Annexin V staining early apoptosis, double positivity (annexin V and PI) indicates late apoptosis. Samples were acquired with a CYAN flow cytometer (DAKO Corporation, San Jose, CA, USA) and analysed using SUMMIT software.

3.8 Measurement of ROS intracellular levels

Basically, cells are incubated with the fluorescent, lipophilic dihydrodichlorofluorescein diacetate (H_2DCF-DA)(Calbiochem) which can diffuse through the cell membrane. Inside, the acetate groups are cleaved by cellular esterases so the resulting H2-DCF cannot leave the cells. Reaction with intracellular ROS, primarily hydrogen peroxide (H2O2), results in the fluorescent molecule DCF (max. emission ~ 530 nm). Breast cancer and primary normal cells were seeded in 6-well plates at density of $3x10^5$ cells/dish and treated with 10µM nelfinavir at different indicated time point. Cells were rinsed with PBS and incubated with 5uM H2DCF-DA in the serum-free fresh medium. After 30 min incubation at 37 ^{0}C in the dark, the cells were washed, harvested and green fluorescence intensity in the cells was examined by FACS (DAKO Corporation, San Jose, CA, USA) analysis using SUMMIT software.

3.9 Lipid peroxidation analysis

Lipid peroxidation was analysed using the parameters indicated in the Lipid Peroxidation (MDA) assay kit instructions (Abcam). Briefly, cells were seeded at density of $1x10^6$cells, treated with nelfinavir at indicated time, lysated on ice in MDA lysis buffer and centrifuged (13000xg, 10 min) to remove insoluble material. The supernatants were placed into new vials with Thiobarbituric Acid (TBA) solution for 60 min at 95^{o}C and cooled in ice bath for 10 min. The MDA-TBA adducts were quantified colorimetrically at 532nm using a microplate reader.

3.10 SOD activity assay

SOD Activity Assay kit (Abcam) was used to determine the SOD activity in breast cancer cell lines treated for 30 min, 3h, 24h and 48h with 10μM nelfinavir. The analysis of enzymatic activity was based on detection of WST-1 products (water-soluble formazan dye) upon reduction with superoxide anion. Briefly, cells were homogenized in ice cold 0.1M Tris/HCl, ph 7.4 containing 0.5 %Triton X-100, 5mM β-ME, 0.1mg/ml PMSF. After centrifugation (14000xg 5min at 4°C), supernatants were incubated with WST Working Solution and Enzyme working solution for 20 min at 37 C. SOD activity (%) was calculated as indicated in the assay kit instructions using absorbance values at 450nm.

3.11 Glutathione reductase assay

Abcam's Glutathione Reductase Assay kit is a highly sensitive colorimetric assay and was used for measuring GR activity in biological samples. Briefly, MCF-7 and MDA-MB231 cells ($1x10^6$ cells) were lysated on ice in assay buffer, then centrifuged at 10000xg for 15 min at 4^oC and supernatants were collected for assay. In the assay, GR reduces glutathione, which reacts with 5,5'-Dithiobis (2-nitrobenzoic acid) (DTNB) to generate yellow TNB^{2-}. The absorbance values were measured at 405 nm by microplate reader.

3.12 Quantitative reverse transcription polymerase chain reaction (qRT-PCR)

Total RNA were extracted from MDA-MB231 cells using trizol reagent (Invitrogen), purificated with Qiagen RNeasy mini-kit and reverse transcribed using a High Capacity Reverse Transcriptase Kit (Applied Biosystems). QRT-PCR was performed using a BioRad IC5 thermo cycler (Bio-Rad laboratories, Hercules, CA) using specific primers (Nakatani et al. 1999):

h-Akt1 5′-ATGAGCGACGTGGCTATTGTGAAG-3′ forward
5′-GAGGCCGTCAGCCACAGTCTGGATG-3′reverse,
h-Akt2 5′-ATGAATGAGGTGTCTGTCATCAAAGAAGGC-3′ forward
5′-TGCTTGAGGCTGTTGGCGACC-3′reverse,
h-Akt3 5′-ATGAGCGATGTTACCATTGT-3′ forward
5′-CAGTCTGTCTGCTACAGCCTGGATA-3′reverse.

Cycle threshold (Ct) values from 3 indipendent experiments were normalized to the internal β-actin control. The ratio of fold change was calculated using the Pfaffl method (Pfaffl 2001).

3.13 Western Blot and immunoprecipitation procedures

Cells were washed in PBS buffer and lysed on ice for 30 min in RIPA buffer (50mM Tris-HCl, pH 7.4, 150mM NaCl, 1% NP-40, 2mM EDTA, 2mM PMSF, 5µg/mL leupeptin, 5µg/mL pepstatin). Lysates were quantified by Biorad DC protein assay. An equal amount of proteins from each sample was loaded with lamely buffer. Protein were resolved by SDS-PAGE and transferred to an Immobilion P membrane (Millipore Corporation, Bedford, MA). Membranes were blocked by incubation with PBS 0,2% tween, 5% nonfat dry milk for one hour at room temperature. the membranes were then incubated overnight with primary antibodies at 4^{o}C, washed for 40 min with PBS 0,2% tween and incubated for one hour with a horseradish peroxidase-conjugated secondary antibodies. finally, protein bands were detected by an enhanced chemiluminescence system (ECL, Amerscham). Computer-acquired images were quantified using ImageQuant software (Amerscham).

For Immunoprecipitation assay, the cells were lysed in RIPA buffer and 500µg of total lysate were incubated with primary antibodies vs protein of interest for one hour and with Protein G plus/protein A agarose beads (Calbiochem) for other two hours. Non immune rabbit or mouse IgG were used as control. Mouse monoclonal antibodies to HSP90, cyclin B, p21, cytochrome c, Bcl-2, β-actin, rabbit polyclonal to MDM2, cyclin A, cyclin D, cyclin E, SOD1, SOD2, Bak and caspase 9 and goat anti-akt were all purchased by Santa Cruz Biotechnology, CA, USA. Rabbit polyclonal to phospho-akt (Ser 473), pospho-PRAS40 (Thr 246) and phospho-Rb (Ser 807/811) were purchased from Cell Signaling, Boston, MA, USA.

3.14 Statistical analysis

Student's t-test was used to assess statistical significance and a p-value<0.05 was deemed significant. Statistics were computed with GraphPad Prism software (San Diego, CA).

RESULTS

4.1 Effect of nelfinavir on viability and proliferation of cancer cells.

To evaluate the anticancer activity of nelfinavir, I performed a cell viability assay and cell-growth analysis in different cancer models: TPC (thyroid), HT-29 (colon), HEPG2 (liver), CALU (lung). As depicted in figure 7, nelfinavir significantly inhibited the growth of all these tumor cells. In particular, 10µM nelfinavir was able to reduce cell population to 40% in HEPG2 cells and HT29 following 24 of treatment, whereas CALU and TPC cells resulted more resistant to drug cytotoxic effects and required the highest concentration of nelfinavir (20µM) to significantly reduced cell viability.

Fig. 7

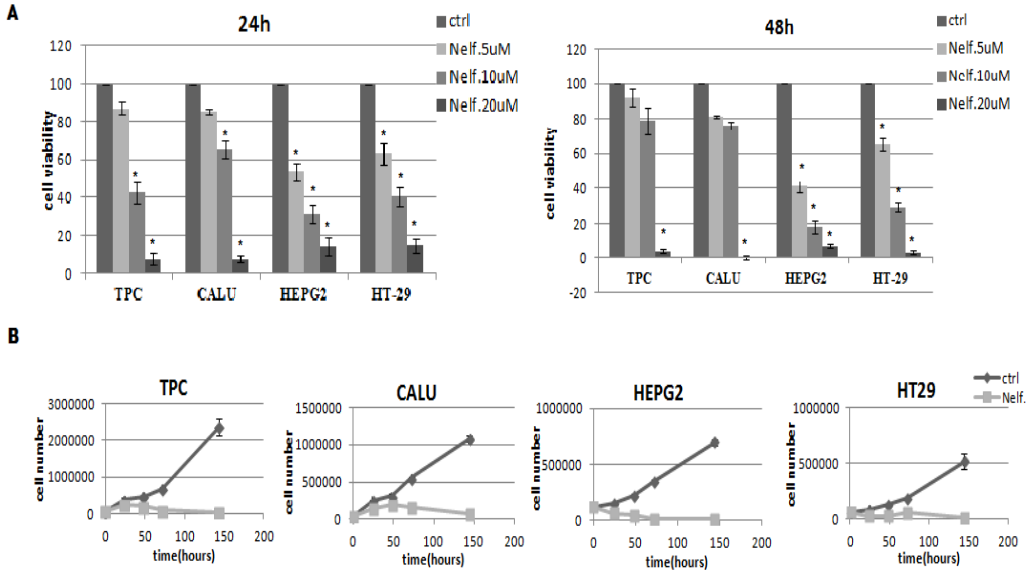

Figure 7. Cytotoxic effect of nelfinavir on cancer cells
A) TPC, CALU, HEPG2, HT-29 were treated with 5µM,10µM, 20µM nelfinavir, and cell viability was measured by MTT assay after 24 and 48 hours (h) of treatment. The histograms represent cell viability percentage relative to untreated cells (control). B) Growth curves of the same cancer cells untreated or treated with 10µM nelfinavir for 24, 48, 72 and 144 hours. Each value is the mean ± S.D. of three indipendent experiments. Significant (* p-value< 0.05) differences in cell viability were observed in cell treated with drug compared to control cells (ctrl).

To determine the effectiveness of anti-proliferative activity of nelfinavir in human breast cancer, I performed a cell viability assay in two different cell lines, MDA-MB231 and MCF-7 cells. These cells are widely used for testing drugs in vitro since they represent two different cell models of breast

carcinomas. These tumor cell lines were treated for 24 hours and 48 hours with 5µM,10µM and 20µM of Nelfinavir, that represent a therapeutic range in HAART protocols. As shown in figure 8, nelfinavir significantly decreased cell viability in a dose-dependent manner in both cell lines although MCF-7 resulted more sensitive to nelfinavir treatment. Breast epithelial cells were drawn from mammary gland of healthy subjects undergoing aesthetic reductive surgery, and used to determine whether nelfinavir reduced viability of normal cells. Data suggest that nelfinavir affected the viability of breast normal cells only at high concentration (20µM). The analysis of the growth of MDA, MCF-7 and breast primary normal cells confirmed the selectivity of the anti-proliferative action of nelfinavir (10µM) on tumor cells. For this reason all the following experiments were performed with 10µM nelfinavir.

Fig.8

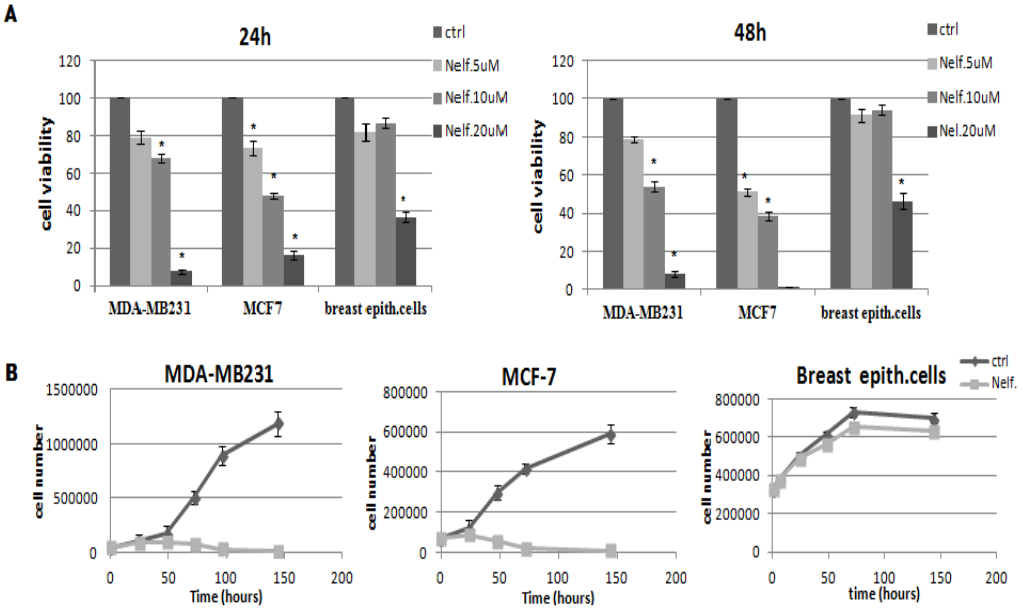

Figure 8. Nelfinavir exhibits anti-proliferative effects in breast cancer cell lines
A) MTT assay to assess cell viability in MDA-MB231, MCF-7 and normal breast epithelial cells, treated with indicated concentration of nelfinavir for 24 and 48 hours. B) Growth curves for 10µM nelfinavir at indicated times in MDA-MB231, MCF-7 and breast epithelial cells. The data show the mean ± S.D. of three indipendent experiments. Significant (* p-value< 0.05) differences in cell viability were observed in cell treated with the drug compared to control cells (ctrl).

4.2 Cell-cycle profile and cell-death analysis in nelfinavir-treated cells.

The inhibition of cell-growth/viability in tumor cells treated with nelfinavir can sustain different biological mechanisms such as cell cycle block, apoptosis, necrosis and senescence. Firstly, I evaluated cell cycle in MDA-MB231 and MCF-7 cells. FACS analysis revealed that nelfinavir induced a slight increase of G1 phase population percentage and decrease of S and G2 phase cell percentage following 24 hours of treatment of MDA-MB231 cells. Otherwise, nelfinavir did not affect MCF-7 cell-cycle (figure 9).

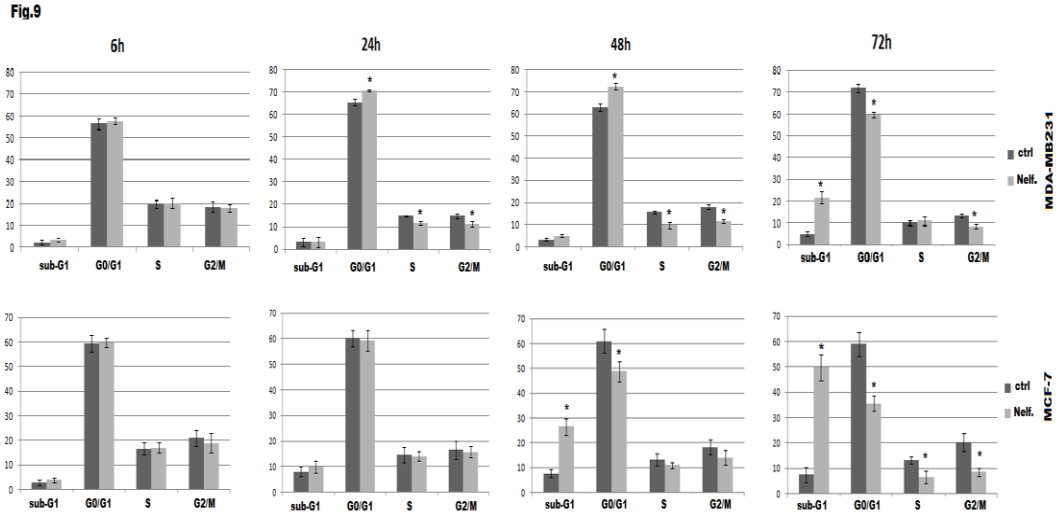

Figure 9. Cell-cycle analysis in nelfinavir treated breast cancer cell lines
MDA-MB231 and MCF-7 cells were treated with 10μM nelfinavir for 6-72 hours (h). Thereafter, the cells were washed, fixed and stained with propidium iodide, and analyzed for DNA content by flow cytometry as described in Material and Methods. These data represent the mean ± S.D. of four indipendent experiments. * p-value< 0.05, versus control cells (ctrl).

To better investigate the induction drug-mediated of cell-cycle arrest, I performed a Western Blot analysis of different proteins involved in cell-cycle progression control such as Rb, p21, cyclins A, B, D, E. As shown in figure 10, nelfinavir reduced the levels of phosphorylated Rb, cyclin A, cyclin B, cyclin D, increased the expression levels of p21 in breast cancer cell lines but not in normal cells. Moreover, the expression of cyclin E was modified only in MDA-MB231. Although both cell lines showed a similar protein expression profile, biological effects of nelfinavir treatment resulted different in MDA-MB231 and MCF-7 cells. Indeed, whereas in the former I observed a Go/G1 block, MCF-7 cell-cycle was not affected by nelfinavir.

Fig.10

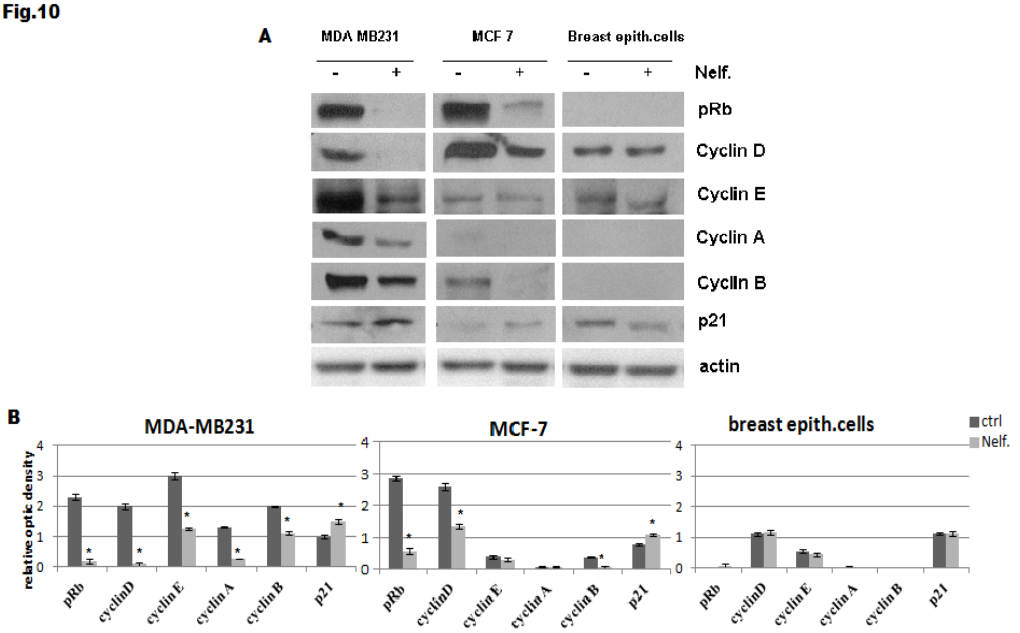

Figure 10. Specific anti-proliferative activity of nelfinavir in breast cancer cells compared to normal cells A) MDA-MB23, MCF-7 and primary breast epithelial cells were treated with 10μM nelfinavir for 24 hours and protein lysates immunoblotted for different cell-cycle regulators: pRB, cyclin A, B, D, E, p21 and β-actin, used as loading control. B) Densitometric analysis of proteins signals relative to actin signal. The values represent the means ± S.D. of three indipendent experiments and compared to control value (* p-value < 0.05)

Cell-cycle analysis also revealed that nelfinavir increased the fraction of tumor cells with sub-G1 DNA content. Therefore, I investigated whether this result, as well as the reduction of cell growth/viability, was correlated to cell death mechanisms. To this aim, breast cancer cells were treated with 10µM nelfinavir for different time points and stained with Annexin V conjugated with FITC, which marks apoptotic cells, and propidium iodide as a general cell death marker. Nelfinavir treatment resulted in time-dependent increase in proportions of apoptotic and necrotic cells (figure 11). In particular, nelfinavir rapidly induced necrosis followed by apoptotic process in both cell lines. A comparison between these cell lines death profile pointed out different cell death timetables. Indeed 12 hours of nelfinavir treatment increased to 20% the cell-death percentage achieving about 50% of necrotic and apoptotic cells after 48 hours of treatment in MCF-7 cells. In MDA-MB231 cells, no change in the cell-death pathways accured before 48 hours of nelfinavir treatment, and more than 72 hours of drug treatment were required to determine a massive increase of propidium iodide-positive and annexin V-positive cells.

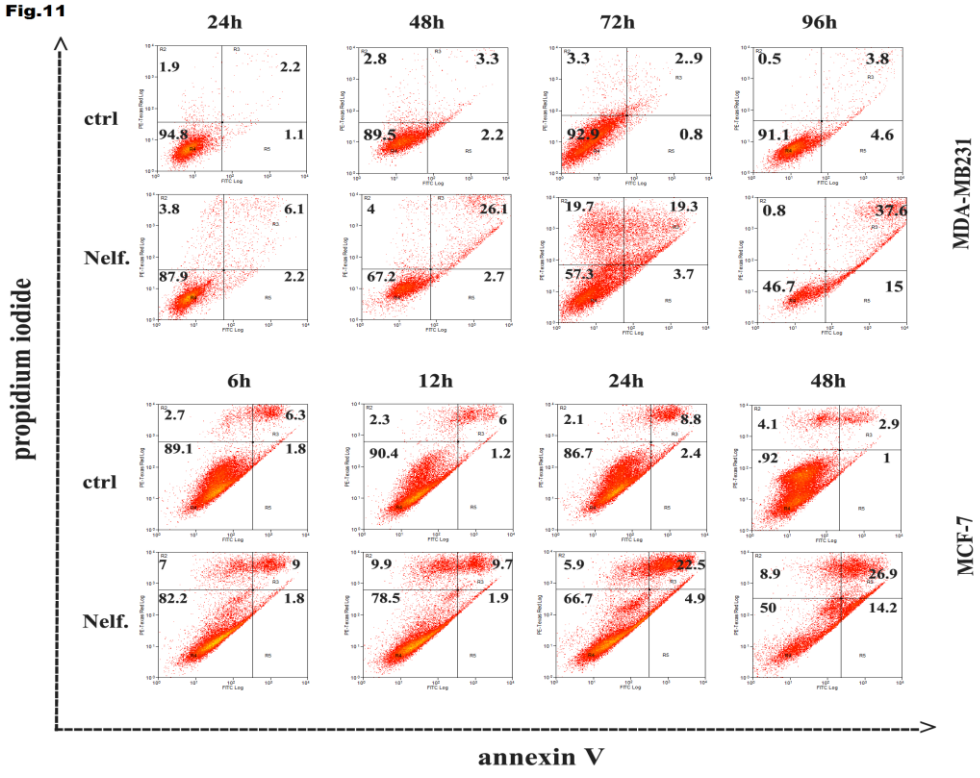

Figure 11. Nelfinavir induces necrosis and apoptosis in breast cancer cell lines
MDA-MB231 and MCF-7 cells were treated with 10µM nelfinavir for indicated time points and cells were subsequently stained with FITC-conjugated annexin V and propidium iodide and analyzed by flow cytometry.

To confirm the induction of cell death by nelfinavir, I tested the effects of this drug on the proteins involved in cell death pathway by western blot analysis. As shown in figure 12, nelfinavir-treated cells increased the expression levels of pro-apoptotic mitochondrial factor Bak, induced a citochrome c release from mitochondria, and subsequently the activation of caspase 9 in time-dependent manner. Therefore, parallel to the cytotoxic effect revealed by MTT and FACS analysis, treatment of MDA-MB231 and MCF-7 cells with nelfinavir, for 72 and 24 hours respectively, increased the levels of apoptotic markers. So, the short-term nelfinavir-treatment induced directly cell-death in MCF-7cells and did not have a prominent cytotoxic effect in MDA-MB231, which resulted blocked in G0/G1 phase. However, prolonged cell-cycle block induced necrosis and activation of the apoptotic process. These data suggest a greater resistance of MDA-MB231 cells to nelfinavir-induced cytotoxicity.

Fig.12

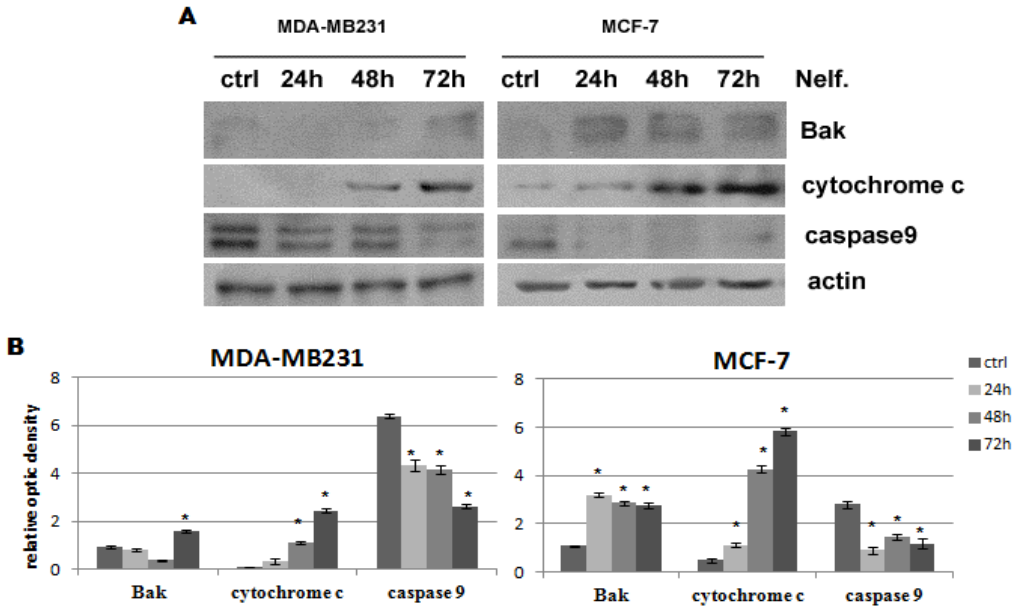

Figure 12. Time-course of apoptosis regulators affected by nelfinavir
A) Western blot analysis was performed in MDA-MB231 and MCF-7 treated with 10μM nelfinavir at indicated time points and bak, cytochrome c and pro-caspase 9 proteins were revealed using specific antibodies. β-actin immunoblotting was used as loading control. B) Densitometric analysis of proteins signals relative to actin signal. The present data represent the means ± S.D. of three indipendent experiments and compared to control value (* p-value< 0.05)

4.3 Breast cancer cells treated with nelfinavir downregulate akt pathway

Akt signaling pathway has been implicated in the regulation of cell cycle progression and cell proliferation. Activation of akt is also associated with protection of cells from apoptosis (Datta et al. 1997; Burgering and Medema 2003; LoPiccolo et al. 2008). To analyze whether inhibition of akt is related to nelfinavir-induced cell cycle arrest and/or apoptosis, I evaluated akt expression and phosphorylation by western blot. MDA-MB231 and MCF-7 cells were treated with nelfinavir for different times, depending from cell-death profile: 3, 6, 24, 48, 72 hours for MDA-MB231 cells and 30 minutes, 3, 6 and 24 hours for MCF-7 cells. As shown in figure 13, the treatment with nelfinavir for 6 hours determined a significant reduction of akt phosphorylation in both cell lines. An interesting data is that also total akt protein was downregulated following 24 hours of drug treatment: this suggests that enhanced akt de-phosphorylation at this time point could be explained by reduction in total akt protein levels.

To determine whether the downregulation of akt affects downstream targets and is specific for tumor cell lines, I analyzed the expression levels of the most representative proteins involved in akt signaling in breast cancer cells and normal breast epithelial cells. Western blot analysis revealed a reduction of all akt analyzed targets such as phospho-PRAS, MDM2 and Bcl2, in MDA-MB231 and MCF-7 cells, while no effects were observed in normal cells (figure 13C).

Fig.13

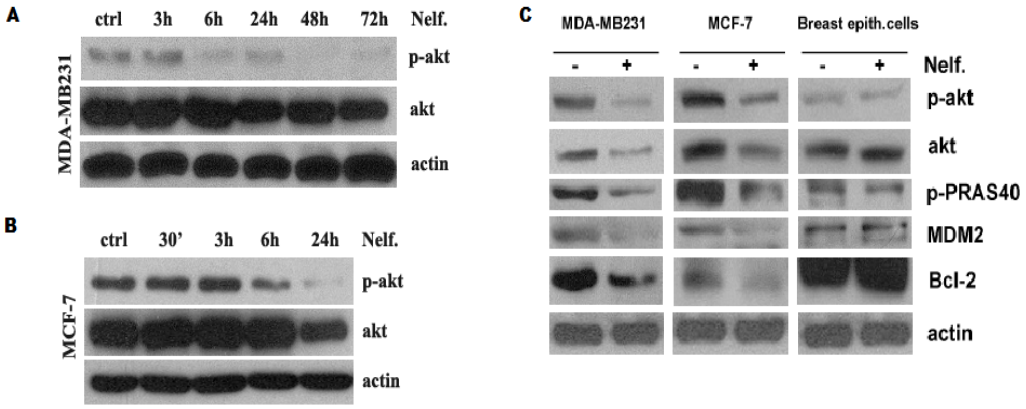

Figure 13. Nelfinavir inhibits akt signaling in cancer but not in normal breast cells
Protein lysates from MDA-MB231 cells (A) or MCF-7 cells (B), subjected to 10μM nelfinavir treatment for the indicated time points, were immunoblotted for phosphorylated and total akt. C) MDA-MB231, MCF-7 and normal breast epithelial cells were treated with 10μM nelfinavir and lysed after 24 hours. Protein lysates were subjected to western blot analysis of akt and its effectors phospho-PRAS, MDM2 and Bcl-2, using specific antibodies. β-actin immunoblotting was used as loading control.

4.4 Nelfinavir induces akt downregulation by disruption of akt-HSP90 complex

In order to understand whether akt decrease occurred at transcriptional level, I analyzed the expression of akt mRNA in MDA-MB231 cells by a reverse transcription-PCR experiment. As shown in figure 14A, the treatment with nelfinavir for 24 hours did not inhibit the expression of all three akt isoforms (Akt1, 2, 3) mRNA. To investigate whether nelfinavir-mediated akt regulation was at post-transcriptional level, I analyzed akt stability, treating MDA-MB231 cells with cycloheximide to block new protein synthesis.

Figure 14B showed that nelfinavir modified akt turnover reducing of 20% akt expression levels in presence of cycloheximide compared to values derived from single cycloheximide treatment. The result suggested that nelfinavir does not affect de novo protein synthesis.

Because akt stability is mainly dependent from its association with chaperone HSP90, I evaluated the association between akt and HSP90 by co-immunoprecipitation assay. As shown in figure 14C, nelfinavir reduced akt/HSP90 association after 6 hours of treatment without affecting akt and HSP90 expression levels. Nelfinavir-mediated disruption of HSP90/akt complex could explain the significant and fast de-phosphorylation of akt and downregulation of total akt. To determine whether nelfinavir induces akt degradation and whether proteasome mediates this process, cells were treated with MG132, a proteasome inhibitor, and akt was detected by western blot analysis (figure 14D). Proteasome inhibitor impaired nelfinavir effects restoring akt protein levels, thus suggesting that nelfinavir induced akt degradation via proteasome

Fig.14

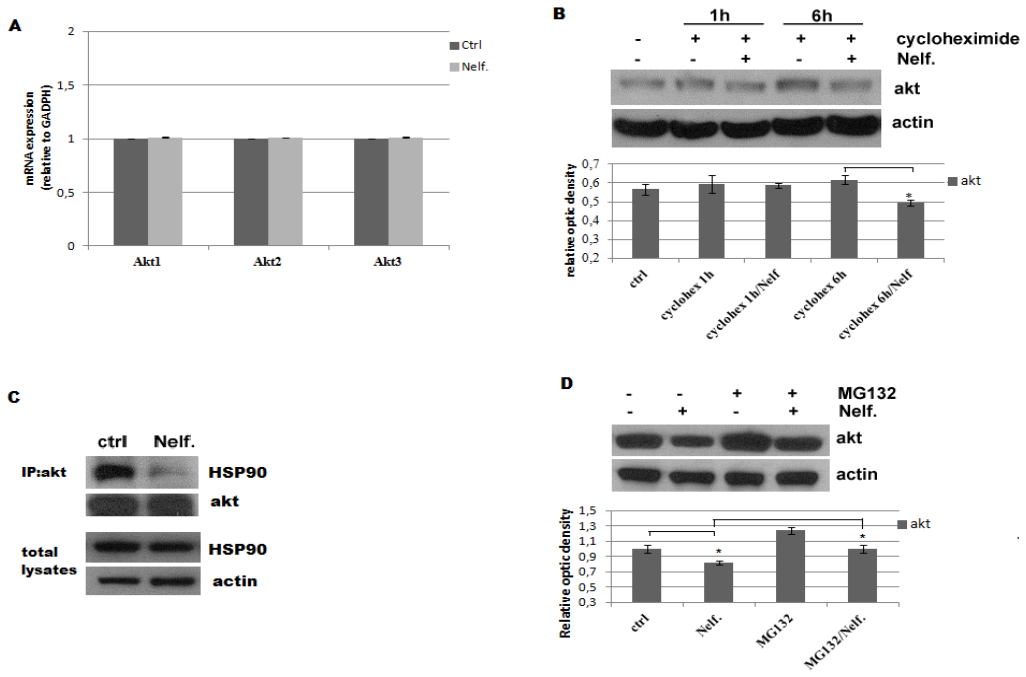

Figure 14. Nelfinavir causes a dissociation of akt/HSP90 complex and akt degradation via proteasome A) MDA-MB231 cells were treated with 10μM nelfinavir for 24 hours and mRNA expression levels of three akt isoforms were analyzed by RT-PCR as indicated in Material and Methods. The values represent mean ± SD of three indipendent experiments normalized to untreated cell values. B) MDA-MB231 cells were treated with 10μM nelfinavir for 24 h and incubated with 0,5μg/mL cycloheximide for the last 1 hour or 6 hours of treatment. Protein lysates were subjected to western blot analysis for akt and β-actin. C) Cells were treated with nelfinavir for 6 h, then lysed, immunoprecipitated (IP) using akt antibody and immunoblotted for HSP90 or akt. D) Lysates from MDA-MB231 cells co-treated with nelfinavir for 24 hours and proteasomal inhibitor MG132 (10μM) for the last 8 hours of drug treatment were subjected to western blot for akt and β-actin. Akt signal following the indicated treatments were quantified by densitometry and normalized on β-actin values. The values are representative of three indipendent experiments. Error bars represent S.D. and *p-value < 0.05.

4.5 Sinergistic effect of nelfinavir with PI3K or HSP90 inhibitors

To confirm the involment of akt pathway and HSP90 activity in nelfinavir-mediated anti-cancer effects, I determined whether canonical inhibitors of akt pathway or HSP90 activity were able to reduce tumor cell-growth. Cells were treated with 17-AAG, inhibitor of HSP90 chaperone activity and LY 294002, PI3k inhibitor. First I analyzed the expression levels of phosphorylated and total akt in MDA-MB231 cells treated with different concentrations of these inhibitors. As shown in figure 15, both 17-AAG and LY294002 determined a reduction of akt phosphorylation. In addition, 1µM 17-AAG caused a downregulation of total akt, thus confirming the important role of HSP90 in akt stability. To determine whether these compounds as well as nelfinavir affect cell growth, I performed cell counts at 24, 48 and 72 hours of treatments. Both 17-AAG and LY294002 determined a reduction of cell number in a time dependent manner, even if nelfinavir showed more efficacy than the other two compounds (figure 15C).

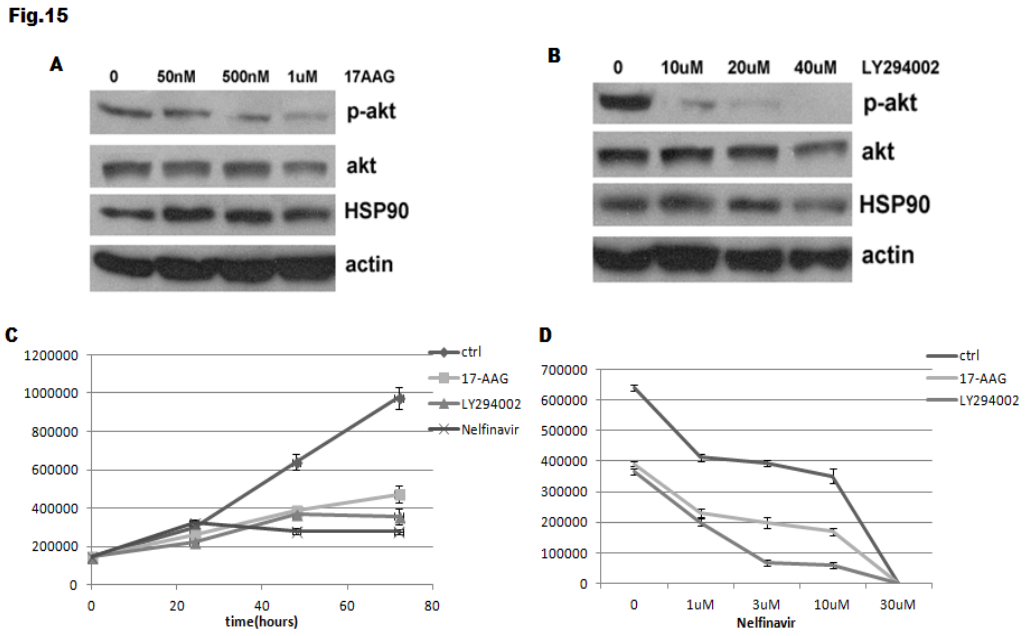

Figure 15. 17-AAG and LY294002 enhance nelfinavir anti-proliferative efficacy
Dose-response curve of 17-AAG (A) at 12 hours and of LY204002 (B) at 24 hours in MDA-MB231. Total cell lysate was used to perform western blot analysis of phopho-akt, akt, HSP90 and β-actin by specific antibodies. β-actin immunoblotting was used as a loading control. C) MDA-MB231 cells were treated with 500nM 17-AAG, 10µM LY294002 or 10µM nelfinavir for the indicated time points to assess cell-growth curve. D) MDA-MB231 cells were incubated with 500nM 17-AAG or 10µM LY294002 in presence of different nelfinavir concentration and cell number analyzed at 48 hours of treatments. Values represent the means ± S.D. of three indipendent experiments.

According to the literature (Gupta et al. 2007), these data suggest that nelfinavir has a broad spectrum of activity, not only restricted to akt downregulation. Moreover, the combination of nelfinavir with 17AAG and LY294002 improved both its anticancer efficacy and antiproliferative activity, as shown in figure 15D. Indeed, these two inhibitors showed a synergistic effect with nelfinavir, reducing tumor cell growth in nelfinavir dose-dependent manner.

4.6 Nelfinavir induces the increase of ROS production and lipid peroxidation in breast cancer but not in normal cell lines

The degradation of akt protein and the presence of high percentage of necrotic cells in nelfinavir-treated cells suggested an involvment of a fast-acting mechanism such as reactive oxygen species. To assess ROS production in these cells, I performed a FACS analysis through the observation of H2DCF-DA oxidation. As shown in figure 16, nelfinavir induced time-dependent production of ROS with different trend in the analyzed cell-lines. The increase of ROS production was fast in MCF-7 cells, starting at 30minutes, and was progressively reduced until 24 hours of nelfinavir-treatment. MDA-MB231 cells treated with this drug exhibited a slight increase of intracellular ROS levels within 3 hours, that gradually enhanced in a time-dependent manner. These different trends of ROS levels reflected also the cell-death schedule observed in these two cell lines. Therefore, the high levels of ROS at 30 minutes in MCF7 cells could explain the earlier cell-death induction in MCF-7 cells compared to MDA-MB231 cells. In both cell lines a massive ROS production rapidly caused necrosis, while a slight increase of ROS levels occurring in the second part of the time course was able to regulate apoptotic pathways as described in other studies (Chandra et al. 2000; Achanta and Huang 2004; Conklin 2004). On the contrary, in normal primary breast cell, only long term nelfinavir treatment induced a not statistically significant increase of ROS production.

Fig.16

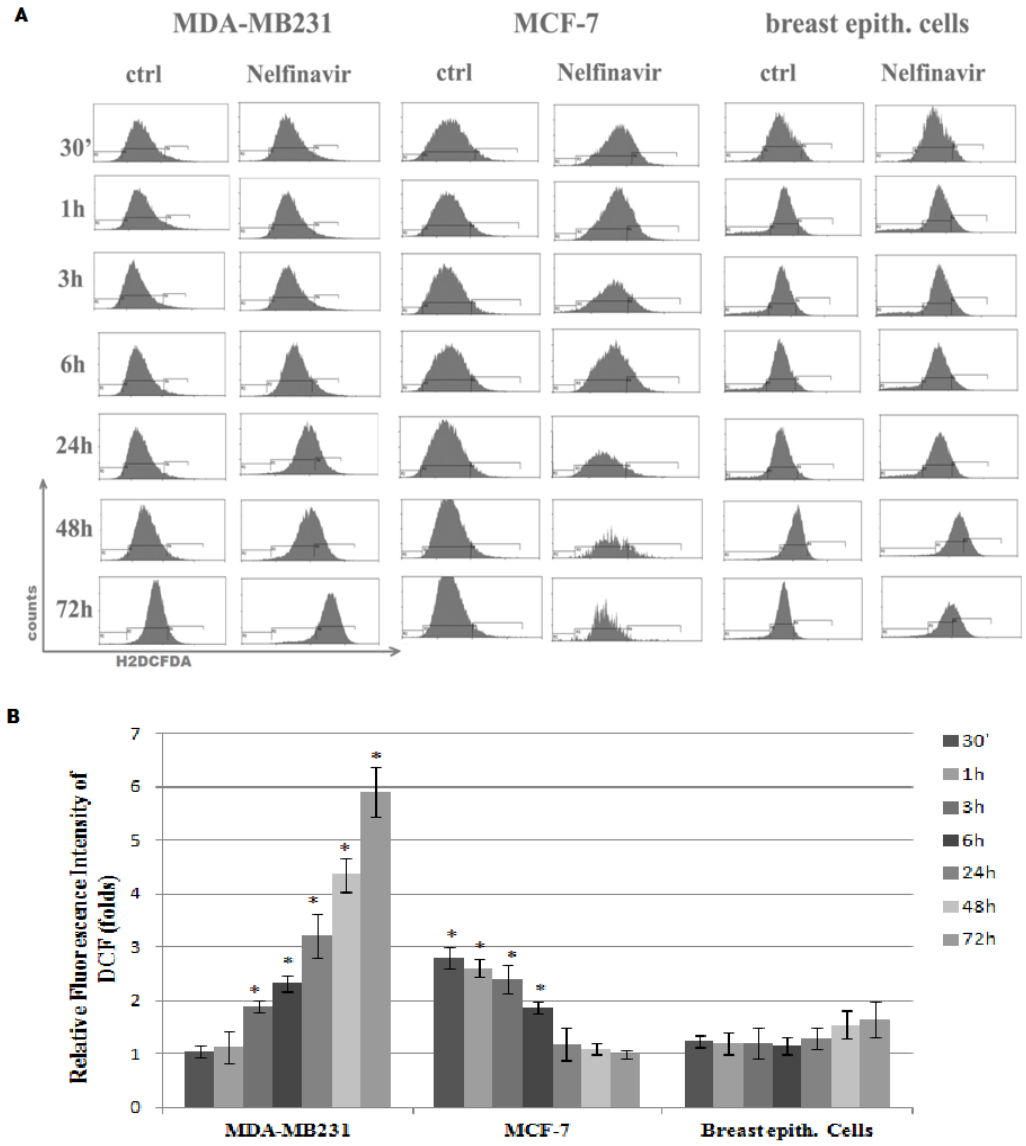

Figure 16. Nelfinavir induces ROS accumulation in a time-dependent manner in breast cancer cells MDA-MB231, MCF-7 and primary breast epithelial cells were subjected to 10μM nelfinavir treatment for 30 minutes-72 hours (h). ROS production was measured by H2DCF-DA staining and fluorescence intensity was shown as representative FACS-based method (A) or expressed as MFI normalized to untreated cell values (B). Each value is the mean ±S.D. of three different experiments. *p< 0.05 compared to control cells.

Since ROS cause macromolecular damage with rapid attack to the polyunsatured fatty acids of the membrane, I investigated whether nelfinavir induced lipid peroxidation. To this aim, I treated MCF-7 and MDA-MB231 cells with 10μM nelfinavir for 30 minutes, 3, 24 and 72 hours and quantified the malondialdehyde (MDA) concentration, a lipid peroxidation marker, by colorimetric assay. As depicted in figure 17, while in MDA-MB231cells nelfinavir induced a progressive increase of lipid peroxidation starting from 3 hours up to 72 hours, in MCF-7 cells this effect began at 24 hours of treatment. No significative modification of lipid oxidation status was observed in normal cells, although 30 min nelfinavir incubation caused a slight reduction of lipid peroxidation in all analized cell lines. From this assay appeared an early detoxifying response of cells to redox state perturbation induced by the drug, that was suppressed after 3 hours in tumoral cells. These data indicated a protective response of normal cells to nelfinavir-induced oxidative stress, whereas breast cancer cell lines did not shown a full detoxifing capability.

Fig.17

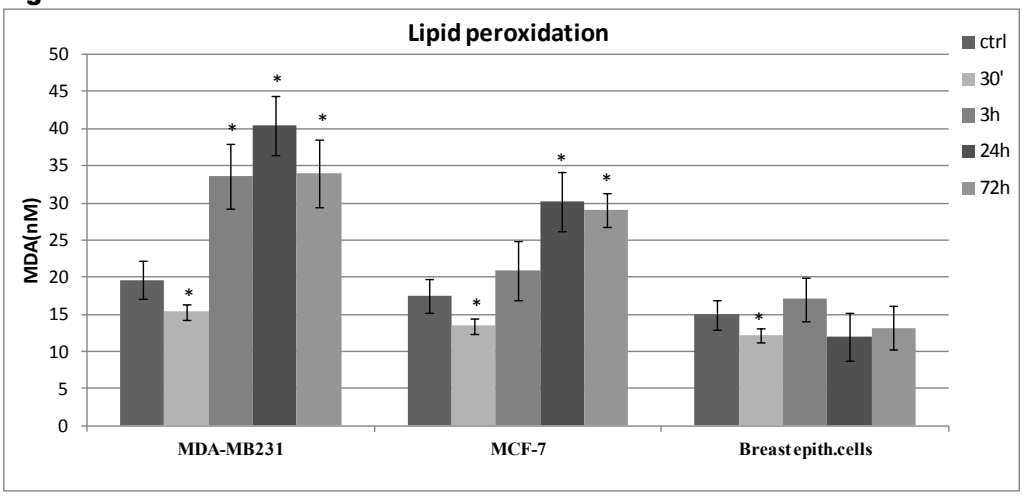

Figure 17. Nelfinavir treatment causes an increased lipid peroxidation in tumor cells Breast cancer cells and normal mammary cells were treated with 10μM nelfinavir for the indicated time points, and processed as indicated in material and methods. Colorimetric analysis revealed the concentration of MDA (nM), a lipid peroxidation marker. The present data derived from three different experiments. *(p-value< 0.05) indicates statistical significance relative to control (ctrl).

4.7 Nelfinavir perturbs cell redox state by affecting ROS-scavengers enzymes

To better investigate redox alterations induced by nelfinavir in breast cancer cells and identify the source of ROS production, I analyzed the activity of the main ROS detoxifying-enzymes: superoxide dismutase (SOD) and glutathione reductase (GR). In MDA-MB231 and MCF-7 cells, nelfinavir increased SOD activity in a time dependent manner (figure 18A). Since SOD acts both as antioxidant enzyme for removing superoxide anion and as ROS inducer for production of hydrogen peroxide, the increase of SOD activity could be a pro- and anti-oxidant condition. For this reason, the enhanced SOD activity after the treatment with nelfinavir could represent a source of ROS production as well as the effect of oxidative stress response. To better investigate the role of SOD, I analyzed SOD1 and SOD2 protein expression levels following nelfinavir treatment in breast cancer cell lines and normal breast epithelial cells. Western blot analysis revealed a time and cell-type dependent regulation of SOD 1 and SOD2 expression levels (figure 18B).

Fig.18

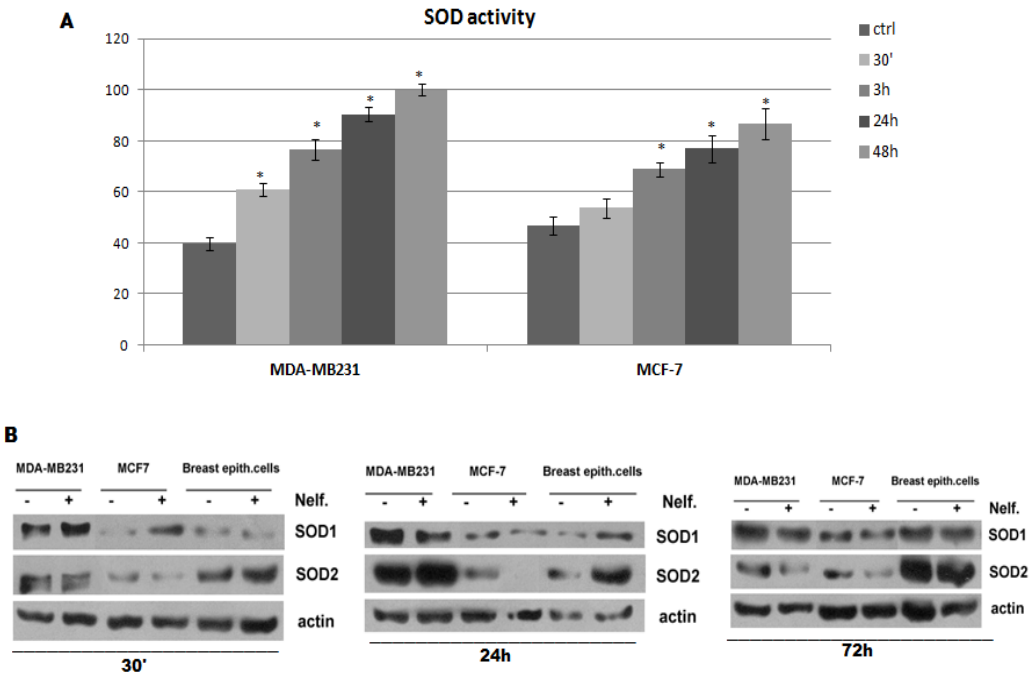

Figure 18. Nelfinavir regulates SOD activity and expression in a time-dependent manner A) Breast cancer cells were treated with 10μM nelfinavir at indicated times and SOD activity (inhibition rate %) analyzed as indicated in Material and Methods. Values are representative of three independent experiments (means ± S.D., *p-value< 0.05). B) Protein lysates derived from MDA-MB231, MCF-7, or breast epithelial cells, treated with 10μM nelfinavir for the indicated time points, were immunoblotted with anti- SOD1 and anti-SOD2. β-actin was used as loading control.

In particular, at an early time of 30 minutes of nelfinavir treatment, SOD1 was upregulated in MDA-MB231 and in MCF7 cells, while SOD2 levels increased following 24 hours of treatment. Although also normal cells showed an increase of SOD1 and SOD2 expression at an early time of nelfinavir treatment, long term treatment did not affect the levels of SOD1 and SOD2.

On the another hand, in tumoral cell lines, the initial increase of SOD1 and SOD2 levels was followed by a strong reduction of the expression of both protein expression at 72 hours of treatment. This analysis suggests an involvement of SOD1 at an early step of nelfinavir anti-cancer activity.

To determine whether SOD1 upregulation at this early stage was responsable for the increase of ROS production or rather it represented a ROS-induced effect in breast cancer cells, I treated these cells with tocopherol, and analyzed SOD expression by western blot. As shown in figure 19, both the upregulation of SOD1 after 30 minutes of drug treatment and its reduction at 24 hours, were dependent by ROS production, since the antioxidant tocopherol restored basal SOD1 expression levels. These data suggested that SOD1 and SOD2 do not act as ROS-producers but rather their activity and expression levels are regulated by reactive species following the treatment with nelfinavir.

Fig.19

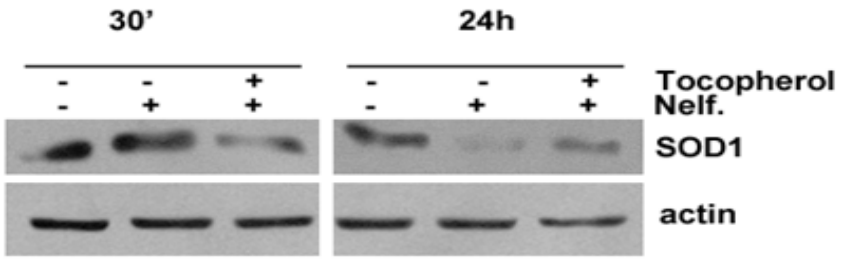

Figure 19. Nelfinavir-enhanced ROS levels modulate SOD1 expression
MCF-7 cells, treated with 10μM nelfinavir ± 35μM tocopherol for 30 minutes or 24 hours, were lysed and subjected to western blot analysis for SOD1. β-actin was used as loading control.

To investigate whether other detoxifying enzymes were activated by nelfinavir-mediated oxidative stress, I measured the activity of GR at different times of nelfinavir treatment. As shown in figure 20, GR activity enhanced after 3 hours of drug incubation and was strongly reduced after 24 hours of treatment in MCF-7 or 48 hours in MDA-MB231. The rapid activation and the subsequent downregulation of GR activity reflected ROS production trend and SOD1 and SOD2 expression level changes.

Fig.20

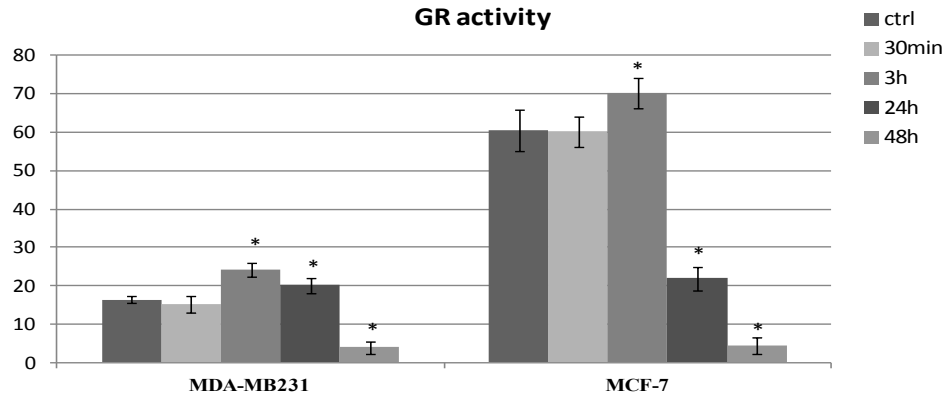

Figure 20. Nelfinavir regulates GR activity
Cells were treated with 10μM nelfinavir at indicated time points, then lysed and processed as indicated in Materials and Methods. GR activity is expressed in mU/ml, values are means± S.D. of three independent experiments.*p-value< 0.05.

4.8 The disruption of akt-hsp90 complex in nelfinavir-treated cancer cells is ROS mediated

In physiological conditions, ROS are very important regulators of many intracellular pathways such as cell proliferation and metabolism, but at higher concentration they can determine the opposite effects by blocking survival pathways and inducing apoptosis and necrosis. To investigate whether ROS were responsable for akt downregulation and akt/HSP90 complex dissociation, breast cancer cells were treated with nelfinavir in presence of antioxidant tocopherol, and HSP90/akt complex were co-immunoprecititated to perform western blot analysis. As shown in figure 21, in breast cancer cell lines, the presence of tocopherol impaired nelfinavir-induced disruption of akt/HSP90 complex. This result puts ROS production as an earlier event than akt downregulation. According to literature, this result suggests an important correlation between high intracellular ROS levels and akt/HSP90 downregulation (Beck et al. 2012; Sarkar et al. 2013). Because ROS promote disruption of akt/HSP90 complex in tumoral cells treated with nelfinavir, I also evaluated the protein expression levels of other two HSP90 clients such as cyclinD and ERα. Figure 21B shows that these proteins were reduced by nelfinavir treatment while the addition of tocopherol restored their expression levels at those of untreated cells.

Fig.21

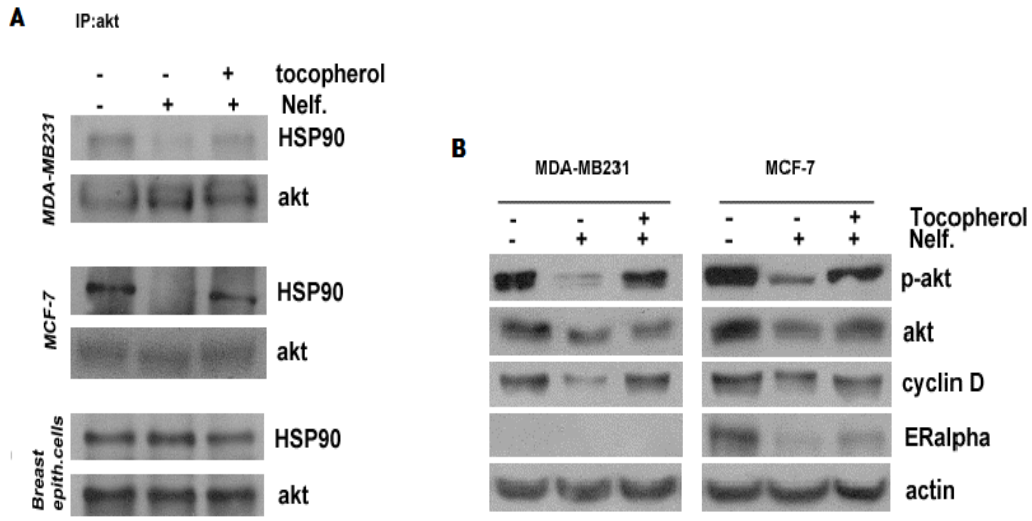

Figure 21. T**he nelfinavir-induced akt/HSP90 complex disruption is ROS-mediated**
A) MDA-MB231, MCF7 and breast epithelial cells were treated with 10μM nelfinavir and 35μM tocopherol for 6 hours, and equal amounts of protein lysate were immunoprecipitated (IP) using akt antibody followed by immunoblotting with anti-HSP90 and anti-akt. B) MDA-MB231 and MCF-7 cells were treated with 10μM nelfinavir and 35μM tocopherol for 24 hours and phospho-akt, akt, cyclin D, ERα, β-actin levels were monitored using the respective antibody by western blot on total lysate. β-actin immunoblotting was used as a loading control.

4.9 The free radical scavenger tocopherol completely suppresses cell death induced by nelfinavir

To confirm the primary role of ROS in the mechanism of action of nelfinavir, I assessed the capability of tocopherol to prevent nelfinavir-induced cell death. MCF-7 and MDA-MB231 cells were treated with nelfinavir for 24 and 48 hours respectively, and necrosis and apoptosis were evaluated by annexin V/PI assay. The presence of tocopherol in tumor cells treated with nelfinavir impaired ROS overproduction and subsequent apoptotic and necrotic processes (figure 22).

Fig.22

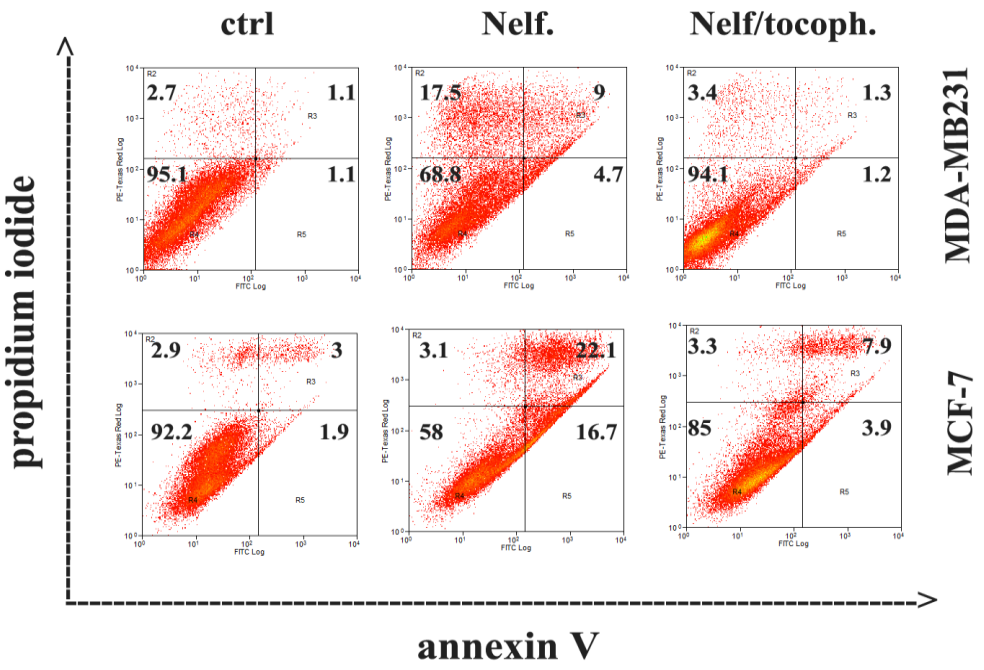

Figure 22. Nelfinavir induces tumor cell-death by increased ROS production
MDA-MB231 and MCF-7 cells were treated with nelfinavir (for 72 and 24 hours respectively) in the absence or presence of 35µM tocopherol**.** Cell-death profile was examined by cytofluorimetric analysis of annexin V/ propidium iodide (PI) positivity. The cell percentage are reported in corresponding areas of dot-plot. Three different experiments confirmed this cell distribution.

4.10 Identification of new series of nelfinavir-derivatives

The study of the mechanisms at the basis of anti-cancer activity of nelfinavir and the identification of the main targets of the drug have accounted for and directed a chemical study of nelfinavir structure. The structure of nelfinavir can be fragmented into five moieties: the 2-methyl-3-hydroxy-benzamide portion A, the S-phenyl group B, the tert-butyl carboxamide moiety C, the lipophilic dodecahydroisoquinoline ring D and the central hydroxyl group E (figure 23). The benzamide ring A in the predicted conformations superimposes well onto the aromatic groups of the co-crystallized inhibitors and plays a critical role in molecular recognition (Aronov et al. 2008).

Fig.23

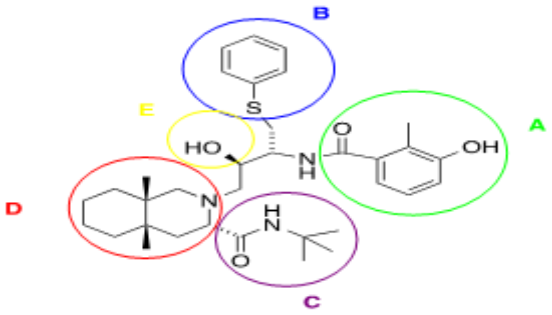

Figure 23. **Structure of Nelfinavir**

In this work we synthesized several peptidomimetics derived from nelfinavir. Peptidomimetics are caracterized by improved chemical accessibility and allow to obtain molecular diversity. The synthesized molecules mainteined crucial residues for the activity: A, B, C, D (figure 23) but the dodecahydroisoquinoline ring D was replaced with a 1,2,3,4-tetrahydroisoquinoline ring to reduce the flexibility and remain the two aromatic rings A and B, introducing as A a phenilalanine (ND1) and a tyrosine (ND2) in order to mantain the hydroxilic group on the aromatic ring (figure 24A). Viability assay revealed that ND1 e ND2 preserved anti-tumoral potential of nelfinavir at 10μM in MCF-7 cells (figure 24B). However, these two compounds showed less efficacy in MDA-MB231 cells and more cytotoxic activity versus normal breast cell than nelfinavir. This result suggested that the new chemical modifications were not useful to improve anti-tumoral efficacy, although they highlighted the tridimensional pharmacophoric structure of nelfinavir.

Fig.24

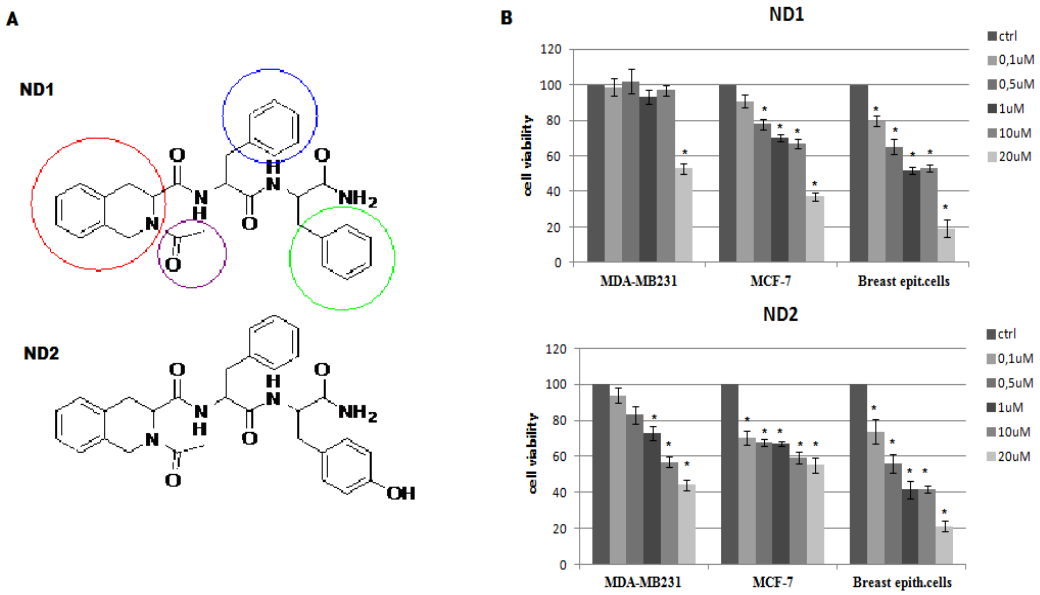

Figure 24. ND1 e ND2 preserve nelfinavir cytotoxic activity in breast cancer cells
A) Structure of ND1 and ND2. B) Cell viability analysis in MDA-MB231, MCF-7 and normal breast epithelial cells treated with different concentrations of ND1 or ND2 for 24 hours. Each value represents the mean ± S.D. of three different experiments.*p-value< 0.05.

We also used this template to construct new heterocyclic systems designed as potential modulators of cell proliferation. We synthesized focused libraries of compounds based on the spiro (oxindole-3,3-thiazolidine) nucleus (series 100) and the corresponding spiro[imidazo[1,5-c]-thiazole-3,3-indoline]-2',5,7(6H,7aH)-trione derivatives (series 200) (figure 25).

Fig.25

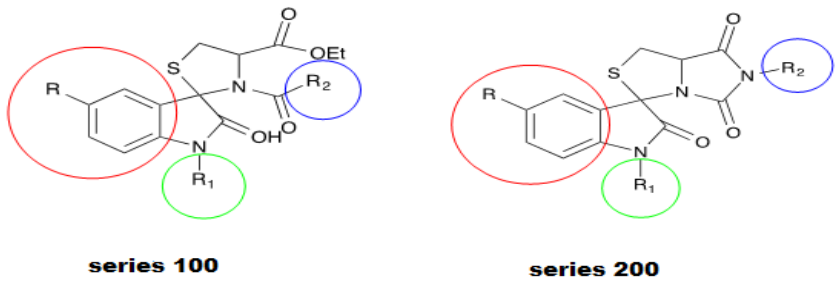

Figure 25. Structure of series 100 and series 200
In both series R = H, CH_3, Br; R' = benzyl derivatives or alkyl; R" = H or acyl derivatives.

I focused my attention on series 200 compounds, and tested their cytototoxic activity in MCF-7 as primary screening. The most part of these new compounds showed a lower IC_{50} than nelfinavir (table 3), suggesting that the novel chemical modification improved citotoxic efficacy of nelfinavir in breast cancer cells. Among these nelfinavir-derivatives, 4n proved to be the most potent compound with an IC_{50} of 50nM resulting as a new candidate for further biological studies.

Table 3

Series 200				IC_{50} (μM±SD)[a]
C	R	R_1	R_2	MCF-7[b]
4a	H	H	$CH_2C_6H_4$(4-Cl)	>5
4b	CH_3	H	$CH_2C_6H_4$(4-Cl)	4.81±1.0
4c	Br	H	$CH_2C_6H_4$(4-Cl)	2.90±0.8
4d	H	H	C_6H_4(4-Cl)	2.15±0.7
4e	CH_3	H	C_6H_4(4-Cl)	2.12±0.7
4f	Br	H	C_6H_4(4-Cl)	0.90±0.2
4g	Br	H	C_6H_4(4-Cl)	3.0 ±0.20
4h	H	CH_3	C_6H_4(4-Cl)	4.52±1.1
4i	CH_3	CH_3	C_6H_4(4-Cl)	1.23±0.4
4j	Br	CH_3	C_6H_4(4-Cl)	0.52±0.3
4k	Br	CH_3	$CH_2C_6H_4$(4-Cl)	0.27±0.1
4l	Br	CH_3	C_6H_5	0.31±0.1
4m	Br	CH_3	C_6H_4(4-CH_3)	0.06±0.05
4n	Br	CH_3	Cyclohexyl	0.04±0.01
4o	CH_3	CH_3	Cyclohexyl	1.20±0.6
4p	H	CH_3	Cyclohexyl	2.30±0.8
4q	Br	H	Cyclohexyl	0.22±0.1
4r	Br	CH_3	Cyclohexyl	2.01±0.9
5a	H	COC_6H_4(4-Cl)	H	1.01±0.6
5b	CH_3	COC_6H_4(4-Cl)	H	3.46±0.9
5c	Br	COC_6H_4(4-Cl)	H	0.15±0.1
5d	Br	Cyclohexyl	H	2.08±0.8
6b	CH_3	COC_6H_4(4-Cl)		2.78±0.9
6c	Br	COC_6H_4(4-Cl)		0.86±0.4
6d	Br	Cyclohexyl		1.63±0.6

Table 3. 4n reduces MCF-7 cells viability in a nanomolar range
Screening of nelfinavir-derivative compounds by cell viability analysis in MCF-7 cells. The numbers reported represent IC50 values (μM) ± S.D. Each value is the mean of three indipendent experiments.

4.11 4n is the most potent nelfinavir-derivative with anti-cancer activity

I further investigated the cytotoxic effect of 4n in MDA-MB231 cells and primary normal breast cells. Figure 26 demonstrated that 4n was also capable to reduce MDA-MB231 cell viability without affecting normal cells viability when it was used at 50nM-1µM concentration range. Subsequently, I evaluated whether 4n compound retained the same biological effects and molecular targets of the lead compound, nelfinavir. To this purpose, I analyzed akt regulation and ROS production in MCF7 cells treated with 4n. As shown in figure 26, 4n as well as nelfinavir reduced akt expression levels after 24, 48 and 72 hours of treatment. The FACS analysis of ROS intracellular levels revealed that, likewise nelfinavir, also 4n is able to induce ROS production.

Fig.26

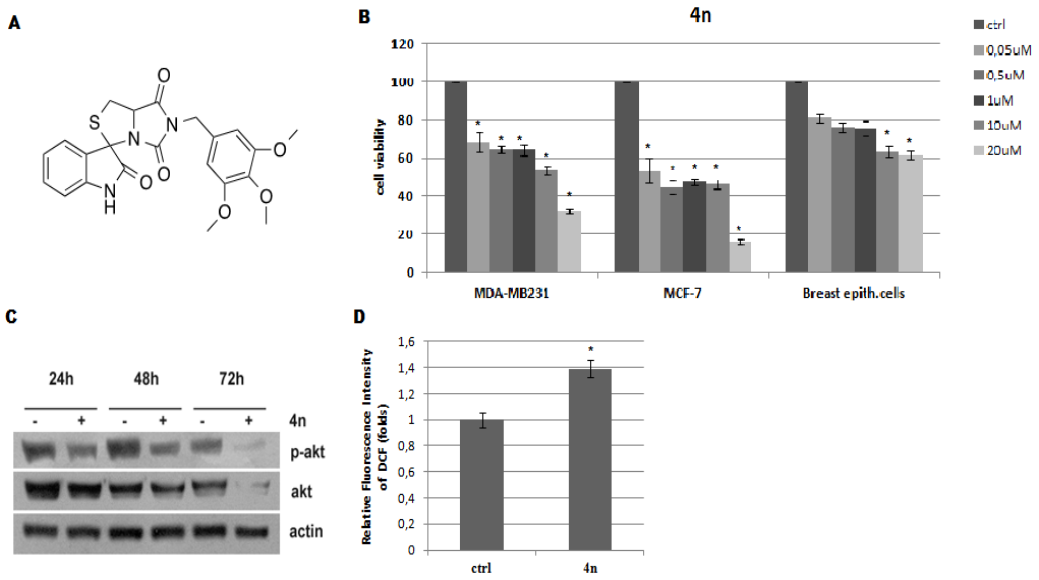

Figure 26. 4n preserves anti-cancer molecular mechanism of nelfinavir
A) Chemical structure of 4n. B) MTT assay performed in MDA-MB231, MCF-7 and primary breast epithelial cells, treated with indicated concentration of 4n for 24 hours. C) Western blot analysis of phospho- and total akt in MCF-7 cells treated with 50nM 4n at indicated time points. β-actin immunoblotting was used as a loading control. D) MCF-7 cells were treated with 50 nM 4n and after 30 minutes, ROS production was assessed in terms of oxidation of H2DCF-DA and compared to control (ctrl) cells. Each value represents the mean ± S.D. of three different experiments.* p-value< 0.05.

5. DISCUSSION

Identification and characterization of new pharmacological activities from existing drugs represents an effective way to accelerate the translation of discoveries from the bench to clinical applications. HIV-PI, rationally designed to block viral protease, have shown an anti-tumoral activity in several cancers, thus encouraging the study of the intracellular pathways at the basis of their anti-cancer activity. Among HIV-PIs, nelfinavir is considered the most potent antitumoral compound, and has entered several clinical trials as either a chemotherapeutic agent or a radiosensitizer for cancer therapy (Chow et al. 2006; Yang et al. 2006b; Gills et al. 2007). Many studies suggested that inhibition of PI3k and akt signalling are responsible for its pro-apoptotic effects on tumor cells, enhancing the efficacy of radiation therapy in different types of cancer (Yang et al. 2006b; Gills et al. 2007; Gupta et al. 2007; Bernstein and Dennis 2008; Plastaras et al. 2008). Despite extensive studies on the anticancer and radiosensitizing activity of nelfinavir, the specific molecular mechanism underlying its antiproliferative activity and its inhibitory effect on PI3K and akt signaling pathway remains unknown. Aim of the present thesis is to study the anticancer activity of nelfinavir in breast cancer model, where few and controversal data prevent its employment in clinical trials. Breast cancer is the most frequent cancer in the female population and, despite recent advances in chemo- and endocrine therapy, significant proportion of breast cancer patients fail to heal for the lack of selectivity in the activity of chemotherapeutics and, and for the acquisition of chemoresistance and endocrine resistance. Moreover, it has been demonstrated that PI3K mutations in addition to alterations of other pro-tumoral molecules play a role in resistance to some of the endocrine therapies. In this context, I investigated whether nelfinavir exerts anti-cancer activity in breast cancer cells, and I evaluated the role of PI3K/akt pathway in drug-mediated anti-proliferative effect. To this aim, I used breast cancer cell lines that were either estrogen-dependent (MCF-7) or estrogen and progesterone receptor negative (MDA-MB231). MCF-7 and MDA-MB-231 cell lines are dependent on Akt for proliferation (Fujita et al. 2002; Acosta et al. 2003), making them also informative for the effects of nelfinavir on Akt signaling, that may regulate breast cancer proliferation and survival. Firstly, I validated the anti-proliferative and cytotoxic activity of nelfinavir in a panel of different tumor types, focusing the attention on breast cancer cell lines. I observed that 10μM nelfinavir was able to reduce tumor cell viability without affecting normal primary breast cell-viability/growth. Extensive pharmacokinetics studies have shown that nelfinavir has an average peak plasma level of 8-10μM, that represents the IC_{50} used for breast cancer cell lines, and suggesting that it may be effective in breast cancer patients with the current dosage regimen (Bernstein and Dennis 2008). In this work, I demonstrated that nelfinavir induces cell-cycle arrest in G0/G1 phase and subsequently cell death in MDA-MB231, whereas it causes directly the death in

MCF-7 cells. FACS analysis of cell-cycle was further supported by the observation of changes in the expression of cell-cycle regulators. Indeed, nelfinavir reduced the levels of phosphorylated Rb, cyclin A, cyclin B, cyclin D, increased the expression levels of p21 in breast cancer cell lines but not in normal cells. Furthermore, cyclin E resulted downregulated only in MDA-MB231. Although tumor cell lines showed a similar protein expression profile, biological effects of nelfinavir treatment resulted different in MDA-MB231 and MCF-7 cells. Indeed, whereas in the former I observed a Go/G1 block, MCF-7 cell-cycle was not affected by nelfinavir. Probably, the different basal levels of expression of cyclins and the significant reduction of cyclin E limited to MDA-MB231 cells, could play a role in the different response of cell lines to nelfinavir in cell-cycle progression. It is also possible that other mediators that I did not investigated mediators are involved in this different cellular response. The study of apoptotic and necrotic populations, differentiated by annexin V/PI staining, and the evaluation of apoptotic markers such as Bak, cytocrome C and caspase 9, revealed a fast induction of necrosis followed by an apoptotic process both in MDA-MB231 and in MCF-7 cells. These results suggest a direct cytotoxic action of nelfinavir on tumor cell. A comparison between the death profile of these cell lines pointed out different cell death timetables. Indeed, 12 hours of nelfinavir treatment increased to 20% the necrotic cells percentage, achieving about 50% of necrotic and apoptotic cells following 48 hours of treatment in MCF-7 cells while more than 72 hours of drug treatment were required to determine a massive increase of cell-death in MDA-MB231 cells. Therefore, nelfinavir-treated cells increased the expression levels of pro-apoptotic mitochondrial factor Bak, induced a citochrome c release from mitochondria, and subsequently the activation of caspase 9 in a time-dependent manner. So, the short-term nelfinavir-treatment induced cell-death directly in MCF-7cells, and did not have a prominent cytotoxic effect in MDA-MB231, which resulted blocked in G0/G1 phase. However, prolonged cell-cycle block induced necrosis and activation of the apoptotic process. These data suggest a greater resistance of MDA-MB231 cells to nelfinavir-induced cytotoxicity compared to MCF-7 cells.

It was well established that inhibition of akt phosphorylation is an important mechanism by which nelfinavir exerts anti-tumour activity in several cancer types (Gupta et al. 2005; Yang et al. 2006b; Cuneo et al. 2007), although its involvment in breast cancer has not been elucidated. My results demonstrated that nelfinavir is effectively able to downregulate akt signaling in breast cancer cell models, as suggested by reduction of phosphorylated-akt and akt-targets such as cyclin D, PRAS40, MDM2, and Bcl-2 in tumor cells but not in normal cells. Surprisingly, also total akt was reduced by the drug, leading us to analyze akt mRNA expression levels and akt protein stability. Our data suggested that nelfinavir-mediated akt regulation does not accurr at transcriptional level, but rather nelfinavir enhances akt protein turnover by affecting akt stability. Because akt stability is mainly dependent from its

association with chaperone HSP90, I evaluated the association between akt and HSP90 by co-immunoprecipitation assay. The result demonstrated that nelfinavir reduces akt/HSP90 association after 6 hours of treatment without affecting akt and HSP90 expression levels. The nelfinavir-mediated disruption of HSP90/akt complex could explain the significant and fast de-phosphorylation of akt and subsequent downregulation of total akt. Indeed, akt when dissociated from its chaperon became more sensitive to PP2A-mediated dephosphorylation and to ubiquitination and degradation by proteasome (Sato et al. 2000). To determine whether nelfinavir induced akt degradation and whether proteasome mediated this process, breast cancer cells were treated with MG132, a proteasome inhibitor, and akt was detected by western blot analysis. Proteasome inhibitor impaired nelfinavir effects restoring akt protein levels, thus suggesting that nelfinavir induced akt degradation via proteasome. Although in different breast cancer cell lines, the effect of nelfinavir on akt/HSP90 complex dissociation has been recently observed (Shim et al. 2012). To confirm the involvement of akt pathway and HSP90 activity in nelfinavir-mediated anti-cancer effects, I determined whether canonical inhibitors of akt pathway or HSP90 activity were able to reduce breast cancer cell-growth. Both 17-AAG and LY294002 reduced cell-growth and determined a downregulation of akt, thus confirming the important role of HSP90 in akt stability and in breast cancer cell viability. However, nelfinavir showed more efficacy than the other two inhibitors, suggesting, in agreement with existing literature (Gills et al. 2007; Gupta et al. 2007), that nelfinavir has a broad spectrum of activity not only restricted to akt downregulation. Moreover, the combination of nelfinavir with 17-AAG and LY294002 improved both its anticancer efficacy and antiproliferative activity. Indeed, these two inhibitors showed a synergistic effect with nelfinavir, reducing tumor cell growth in a nelfinavir-dose-dependent manner.

Contrary to the hypothesis of HSP90 as primary nelfinavir target (Shim et al. 2012), I demonstrated that akt/HSP90 disruption is dependent upon nelfinavir-induced oxidative stress. A number of evidences led me to hypothesyze that ROS could play a primary role in anti-cancer activity of nelfinavir: the presence of high necrotic cell percentage following nelfinavir short-term treatment in breast cancer cells; the observation that dissociation of HSP90/client complex could be due to oxidation and loss of function of the chaperon protein (Beck et al. 2012; Sarkar et al. 2013); clinical studies on nelfinavir as anti-viral drug that revealed an involvement of ROS in the side-effects development (Moskowitz and Kukin 1999; Irani 2000; Bloch-Damti and Bashan 2005; Rudich et al. 2005; Gotoh and Mori 2006). For these reasons, I evaluated ROS production in breast cancer cells and in normal breast cells. The analysis revealed a significant increase of ROS intracellular levels limited to tumor cells. The increase of ROS production was fast in MCF-7 cells and was progressively reduced until 24 hours of nelfinavir-treatment. MDA-MB231 cells treated with this drug exhibited a slight increase of intracellular ROS

levels within 3 hours, that gradually enhanced in a time-dependent manner. The different trends of ROS levels reflected also the cell-death schedules observed in these two cell lines. Therefore, the high levels of ROS at 30 minutes in MCF7 cells could explain the earlier cell-death induction compared to MDA-MB231 cells. In both cell lines, a massive ROS production caused necrosis, while a slight increase of ROS levels occurring in the second part of the time course was able to regulate apoptotic pathways, as described in previous studies (Chandra et al. 2000; Achanta and Huang 2004; Conklin 2004). The observation of ROS-generating capability of nelfinavir is further supported by the observation of drug-mediated increase of lipid peroxidation. Comparing tumor and normal breast cells it resulted evident that, although both cell types showed an early protective response to oxidative stress, only normal cells restored basal redox status, whereas cancer cells did not retain full detoxifying capability. It has been well established that breast cancer cells present higher ROS levels than normal cells in basal conditions (Toyokuni et al. 1995; Portakal et al. 2000; Brown and Bicknell 2001), in order to promote genome instability and alterations in cell signaling processes related to survival, proliferation, resistance to apoptosis, angiogenesis and metastasis (McEligot et al. 2005; Sablina et al. 2005; Reliene and Schiestl 2006; Lu et al. 2007). Since tumor and normal cells show different redox balance, one interesting therapeutic strategy might be the induction of cytotoxic oxidative stress (De Miguel and Cordero 2012). I demonstrated that anti-cancer effects of nelfinavir are due to the capability of redox status regulation, thus explaining its greater efficacy in tumor cells compared to normal cells. The different behaviour between cancer and normal cells could be related to loss of activity or impairment of antioxidants (Oberley and Buettner 1979; Oberley et al. 2004; Ridnour et al. 2004; Sinha et al. 2009), or to an upregulation of ROS-producer enzymes (Sundaresan et al. 1996; Brown et al. 2000; Meitzler et al. 2013). To further investigate the molecular source of nelfinavir-induced ROS, I determined whether nelfinavir enhances ROS levels by downregulation of antioxidant signaling. Among the different intracellular detoxifying-enzymes that are differently modulated in breast cancer cells compared to normal cells, SOD represents the main redox status regulator (Oberley and Buettner 1979; Sinha et al. 2009; Radenkovic et al. 2013). Surprisingly, my results demonstrated that nelfinavir increased SOD activity in a time-dependent manner in breast cancer cell lines. However, the increase of SOD activity has been reported not only as antioxidant but also as pro-oxidant condition. Indeed, since SOD acts both as antioxidant enzyme for removing superoxide anion and as ROS inducer for production of hydrogen peroxide, the enhanced SOD activity after the treatment with nelfinavir could represent a source of ROS production as well as the effect of oxidative stress. My results suggested that nelfinavir regulates not only the activity but also the expression levels of SOD1 and SOD2 both in tumor and normal breast cells. In particular, it determines a rapid increase of SOD1 (at 30 min) and SOD2 (at 24 hours) levels, followed by

restoring of basal levels in normal cells or strong reduction of their expression in cancer cells. To determine whether SOD1 upregulation at an early state was responsable for the increase of ROS production, or rather it represented a ROS-induced effect in breast cancer cells, I analyzed SOD expression in cells treated with nelfinavir in the presence of tocopherol. The analysis revealed that both the upregulation of SOD1 after 30minutes of drug treatment and its subsequent reduction, were dependent by ROS production, since antioxidant restored basal SOD1 expression levels. These data suggest that SOD1 is not the primary target of nelfinavir, but is first upregulated, and then downregulated following redox status modification induced by the drug. Another investigated antioxidant, GR, is regulated by nelfinavir, that primarily enhances and subsequently reduces GR activity. The rapid activation and the following downregulation of GR activity reflected ROS production kinetics and the expression of SOD1 and SOD2. While it was well established that detoxifying enzymes can be activated and upregulated by ROS (De Miguel and Cordero 2012), their decrease in oxidative stress condition is not completely understood. However many authors suggest that decrease of SOD (Manoharan et al. 2004; Ezzi et al. 2007) and GR activity could be related to the generation of free radicals that cause direct damage to the enzyme (Veal et al. 2007). It is possible that also nelfinavir-induced oxidative stress determines a reduction of antioxidants levels by oxidation, which further enhances ROS levels. Another explaination might be that the nelfinavir-mediated downregulation of akt signaling causes a reduction of antioxidant enzymes expression by NFkB regulation (Rojo et al. 2004). In physiological conditions, ROS are involved in the regulation of cell proliferation and metabolism, but at higher concentrations they can determine the opposite effects by blocking survival pathways and inducing apoptosis and necrosis. To investigate whether ROS are responsible of AKT downregulation and akt/HSP90 complex dissociation, breast normal and cancer cells were treated with nelfinavir in presence of antioxidant tocopherol. My results demonstrated that in breast cancer cell lines, the presence of tocopherol impaired nelfinavir-induced disruption of akt/HSP90 complex, whereas nelfinavir did not affect akt/HSP90 association in normal cells. These results put ROS production as an earlier event than akt downregulation. According to the literature, these results demonstrate an important correlation between high intracellular ROS levels and akt/HSP90 downregulation (Clark et al. 2009; Beck et al. 2012; Sarkar et al. 2013). To confirm the primary role of ROS in the mechanism of action of nelfinavir, I assessed the capability of tocopherol to prevent nelfinavir-induced cancer cell death. My analysis showed that the presence of antioxidant in cells treated with nelfinavir, impaired apoptosis and necrosis development. Although nelfinavir induced cell death in the two breast cancer cell lines I tested, the data also indicate that the cell lines respond quite differently to nelfinavir, regarding the effect on cell cycle and timetable of ROS production and cell-death. This variation might be due to the different hormone receptor status of the cells, but also to different redox

adaptation and to the different malignancies of the tumours from which these cell lines have been derived.

It is plausible that oxidative stress produced by nelfinavir affects other pathways in addition to akt/HSP90 signaling to cause cell death. Indeed, other HSP90 clients resulted downregulated by the drug such as ER and cyclin D, leading to the hypothesis that many oncogenic kinases HSP90 clients, such as Raf-1, Bcr-Abl and ErbB2 (Zuehlke and Johnson 2010), might be regulated by the drug. This fact could explain the broad spectrum of nelfinavir anti-cancer molecular mechanisms and the large amount of molecular targets reported in the literature.

Therefore, the suggested temporary sequence of nelfinavir activities in breast cancer cells is as follows: pertubation of redox state with increase of ROS production; akt/HSP90 disruption by oxidation; akt degradation via proteasome; cell cycle block and/or cell death. These nelfinavir-mediated biological effects are represented in figure 27.

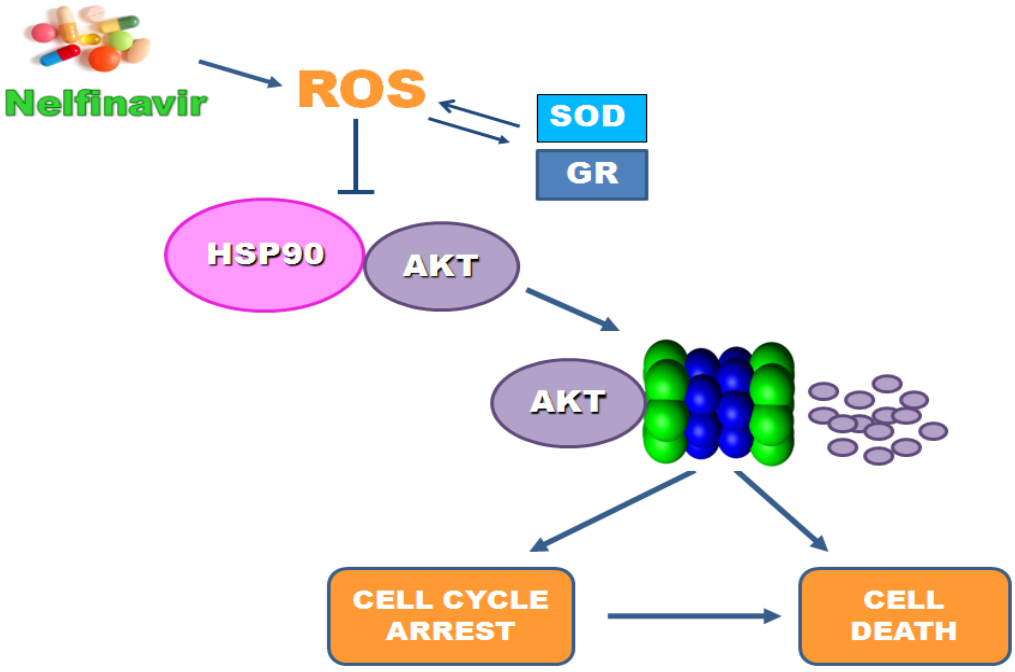

Figure 27. A possible nelfinavir mechanism of action in breast cancer

Despite this wide spectrum of activity, nelfinavir is not very potent, since it requires 10µM concentration to achieve cell activity, and the maximum concentrations achieved in patients are 7-9µM (Bernstein and Dennis 2008). Therefore, long term treatment with this concentration of nelfinavir can cause important side effects. These evidences drove me to characterize nelfinavir structure in order to synthesize new peptidomimetics with anti-cancer activity.

In this work we synthesized nelfinavir-derivatives, manteining crucial lead compound-residues for the activity. The first two compounds ND1 and ND2 preserved anti-tumoral efficacy of nelfinavir, even if they showed more cytotoxic activity than nelfinavir versus normal breast cells. These results suggested that the new chemical modifications were not useful to improve anti-tumoral efficacy although they highlighted the tridimensional pharmacophoric structure of nelfinavir, that was important for the development of second class of nelfinavir-derivatives, named series 200. The most part of these new compounds showed a lower IC_{50} than nelfinavir, suggesting that the novel chemical modification improved citotoxic activity of nelfinavir in breast cancer cells. Among these nelfinavir-derivatives, 4n resulted the most potent compound, with an IC_{50} of 50 nM in breast cancer cells and low toxicity versus normal cells. Therefore, the analysis of akt expression and ROS production in breast cancer cells revealed that 4n as well as nelfinavir reduced akt expression levels and induced a significant increase of ROS intracellular levels.

In order to better define the anti-cancer activity of 4n, I investigated new hypothetical molecular targets of this new compound. Starting from the chemists observation that 4n, as well as all class of compounds, show structural analogy with nutlin, I determined whether 4n affects p53-MDM2 interaction in MCF7 cells. This part of study has been the subject of publication attached to the present thesis (Bertamino et al. 2013), that demonstrates a direct involvement of 4n in a p53/MDM2 dissociation with subsequent p53 accumulation and induction of p53-dependent apoptosis.

6. CONCLUSIONS

Chemotherapy resistance remains a major obstacle for successful breast cancer treatment. Thus, the continuous development of new anti-cancer drugs could help address drug resistance by offering a broader spectrum of alternative anticancer agents. Nelfinavir, initially designed to block HIV-protease, has shown an important anti-cancer activity by affecting many intracellular pathways involved in tumor cell proliferation and cell-death resistance mechanisms. Elucidation of its mechanism of action could have important implications in the development of nelfinavir and its analogs as new anticancer agents. In the present study, I demonstrated that nelfinavir reduces breast cancer cell viability/growth by induction of cell-cycle block or cell-death, depending on cell line. Indeed, nelfinavir directly causes necrosis and apoptosis in MCF-7 while it determines cell-cycle arrest in G1 phase and subsequent cell-death in MDA-MB231cells.

Investigating the role of akt pathway in nelfinavir mediated cycle arrest and/or apoptosis, I can assert that nelfinavir strongly reduces akt signaling, proving this drug as effective chemotherapeutic agent or a radiosensitizer for cancer therapy. I have also shown that akt downregulation is related to a dissociation of akt/HSP90 complex that causes akt via proteasome degradation. The use of specific HSP90 or akt signal inhibitors confirmed the important function of akt/HSP90 complex in breast cancer cell proliferation. In addition, nelfinavir resulted more effective than these two inhibitors to reduce cell growth, suggesting that it has a broad spectrum of activity, not only restricted to akt downregulation.

Importantly, I proved that both akt/HSP90 disruption and cell-death induced by nelfinavir in breast cancer cells, are related to ROS production. Indeed, the analysis of antioxidant enzymes such as SOD and GR revealed that nelfinavir induces redox status alterations, thus leading to oxidative stress.

These findings sustained both design and identification of novel nelfinavir-derivatives. I presented a new class of peptidomimetics derived from nelfinavir with enhanced anti-cancer efficacy. Among these compounds, 4n represents the most potent compound, which retains nelfinavir molecular target, working in a nanomolar range of concentration compared to 10μM nelfinavir. However, further studies are needed to better define all 4n-molecular and cell targets, as well as its anti-cancer efficacy in vivo.

Development of novel compounds capable to selectively inhibit tumor cell growth with more efficacy than actual chemotherapeutic agents is urgently required for cancer therapy, thus my work provides a molecular basis to explain the broad-spectrum anti-cancer effect of nelfinavir and prepare the ground for the development of new nelfinavir derivatives with more specific anti-cancer activity.

7. AKNOWLEDGEMENTS

I thank Prof. Massimo Santoro for allowing me to attend the doctorate program in Molecular Oncology and Endocrinology under his supervision.

Thanks to Dr. Maddalena Illario who gave me the opportunity to work in her lab and significantly contributed to my scientific growth.

A special thank to Prof. Pietro Campiglia and Dr. Dario D'angelo whose collaboration was fundamental for this thesis.

Many thanks to Prof. Nunzia Montuori for her precious advices in experimental planning.

Thanks to Prof. Pietro Formisano for the critical discussion of the data and to Prof. Francesco Bequinot, a leading guide of my working group.

I thank Prof. Hilmar Bading who gave me the important opportunity to join his laboratory, extending my scientific knowledge and technical skills.
Thanks To Dr. Sara Monaco who made me feel at home in Germany. I'm grateful to her way of seeing the science and for all that she thought me.

Thanks to Dr. Maria Rosaria Rusciano who helped me to overcome technical difficulties and my “statistical limits”.
I thank my deskmate, Dr. Serena Maione, for constant practical and moral support. Our “highly scientific moments” and deserved breaks made my work almost enjoyable.
Thanks to my colleagues Catherine Crola, “the blond”, and Mario Neri “the confessor”, with whom I started the research activity in Illario’s lab.

I'm gratful to Rosaria Landi, my “peaceful friend”, for her extraordinary listening ability and great avaiability to help me everytime I needed.
Thanks to Rossella Delle Donne, Carmela Passaro, Antonio Pezone, Iaccarino's lab and all kind collegues for “the loaned reagents” and technical advices. They contributed pratically to my experiments fulfillment.

I thank my friends that I have often left aside during these “doctorate years” for their understanding and affection.

Thanks to Agostino for supporting with love my dreams and aspirations.
Lastly, I want to thank my family for all that I have and all that I am.

8. REFERENCES

Abate C, Patel L, Rauscher FJ, 3rd, Curran T. 1990. Redox regulation of fos and jun DNA-binding activity in vitro. Science 249(4973): 1157-1161.

Achanta G, Huang P. 2004. Role of p53 in sensing oxidative DNA damage in response to reactive oxygen species-generating agents. Cancer research 64(17): 6233-6239.

Acosta JJ, Munoz RM, Gonzalez L, Subtil-Rodriguez A, Dominguez-Caceres MA, Garcia-Martinez JM, Calcabrini A, Lazaro-Trueba I, Martin-Perez J. 2003. Src mediates prolactin-dependent proliferation of T47D and MCF7 cells via the activation of focal adhesion kinase/Erk1/2 and phosphatidylinositol 3-kinase pathways. Molecular endocrinology 17(11): 2268-2282.

Ahmed KBR, Davies MA. 2011. New Molecular Targets for the Systemic Therapy of Melanoma. Murph M, editor. Research on Melanoma-A Glimpse into Current Direction and Future Trends. Intech. Chapter 8.

Alfadda AA, Sallam RM. 2012. Reactive oxygen species in health and disease. Journal of biomedicine & biotechnology 2012: 936486.

Allen RG, Tresini M. 2000. Oxidative stress and gene regulation. Free radical biology & medicine 28(3): 463-499.

Ammendola R, Mesuraca M, Russo T, Cimino F. 1994. The DNA-binding efficiency of Sp1 is affected by redox changes. European journal of biochemistry / FEBS 225(1): 483-489.

Andre P, Groettrup M, Klenerman P, de Giuli R, Booth BL, Jr., Cerundolo V, Bonneville M, Jotereau F, Zinkernagel RM, Lotteau V. 1998. An inhibitor of HIV-1 protease modulates proteasome activity, antigen presentation, and T cell responses. Proceedings of the National Academy of Sciences of the United States of America 95(22): 13120-13124.

Aronov AM, McClain B, Moody CS, Murcko MA. 2008. Kinase-likeness and kinase-privileged fragments: toward virtual polypharmacology. Journal of medicinal chemistry 51(5): 1214-1222.

Barbaro G, Barbarini G. 2007. HIV infection and cancer in the era of highly active antiretroviral therapy (Review). Oncology reports 17(5): 1121-1126.

Barillari G, Iovane A, Bacigalupo I, Palladino C, Bellino S, Leone P, Monini P, Ensoli B. 2012. Ritonavir or saquinavir impairs the invasion of cervical intraepithelial neoplasia cells via a reduction of MMP expression and activity. Aids 26(8): 909-919.

Baselga J. 2011. Targeting the phosphoinositide-3 (PI3) kinase pathway in breast cancer. The oncologist 16 Suppl 1: 12-19.

Beck KF, Eberhardt W, Frank S, Huwiler A, Messmer UK, Muhl H, Pfeilschifter J. 1999. Inducible NO synthase: role in cellular signalling. The Journal of experimental biology 202(Pt 6): 645-653.

Beck R, Dejeans N, Glorieux C, Creton M, Delaive E, Dieu M, Raes M, Leveque P, Gallez B, Depuydt M et al. 2012. Hsp90 is cleaved by reactive oxygen species at a highly conserved N-terminal amino acid motif. PloS one 7(7): e40795.

Beckman JS, Koppenol WH. 1996. Nitric oxide, superoxide, and peroxynitrite: the good, the bad, and ugly. The American journal of physiology 271(5 Pt 1): C1424-1437.

Bellacosa A, de Feo D, Godwin AK, Bell DW, Cheng JQ, Altomare DA, Wan M, Dubeau L, Scambia G, Masciullo V et al. 1995. Molecular alterations of the AKT2 oncogene in ovarian and breast carcinomas. International journal of cancer Journal international du cancer 64(4): 280-285.

Ben-Romano R, Rudich A, Etzion S, Potashnik R, Kagan E, Greenbaum U, Bashan N. 2006. Nelfinavir induces adipocyte insulin resistance through the induction of oxidative stress: differential protective effect of antioxidant agents. Antiviral therapy 11(8): 1051-1060.

Ben-Romano R, Rudich A, Tirosh A, Potashnik R, Sasaoka T, Riesenberg K, Schlaeffer F, Bashan N. 2004. Nelfinavir-induced insulin resistance is associated with impaired plasma membrane recruitment of the PI 3-kinase effectors Akt/PKB and PKC-zeta. Diabetologia 47(6): 1107-1117.

Berns K, Horlings HM, Hennessy BT, Madiredjo M, Hijmans EM, Beelen K, Linn SC, Gonzalez-Angulo AM, Stemke-Hale K, Hauptmann M et al. 2007. A functional genetic approach identifies the PI3K pathway as a major determinant of trastuzumab resistance in breast cancer. Cancer cell 12(4): 395-402.

Bernstein WB, Dennis PA. 2008. Repositioning HIV protease inhibitors as cancer therapeutics. Current opinion in HIV and AIDS 3(6): 666-675.

Bertamino A, Soprano M, Musella S, Rusciano MR, Sala M, Vernieri E, Di Sarno V, Limatola A, Carotenuto A, Cosconati S et al. 2013. Synthesis, in vitro, and in cell studies of a new series of [indoline-3,2'-thiazolidine]-based p53 modulators. Journal of medicinal chemistry 56(13): 5407-5421.

Betteridge DJ. 2000. What is oxidative stress? Metabolism: clinical and experimental 49(2 Suppl 1): 3-8.

Bloch-Damti A, Bashan N. 2005. Proposed mechanisms for the induction of insulin resistance by oxidative stress. Antioxidants & redox signaling 7(11-12): 1553-1567.

Bonini C, Chiummiento L, De Bonis M, Di Blasio N, Funicello M, Lupatelli P. 2004. Synthesis of a first thiophene containing analog of the HIV protease

inhibitor nelfinavir. Tetrahedron Letters 45: 2797-2799.

Bonini C, Chiummiento L, De Bonis M, Di Blasio N, Funicello M, Lupatelli P, Suanno G, Bertib F, Campaner P. 2005. Synthesis, biological activity and modelling studies of two novel anti HIV PR inhibitors with a thiophene containing hydroxyethylamino core. Tetrahedron 61: 6580-6589.

Bonini C, Chiummiento L, De Bonis M, Di Blasio N, Funicello M, Lupattelli P, Pandolfo R, Tramutola F, Berti F. 2010. Synthesis of new thienyl ring containing HIV-1 protease inhibitors: promising preliminary pharmacological evaluation against recombinant HIV-1 proteases. Journal of medicinal chemistry 53(4): 1451-1457.

Bono C, Karlin L, Harel S, Mouly E, Labaume S, Galicier L, Apcher S, Sauvageon H, Fermand JP, Bories JC et al. 2012. The human immunodeficiency virus-1 protease inhibitor nelfinavir impairs proteasome activity and inhibits the proliferation of multiple myeloma cells in vitro and in vivo. Haematologica 97(7): 1101-1109.

Bredt DS. 1999. Endogenous nitric oxide synthesis: biological functions and pathophysiology. Free radical research 31(6): 577-596.

Brognard J, Sierecki E, Gao T, Newton AC. 2007. PHLPP and a second isoform, PHLPP2, differentially attenuate the amplitude of Akt signaling by regulating distinct Akt isoforms. Molecular cell 25(6): 917-931.

Brown NS, Bicknell R. 2001. Hypoxia and oxidative stress in breast cancer. Oxidative stress: its effects on the growth, metastatic potential and response to therapy of breast cancer. Breast cancer research : BCR 3(5): 323-327.

Brown NS, Jones A, Fujiyama C, Harris AL, Bicknell R. 2000. Thymidine phosphorylase induces carcinoma cell oxidative stress and promotes secretion of angiogenic factors. Cancer research 60(22): 6298-6302.

Bruning A, Burger P, Vogel M, Rahmeh M, Gingelmaiers A, Friese K, Lenhard M, Burges A. 2009. Nelfinavir induces the unfolded protein response in ovarian cancer cells, resulting in ER vacuolization, cell cycle retardation and apoptosis. Cancer biology & therapy 8(3): 226-232.

Bruning A, Friese K, Burges A, Mylonas I. 2010. Tamoxifen enhances the cytotoxic effects of nelfinavir in breast cancer cells. Breast cancer research : BCR 12(4): R45.

Brunner TB, Geiger M, Grabenbauer GG, Lang-Welzenbach M, Mantoni TS, Cavallaro A, Sauer R, Hohenberger W, McKenna WG. 2008. Phase I trial of the human immunodeficiency virus protease inhibitor nelfinavir and chemoradiation for locally advanced pancreatic cancer. Journal of clinical oncology : official journal of the American Society of Clinical Oncology 26(16): 2699-2706.

Buijsen J, Lammering G, Jansen RL, Beets GL, Wals J, Sosef M, Den Boer

MO, Leijtens J, Riedl RG, Theys J et al. 2013. Phase I trial of the combination of the Akt inhibitor nelfinavir and chemoradiation for locally advanced rectal cancer. Radiotherapy and oncology : journal of the European Society for Therapeutic Radiology and Oncology 107(2): 184-188.

Burgering BM, Medema RH. 2003. Decisions on life and death: FOXO Forkhead transcription factors are in command when PKB/Akt is off duty. Journal of leukocyte biology 73(6): 689-701.

Cai H. 2005. Hydrogen peroxide regulation of endothelial function: origins, mechanisms, and consequences. Cardiovascular research 68(1): 26-36.

Cantley LC, Neel BG. 1999. New insights into tumor suppression: PTEN suppresses tumor formation by restraining the phosphoinositide 3-kinase/AKT pathway. Proceedings of the National Academy of Sciences of the United States of America 96(8): 4240-4245.

Cao R, Hu Y, Wang Y, Gurley EC, Studer EJ, Wang X, Hylemon PB, Pandak WM, Sanyal AJ, Zhang L et al. 2010. Prevention of HIV protease inhibitor-induced dysregulation of hepatic lipid metabolism by raltegravir via endoplasmic reticulum stress signaling pathways. The Journal of pharmacology and experimental therapeutics 334(2): 530-539.

Cardone MH, Roy N, Stennicke HR, Salvesen GS, Franke TF, Stanbridge E, Frisch S, Reed JC. 1998. Regulation of cell death protease caspase-9 by phosphorylation. Science 282(5392): 1318-1321.

Carr A, Samaras K, Burton S, Law M, Freund J, Chisholm DJ, Cooper DA. 1998. A syndrome of peripheral lipodystrophy, hyperlipidaemia and insulin resistance in patients receiving HIV protease inhibitors. Aids 12(7): F51-58.

Carvalho-Filho MA, Ueno M, Hirabara SM, Seabra AB, Carvalheira JB, de Oliveira MG, Velloso LA, Curi R, Saad MJ. 2005. S-nitrosation of the insulin receptor, insulin receptor substrate 1, and protein kinase B/Akt: a novel mechanism of insulin resistance. Diabetes 54(4): 959-967.

Cavalieri E, Frenkel K, Liehr JG, Rogan E, Roy D. 2000. Estrogens as endogenous genotoxic agents--DNA adducts and mutations. Journal of the National Cancer Institute Monographs(27): 75-93.

Chai H, Yang H, Yan S, Li M, Lin PH, Lumsden AB, Yao Q, Chen C. 2005. Effects of 5 HIV protease inhibitors on vasomotor function and superoxide anion production in porcine coronary arteries. Journal of acquired immune deficiency syndromes 40(1): 12-19.

Chan TO, Rittenhouse SE, Tsichlis PN. 1999. AKT/PKB and other D3 phosphoinositide-regulated kinases: kinase activation by phosphoinositide-dependent phosphorylation. Annual review of biochemistry 68: 965-1014.

Chan TO, Tsichlis PN. 2001. PDK2: a complex tail in one Akt. Science's STKE

: signal transduction knowledge environment 2001(66): pe1.

Chandra J, Samali A, Orrenius S. 2000. Triggering and modulation of apoptosis by oxidative stress. Free radical biology & medicine 29(3-4): 323-333.

Chandra S, Mondal D, Agrawal KC. 2009. HIV-1 protease inhibitor induced oxidative stress suppresses glucose stimulated insulin release: protection with thymoquinone. Experimental biology and medicine 234(4): 442-453.

Chapman TM, Plosker GL, Perry CM. 2004. Fosamprenavir: a review of its use in the management of antiretroviral therapy-naive patients with HIV infection. Drugs 64(18): 2101-2124.

Chen S, Parmigiani G. 2007. Meta-analysis of BRCA1 and BRCA2 penetrance. Journal of clinical oncology : official journal of the American Society of Clinical Oncology 25(11): 1329-1333.

Cheng JQ, Ruggeri B, Klein WM, Sonoda G, Altomare DA, Watson DK, Testa JR. 1996. Amplification of AKT2 in human pancreatic cells and inhibition of AKT2 expression and tumorigenicity by antisense RNA. Proceedings of the National Academy of Sciences of the United States of America 93(8): 3636-3641.

Chow WA, Guo S, Valdes-Albini F. 2006. Nelfinavir induces liposarcoma apoptosis and cell cycle arrest by upregulating sterol regulatory element binding protein-1. Anti-cancer drugs 17(8): 891-903.

Chow WA, Jiang C, Guan M. 2009. Anti-HIV drugs for cancer therapeutics: back to the future? The lancet oncology 10(1): 61-71.

Clark CB, Rane MJ, El Mehdi D, Miller CJ, Sachleben LR, Jr., Gozal E. 2009. Role of oxidative stress in geldanamycin-induced cytotoxicity and disruption of Hsp90 signaling complex. Free radical biology & medicine 47(10): 1440-1449.

Clarke JF, Young PW, Yonezawa K, Kasuga M, Holman GD. 1994. Inhibition of the translocation of GLUT1 and GLUT4 in 3T3-L1 cells by the phosphatidylinositol 3-kinase inhibitor, wortmannin. The Biochemical journal 300 (Pt 3): 631-635.

Clerkin JS, Naughton R, Quiney C, Cotter TG. 2008. Mechanisms of ROS modulated cell survival during carcinogenesis. Cancer letters 266(1): 30-36.

Coffer PJ, Jin J, Woodgett JR. 1998. Protein kinase B (c-Akt): a multifunctional mediator of phosphatidylinositol 3-kinase activation. The Biochemical journal 335 (Pt 1): 1-13.

Collado M, Medema RH, Garcia-Cao I, Dubuisson ML, Barradas M, Glassford J, Rivas C, Burgering BM, Serrano M, Lam EW. 2000. Inhibition of the phosphoinositide 3-kinase pathway induces a senescence-like arrest mediated by p27Kip1. The Journal of biological chemistry 275(29): 21960-21968.

Conklin BS, Fu W, Lin PH, Lumsden AB, Yao Q, Chen C. 2004. HIV protease inhibitor ritonavir decreases endothelium-dependent vasorelaxation and increases superoxide in porcine arteries. Cardiovascular research 63(1): 168-175.

Conklin KA. 2004. Cancer chemotherapy and antioxidants. The Journal of nutrition 134(11): 3201S-3204S.

Cross DA, Alessi DR, Cohen P, Andjelkovich M, Hemmings BA. 1995. Inhibition of glycogen synthase kinase-3 by insulin mediated by protein kinase B. Nature 378(6559): 785-789.

Cullen JJ, Mitros FA, Oberley LW. 2003. Expression of antioxidant enzymes in diseases of the human pancreas: another link between chronic pancreatitis and pancreatic cancer. Pancreas 26(1): 23-27.

Cuneo KC, Tu T, Geng L, Fu A, Hallahan DE, Willey CD. 2007. HIV protease inhibitors enhance the efficacy of irradiation. Cancer research 67(10): 4886-4893.

Dai R, Chen R, Li H. 2009. Cross-talk between PI3K/Akt and MEK/ERK pathways mediates endoplasmic reticulum stress-induced cell cycle progression and cell death in human hepatocellular carcinoma cells. International journal of oncology 34(6): 1749-1757.

Datta SR, Dudek H, Tao X, Masters S, Fu H, Gotoh Y, Greenberg ME. 1997. Akt phosphorylation of BAD couples survival signals to the cell-intrinsic death machinery. Cell 91(2): 231-241.

De Clercq E. 2009. Anti-HIV drugs: 25 compounds approved within 25 years after the discovery of HIV. International journal of antimicrobial agents 33(4): 307-320.

De Miguel M, Cordero MD. 2012. Oxidative therapy against cancer. Lushchak V, editor. Oxidative stress and disease. Intech. Chapter 22.

Dean RT, Fu S, Stocker R, Davies MJ. 1997. Biochemistry and pathology of radical-mediated protein oxidation. The Biochemical journal 324 (Pt 1): 1-18.

Decker P, Muller S. 2002. Modulating poly (ADP-ribose) polymerase activity: potential for the prevention and therapy of pathogenic situations involving DNA damage and oxidative stress. Current pharmaceutical biotechnology 3(3): 275-283.

Deeks SG, Smith M, Holodniy M, Kahn JO. 1997. HIV-1 protease inhibitors. A review for clinicians. JAMA : the journal of the American Medical Association 277(2): 145-153.

Deng W, Baki L, Yin J, Zhou H, Baumgarten CM. 2010. HIV protease inhibitors elicit volume-sensitive Cl- current in cardiac myocytes via mitochondrial ROS. Journal of molecular and cellular cardiology 49(5):

746-752.

Deprez J, Vertommen D, Alessi DR, Hue L, Rider MH. 1997. Phosphorylation and activation of heart 6-phosphofructo-2-kinase by protein kinase B and other protein kinases of the insulin signaling cascades. The Journal of biological chemistry 272(28): 17269-17275.

Di Cristofano A, Pandolfi PP. 2000. The multiple roles of PTEN in tumor suppression. Cell 100(4): 387-390.

Doyon L, Tremblay S, Bourgon L, Wardrop E, Cordingley MG. 2005. Selection and characterization of HIV-1 showing reduced susceptibility to the non-peptidic protease inhibitor tipranavir. Antiviral research 68(1): 27-35.

Dunlop EA, Tee AR. 2009. Mammalian target of rapamycin complex 1: signalling inputs, substrates and feedback mechanisms. Cellular signalling 21(6): 827-835.

Elstrom RL, Bauer DE, Buzzai M, Karnauskas R, Harris MH, Plas DR, Zhuang H, Cinalli RM, Alavi A, Rudin CM et al. 2004. Akt stimulates aerobic glycolysis in cancer cells. Cancer research 64(11): 3892-3899.

Evans JL, Goldfine ID, Maddux BA, Grodsky GM. 2003. Are oxidative stress-activated signaling pathways mediators of insulin resistance and beta-cell dysfunction? Diabetes 52(1): 1-8.

Ezzi SA, Urushitani M, Julien JP. 2007. Wild-type superoxide dismutase acquires binding and toxic properties of ALS-linked mutant forms through oxidation. Journal of neurochemistry 102(1): 170-178.

Flexner C. 2007. HIV drug development: the next 25 years. Nature reviews Drug discovery 6(12): 959-966.

Florescu A, Amir E, Bouganim N, Clemons M. 2011. Immune therapy for breast cancer in 2010-hype or hope? Current oncology 18(1): e9-e18.

Foreman J, Demidchik V, Bothwell JH, Mylona P, Miedema H, Torres MA, Linstead P, Costa S, Brownlee C, Jones JD et al. 2003. Reactive oxygen species produced by NADPH oxidase regulate plant cell growth. Nature 422(6930): 442-446.

Forman HJ. 2007. Use and abuse of exogenous H2O2 in studies of signal transduction. Free radical biology & medicine 42(7): 926-932.

Fridovich I. 1999. Fundamental aspects of reactive oxygen species, or what's the matter with oxygen? Annals of the New York Academy of Sciences 893: 13-18.

Fu W, Chai H, Yao Q, Chen C. 2005. Effects of HIV protease inhibitor ritonavir on vasomotor function and endothelial nitric oxide synthase expression. Journal of acquired immune deficiency syndromes 39(2): 152-158.

Fujita N, Sato S, Katayama K, Tsuruo T. 2002. Akt-dependent phosphorylation

of p27Kip1 promotes binding to 14-3-3 and cytoplasmic localization. The Journal of biological chemistry 277(32): 28706-28713.

Fukuda Y, Takenaka K, Sparreboom A, Cheepala SB, Wu CP, Ekins S, Ambudkar SV, Schuetz JD. 2013. Human immunodeficiency virus protease inhibitors interact with ATP binding cassette transporter 4/multidrug resistance protein 4: a basis for unanticipated enhanced cytotoxicity. Molecular pharmacology 84(3): 361-371.

Gaedicke S, Firat-Geier E, Constantiniu O, Lucchiari-Hartz M, Freudenberg M, Galanos C, Niedermann G. 2002. Antitumor effect of the human immunodeficiency virus protease inhibitor ritonavir: induction of tumor-cell apoptosis associated with perturbation of proteasomal proteolysis. Cancer research 62(23): 6901-6908.

Gage M, Wattendorf D, Henry LR. 2012. Translational advances regarding hereditary breast cancer syndromes. Journal of surgical oncology 105(5): 444-451.

Gao P, Zhang H, Dinavahi R, Li F, Xiang Y, Raman V, Bhujwalla ZM, Felsher DW, Cheng L, Pevsner J et al. 2007. HIF-dependent antitumorigenic effect of antioxidants in vivo. Cancer cell 12(3): 230-238.

Georgakis GV, Younes A. 2005. Heat-shock protein 90 inhibitors in cancer therapy: 17AAG and beyond. Future oncology 1(2): 273-281.

Geyer CE, Forster J, Lindquist D, Chan S, Romieu CG, Pienkowski T, Jagiello-Gruszfeld A, Crown J, Chan A, Kaufman B et al. 2006. Lapatinib plus capecitabine for HER2-positive advanced breast cancer. The New England journal of medicine 355(26): 2733-2743.

Ghosh R, Mitchell DL. 1999. Effect of oxidative DNA damage in promoter elements on transcription factor binding. Nucleic acids research 27(15): 3213-3218.

Giardino Torchia ML, Ciaglia E, Masci AM, Vitiello L, Fogli M, la Sala A, Mavilio D, Racioppi L. 2010. Dendritic cells/natural killer cross-talk: a novel target for human immunodeficiency virus type-1 protease inhibitors. PloS one 5(6): e11052.

Gills JJ, Lopiccolo J, Tsurutani J, Shoemaker RH, Best CJ, Abu-Asab MS, Borojerdi J, Warfel NA, Gardner ER, Danish M et al. 2007. Nelfinavir, A lead HIV protease inhibitor, is a broad-spectrum, anticancer agent that induces endoplasmic reticulum stress, autophagy, and apoptosis in vitro and in vivo. Clinical cancer research : an official journal of the American Association for Cancer Research 13(17): 5183-5194.

Goldenberg MM. 1999. Trastuzumab, a recombinant DNA-derived humanized monoclonal antibody, a novel agent for the treatment of metastatic breast cancer. Clinical therapeutics 21(2): 309-318.

Gotoh T, Mori M. 2006. Nitric oxide and endoplasmic reticulum stress. Arteriosclerosis, thrombosis, and vascular biology 26(7): 1439-1446.

Gow AJ, Chen Q, Hess DT, Day BJ, Ischiropoulos H, Stamler JS. 2002. Basal and stimulated protein S-nitrosylation in multiple cell types and tissues. The Journal of biological chemistry 277(12): 9637-9640.

Granado-Serrano AB, Martin MA, Bravo L, Goya L, Ramos S. 2006. Quercetin induces apoptosis via caspase activation, regulation of Bcl-2, and inhibition of PI-3-kinase/Akt and ERK pathways in a human hepatoma cell line (HepG2). The Journal of nutrition 136(11): 2715-2721.

Gupta AK, Cerniglia GJ, Mick R, McKenna WG, Muschel RJ. 2005. HIV protease inhibitors block Akt signaling and radiosensitize tumor cells both in vitro and in vivo. Cancer research 65(18): 8256-8265.

Gupta AK, Li B, Cerniglia GJ, Ahmed MS, Hahn SM, Maity A. 2007. The HIV protease inhibitor nelfinavir downregulates Akt phosphorylation by inhibiting proteasomal activity and inducing the unfolded protein response. Neoplasia 9(4): 271-278.

Halliwell B. 1996. Antioxidants in human health and disease. Annual review of nutrition 16: 33-50.

-. 1999. Antioxidant defence mechanisms: from the beginning to the end (of the beginning). Free radical research 31(4): 261-272.

Han X, Liehr JG. 1994. 8-Hydroxylation of guanine bases in kidney and liver DNA of hamsters treated with estradiol: role of free radicals in estrogen-induced carcinogenesis. Cancer research 54(21): 5515-5517.

Hanada M, Feng J, Hemmings BA. 2004. Structure, regulation and function of PKB/AKT--a major therapeutic target. Biochimica et biophysica acta 1697(1-2): 3-16.

Hay N, Sonenberg N. 2004. Upstream and downstream of mTOR. Genes & development 18(16): 1926-1945.

Hetz C. 2012. The unfolded protein response: controlling cell fate decisions under ER stress and beyond. Nature reviews Molecular cell biology 13(2): 89-102.

Hirano Y, Yoshida M, Shimizu M, Sato R. 2001. Direct demonstration of rapid degradation of nuclear sterol regulatory element-binding proteins by the ubiquitin-proteasome pathway. The Journal of biological chemistry 276(39): 36431-36437.

Hogg N, Kalyanaraman B. 1998. Nitric oxide and low-density lipoprotein oxidation. Free radical research 28(6): 593-600.

Hosoi T, Hyoda K, Okuma Y, Nomura Y, Ozawa K. 2007. Akt up- and down-regulation in response to endoplasmic reticulum stress. Brain research 1152:

27-31.

Hoyt MT, Palchaudhuri R, Hergenrother PJ. 2011. Cribrostatin 6 induces death in cancer cells through a reactive oxygen species (ROS)-mediated mechanism. Investigational new drugs 29(4): 562-573.

Huang J, Manning BD. 2009. A complex interplay between Akt, TSC2 and the two mTOR complexes. Biochemical Society transactions 37(Pt 1): 217-222.

Hui DY. 2003. Effects of HIV protease inhibitor therapy on lipid metabolism. Progress in lipid research 42(2): 81-92.

Hulgan T, Morrow J, D'Aquila RT, Raffanti S, Morgan M, Rebeiro P, Haas DW. 2003. Oxidant stress is increased during treatment of human immunodeficiency virus infection. Clinical infectious diseases : an official publication of the Infectious Diseases Society of America 37(12): 1711-1717.

Hussain AR, Uddin S, Bu R, Khan OS, Ahmed SO, Ahmed M, Al-Kuraya KS. 2011. Resveratrol suppresses constitutive activation of AKT via generation of ROS and induces apoptosis in diffuse large B cell lymphoma cell lines. PloS one 6(9): e24703.

Irani K. 2000. Oxidant signaling in vascular cell growth, death, and survival : a review of the roles of reactive oxygen species in smooth muscle and endothelial cell mitogenic and apoptotic signaling. Circulation research 87(3): 179-183.

Jareno EJ, Roma J, Romero B, Marin N, Muriach M, Johnsen S, Bosch-Morell F, Marselou L, Romero FJ. 2002. Serum malondialdehyde correlates with therapeutic efficiency of high activity antiretroviral therapies (HAART) in HIV-1 infected children. Free radical research 36(3): 341-344.

Jiang B, Hebert VY, Li Y, Mathis JM, Alexander JS, Dugas TR. 2007a. HIV antiretroviral drug combination induces endothelial mitochondrial dysfunction and reactive oxygen species production, but not apoptosis. Toxicology and applied pharmacology 224(1): 60-71.

Jiang W, Mikochik PJ, Ra JH, Lei H, Flaherty KT, Winkler JD, Spitz FR. 2007b. HIV protease inhibitor nelfinavir inhibits growth of human melanoma cells by induction of cell cycle arrest. Cancer research 67(3): 1221-1227.

Jiang Z, Pore N, Cerniglia GJ, Mick R, Georgescu MM, Bernhard EJ, Hahn SM, Gupta AK, Maity A. 2007c. Phosphatase and tensin homologue deficiency in glioblastoma confers resistance to radiation and temozolomide that is reversed by the protease inhibitor nelfinavir. Cancer research 67(9): 4467-4473.

Kaneki M, Shimizu N, Yamada D, Chang K. 2007. Nitrosative stress and pathogenesis of insulin resistance. Antioxidants & redox signaling 9(3):

319-329.

Kaufman RJ. 2002. Orchestrating the unfolded protein response in health and disease. The Journal of clinical investigation 110(10): 1389-1398.

Kawabata S, Gills JJ, Mercado-Matos JR, Lopiccolo J, Wilson W, 3rd, Hollander MC, Dennis PA. 2012. Synergistic effects of nelfinavir and bortezomib on proteotoxic death of NSCLC and multiple myeloma cells. Cell death & disease 3: e353.

Khanzode SS, Muddeshwar MG, Khanzode SD, Dakhale GN. 2004. Antioxidant enzymes and lipid peroxidation in different stages of breast cancer. Free radical research 38(1): 81-85.

Kim AH, Khursigara G, Sun X, Franke TF, Chao MV. 2001. Akt phosphorylates and negatively regulates apoptosis signal-regulating kinase 1. Molecular and cellular biology 21(3): 893-901.

Kim DI, Lim SK, Park MJ, Han HJ, Kim GY, Park SH. 2007. The involvement of phosphatidylinositol 3-kinase /Akt signaling in high glucose-induced downregulation of GLUT-1 expression in ARPE cells. Life sciences 80(7): 626-632.

Knobbe CB, Reifenberger G. 2003. Genetic alterations and aberrant expression of genes related to the phosphatidyl-inositol-3'-kinase/protein kinase B (Akt) signal transduction pathway in glioblastomas. Brain pathology 13(4): 507-518.

Koster JC, Remedi MS, Qiu H, Nichols CG, Hruz PW. 2003. HIV protease inhibitors acutely impair glucose-stimulated insulin release. Diabetes 52(7): 1695-1700.

Kulisz A, Chen N, Chandel NS, Shao Z, Schumacker PT. 2002. Mitochondrial ROS initiate phosphorylation of p38 MAP kinase during hypoxia in cardiomyocytes. American journal of physiology Lung cellular and molecular physiology 282(6): L1324-1329.

Labarge MA, Garbe JC, Stampfer MR. 2013. Processing of human reduction mammoplasty and mastectomy tissues for cell culture. Journal of visualized experiments : JoVE(71).

Larder BA, Hertogs K, Bloor S, van den Eynde CH, DeCian W, Wang Y, Freimuth WW, Tarpley G. 2000. Tipranavir inhibits broadly protease inhibitor-resistant HIV-1 clinical samples. Aids 14(13): 1943-1948.

Lebon F, Ledecq M. 2000. Approaches to the design of effective HIV-1 protease inhibitors. Current medicinal chemistry 7(4): 455-477.

Lee YJ, Galoforo SS, Sim JE, Ridnour LA, Choi J, Forman HJ, Corry PM, Spitz DR. 2000. Dominant-negative Jun N-terminal protein kinase (JNK-1) inhibits metabolic oxidative stress during glucose deprivation in a human breast carcinoma cell line. Free radical biology & medicine 28(4): 575-584.

Leslie NR. 2006. The redox regulation of PI 3-kinase-dependent signaling. Antioxidants & redox signaling 8(9-10): 1765-1774.

Leslie NR, Bennett D, Lindsay YE, Stewart H, Gray A, Downes CP. 2003. Redox regulation of PI 3-kinase signalling via inactivation of PTEN. The EMBO journal 22(20): 5501-5510.

Levine B, Kroemer G. 2008. Autophagy in the pathogenesis of disease. Cell 132(1): 27-42.

Lewis-Wambi JS, Jordan VC. 2009. Estrogen regulation of apoptosis: how can one hormone stimulate and inhibit? Breast cancer research : BCR 11(3): 206.

Li J, Stouffs M, Serrander L, Banfi B, Bettiol E, Charnay Y, Steger K, Krause KH, Jaconi ME. 2006. The NADPH oxidase NOX4 drives cardiac differentiation: Role in regulating cardiac transcription factors and MAP kinase activation. Molecular biology of the cell 17(9): 3978-3988.

Li JJ, Oberley LW, St Clair DK, Ridnour LA, Oberley TD. 1995. Phenotypic changes induced in human breast cancer cells by overexpression of manganese-containing superoxide dismutase. Oncogene 10(10): 1989-2000.

Li S, Yan T, Yang JQ, Oberley TD, Oberley LW. 2000. The role of cellular glutathione peroxidase redox regulation in the suppression of tumor cell growth by manganese superoxide dismutase. Cancer research 60(14): 3927-3939.

Liao Y, Hung MC. 2004. A new role of protein phosphatase 2a in adenoviral E1A protein-mediated sensitization to anticancer drug-induced apoptosis in human breast cancer cells. Cancer research 64(17): 5938-5942.

-. 2010. Physiological regulation of Akt activity and stability. American journal of translational research 2(1): 19-42.

Liu F, Kovalevsky AY, Tie Y, Ghosh AK, Harrison RW, Weber IT. 2008. Effect of flap mutations on structure of HIV-1 protease and inhibition by saquinavir and darunavir. Journal of molecular biology 381(1): 102-115.

Liu L, Yan Y, Zeng M, Zhang J, Hanes MA, Ahearn G, McMahon TJ, Dickfeld T, Marshall HE, Que LG et al. 2004. Essential roles of S-nitrosothiols in vascular homeostasis and endotoxic shock. Cell 116(4): 617-628.

Lopez D, Gil-Torregrosa BC, Bergmann C, Del Val M. 2000. Sequential cleavage by metallopeptidases and proteasomes is involved in processing HIV-1 ENV epitope for endogenous MHC class I antigen presentation. Journal of immunology 164(10): 5070-5077.

LoPiccolo J, Blumenthal GM, Bernstein WB, Dennis PA. 2008. Targeting the PI3K/Akt/mTOR pathway: effective combinations and clinical considerations. Drug resistance updates : reviews and commentaries in antimicrobial and anticancer chemotherapy 11(1-2): 32-50.

Lu W, Andrieu JM. 2000. HIV protease inhibitors restore impaired T-cell proliferative response in vivo and in vitro: a viral-suppression-independent mechanism. Blood 96(1): 250-258.

Lu W, Ogasawara MA, Huang P. 2007. Models of reactive oxygen species in cancer. Drug discovery today Disease models 4(2): 67-73.

Luber AD, Brower R, Kim D, Silverman R, Peloquin CA, Frank I. 2007. Steady-state pharmacokinetics of once-daily fosamprenavir/ritonavir and atazanavir/ritonavir alone and in combination with 20 mg omeprazole in healthy volunteers. HIV medicine 8(7): 457-464.

Mannick JB, Schonhoff CM. 2002. Nitrosylation: the next phosphorylation? Archives of biochemistry and biophysics 408(1): 1-6.

Manoharan S, Kolanjiappan K, Kayalvizhi M. 2004. Enhanced lipid peroxidation and impaired enzymic antioxidant activities in the erythrocytes of patients with cervical carcinoma. Cellular & molecular biology letters 9(4A): 699-707.

Manza LL, Codreanu SG, Stamer SL, Smith DL, Wells KS, Roberts RL, Liebler DC. 2004. Global shifts in protein sumoylation in response to electrophile and oxidative stress. Chemical research in toxicology 17(12): 1706-1715.

Marnett LJ. 2000. Oxyradicals and DNA damage. Carcinogenesis 21(3): 361-370.

Marshall HE, Merchant K, Stamler JS. 2000. Nitrosation and oxidation in the regulation of gene expression. FASEB journal : official publication of the Federation of American Societies for Experimental Biology 14(13): 1889-1900.

Massaoka MH, Matsuo AL, Figueiredo CR, Farias CF, Girola N, Arruda DC, Scutti JA, Romoff P, Favero OA, Ferreira MJ et al. 2012. Jacaranone induces apoptosis in melanoma cells via ROS-mediated downregulation of Akt and p38 MAPK activation and displays antitumor activity in vivo. PloS one 7(6): e38698.

Mayo LD, Dixon JE, Durden DL, Tonks NK, Donner DB. 2002. PTEN protects p53 from Mdm2 and sensitizes cancer cells to chemotherapy. The Journal of biological chemistry 277(7): 5484-5489.

Mayo LD, Donner DB. 2001. A phosphatidylinositol 3-kinase/Akt pathway promotes translocation of Mdm2 from the cytoplasm to the nucleus. Proceedings of the National Academy of Sciences of the United States of America 98(20): 11598-11603.

McCord JM, Fridovich I. 1969. Superoxide dismutase. An enzymic function for erythrocuprein (hemocuprein). The Journal of biological chemistry 244(22): 6049-6055.

McCoy C. 2007. Darunavir: a nonpeptidic antiretroviral protease inhibitor.

Clinical therapeutics 29(8): 1559-1576.

McEligot AJ, Yang S, Meyskens FL, Jr. 2005. Redox regulation by intrinsic species and extrinsic nutrients in normal and cancer cells. Annual review of nutrition 25: 261-295.

McPherson K, Steel CM, Dixon JM. 2000. ABC of breast diseases. Breast cancer-epidemiology, risk factors, and genetics. Bmj 321(7261): 624-628.

Meitzler JL, Antony S, Wu Y, Juhasz A, Liu H, Jiang G, Lu J, Roy K, Doroshow JH. 2013. NADPH Oxidases: A Perspective on Reactive Oxygen Species Production in Tumor Biology. Antioxidants & redox signaling.

Mimoto T, Hattori N, Takaku H, Kisanuki S, Fukazawa T, Terashima K, Kato R, Nojima S, Misawa S, Ueno T et al. 2000. Structure-activity relationship of orally potent tripeptide-based HIV protease inhibitors containing hydroxymethylcarbonyl isostere. Chemical & pharmaceutical bulletin 48(9): 1310-1326.

Miyamoto S, Murphy AN, Brown JH. 2008. Akt mediates mitochondrial protection in cardiomyocytes through phosphorylation of mitochondrial hexokinase-II. Cell death and differentiation 15(3): 521-529.

Mobley JA, Brueggemeier RW. 2004. Estrogen receptor-mediated regulation of oxidative stress and DNA damage in breast cancer. Carcinogenesis 25(1): 3-9.

Mondal D, Pradhan L, Ali M, Agrawal KC. 2004. HAART drugs induce oxidative stress in human endothelial cells and increase endothelial recruitment of mononuclear cells: exacerbation by inflammatory cytokines and amelioration by antioxidants. Cardiovascular toxicology 4(3): 287-302.

Monini P, Sgadari C, Barillari G, Ensoli B. 2003. HIV protease inhibitors: antiretroviral agents with anti-inflammatory, anti-angiogenic and anti-tumour activity. The Journal of antimicrobial chemotherapy 51(2): 207-211.

Monini P, Sgadari C, Toschi E, Barillari G, Ensoli B. 2004. Antitumour effects of antiretroviral therapy. Nature reviews Cancer 4(11): 861-875.

Moskowitz R, Kukin M. 1999. Oxidative stress and congestive heart failure. Congestive heart failure 5(4): 153-163.

Muise-Helmericks RC, Grimes HL, Bellacosa A, Malstrom SE, Tsichlis PN, Rosen N. 1998. Cyclin D expression is controlled post-transcriptionally via a phosphatidylinositol 3-kinase/Akt-dependent pathway. The Journal of biological chemistry 273(45): 29864-29872.

Muller FL, Liu Y, Van Remmen H. 2004. Complex III releases superoxide to both sides of the inner mitochondrial membrane. The Journal of biological chemistry 279(47): 49064-49073.

Munoz A, Schrager LK, Bacellar H, Speizer I, Vermund SH, Detels R, Saah AJ,

Kingsley LA, Seminara D, Phair JP. 1993. Trends in the incidence of outcomes defining acquired immunodeficiency syndrome (AIDS) in the Multicenter AIDS Cohort Study: 1985-1991. American journal of epidemiology 137(4): 423-438.

Musarrat J, Arezina-Wilson J, Wani AA. 1996. Prognostic and aetiological relevance of 8-hydroxyguanosine in human breast carcinogenesis. European journal of cancer 32A(7): 1209-1214.

Nakatani K, Thompson DA, Barthel A, Sakaue H, Liu W, Weigel RJ, Roth RA. 1999. Up-regulation of Akt3 in estrogen receptor-deficient breast cancers and androgen-independent prostate cancer lines. The Journal of biological chemistry 274(31): 21528-21532.

Neckers L, Ivy SP. 2003. Heat shock protein 90. Current opinion in oncology 15(6): 419-424.

Neckers L, Neckers K. 2005. Heat-shock protein 90 inhibitors as novel cancer chemotherapeutics - an update. Expert opinion on emerging drugs 10(1): 137-149.

Nogueira V, Park Y, Chen CC, Xu PZ, Chen ML, Tonic I, Unterman T, Hay N. 2008. Akt determines replicative senescence and oxidative or oncogenic premature senescence and sensitizes cells to oxidative apoptosis. Cancer cell 14(6): 458-470.

Nordberg J, Arner ES. 2001. Reactive oxygen species, antioxidants, and the mammalian thioredoxin system. Free radical biology & medicine 31(11): 1287-1312.

Oberley LW, Buettner GR. 1979. Role of superoxide dismutase in cancer: a review. Cancer research 39(4): 1141-1149.

Oberley TD, Xue Y, Zhao Y, Kiningham K, Szweda LI, St Clair DK. 2004. In situ reduction of oxidative damage, increased cell turnover, and delay of mitochondrial injury by overexpression of manganese superoxide dismutase in a multistage skin carcinogenesis model. Antioxidants & redox signaling 6(3): 537-548.

Okoh VO, Felty Q, Parkash J, Poppiti R, Roy D. 2013. Reactive oxygen species via redox signaling to PI3K/AKT pathway contribute to the malignant growth of 4-hydroxy estradiol-transformed mammary epithelial cells. PloS one 8(2): e54206.

Olumi AF, Grossfeld GD, Hayward SW, Carroll PR, Tlsty TD, Cunha GR. 1999. Carcinoma-associated fibroblasts direct tumor progression of initiated human prostatic epithelium. Cancer research 59(19): 5002-5011.

Osborne CK, Schiff R. 2011. Mechanisms of endocrine resistance in breast cancer. Annual review of medicine 62: 233-247.

Pajonk F, Himmelsbach J, Riess K, Sommer A, McBride WH. 2002. The

human immunodeficiency virus (HIV)-1 protease inhibitor saquinavir inhibits proteasome function and causes apoptosis and radiosensitization in non-HIV-associated human cancer cells. Cancer research 62(18): 5230-5235.

Pati S, Pelser CB, Dufraine J, Bryant JL, Reitz MS, Jr., Weichold FF. 2002. Antitumorigenic effects of HIV protease inhibitor ritonavir: inhibition of Kaposi sarcoma. Blood 99(10): 3771-3779.

Pelicano H, Xu RH, Du M, Feng L, Sasaki R, Carew JS, Hu Y, Ramdas L, Hu L, Keating MJ et al. 2006. Mitochondrial respiration defects in cancer cells cause activation of Akt survival pathway through a redox-mediated mechanism. The Journal of cell biology 175(6): 913-923.

Pessler D, Rudich A, Bashan N. 2001. Oxidative stress impairs nuclear proteins binding to the insulin responsive element in the GLUT4 promoter. Diabetologia 44(12): 2156-2164.

Pfaffl MW. 2001. A new mathematical model for relative quantification in real-time RT-PCR. Nucleic acids research 29(9): e45.

Plastaras JP, Vapiwala N, Ahmed MS, Gudonis D, Cerniglia GJ, Feldman MD, Frank I, Gupta AK. 2008. Validation and toxicity of PI3K/Akt pathway inhibition by HIV protease inhibitors in humans. Cancer biology & therapy 7(5): 628-635.

Pomerantz RJ, Horn DL. 2003. Twenty years of therapy for HIV-1 infection. Nature medicine 9(7): 867-873.

Pore N, Gupta AK, Cerniglia GJ, Jiang Z, Bernhard EJ, Evans SM, Koch CJ, Hahn SM, Maity A. 2006. Nelfinavir down-regulates hypoxia-inducible factor 1alpha and VEGF expression and increases tumor oxygenation: implications for radiotherapy. Cancer research 66(18): 9252-9259.

Portakal O, Ozkaya O, Erden Inal M, Bozan B, Kosan M, Sayek I. 2000. Coenzyme Q10 concentrations and antioxidant status in tissues of breast cancer patients. Clinical biochemistry 33(4): 279-284.

Powers MV, Workman P. 2006. Targeting of multiple signalling pathways by heat shock protein 90 molecular chaperone inhibitors. Endocrine-related cancer 13 Suppl 1: S125-135.

Pyrko P, Kardosh A, Wang W, Xiong W, Schonthal AH, Chen TC. 2007. HIV-1 protease inhibitors nelfinavir and atazanavir induce malignant glioma death by triggering endoplasmic reticulum stress. Cancer research 67(22): 10920-10928.

Radenkovic S, Milosevic Z, Konjevic G, Karadzic K, Rovcanin B, Buta M, Gopcevic K, Jurisic V. 2013. Lactate dehydrogenase, catalase, and superoxide dismutase in tumor tissue of breast cancer patients in respect to mammographic findings. Cell biochemistry and biophysics 66(2): 287-295.

Ray PD, Huang BW, Tsuji Y. 2012. Reactive oxygen species (ROS) homeostasis and redox regulation in cellular signaling. Cellular signalling 24(5): 981-990.

Reeder JG, Vogel VG. 2008. Breast cancer prevention. Cancer treatment and research 141: 149-164.

Reliene R, Schiestl RH. 2006. Antioxidant N-acetyl cysteine reduces incidence and multiplicity of lymphoma in Atm deficient mice. DNA repair 5(7): 852-859.

Rengan R, Mick R, Pryma D, Rosen MA, Lin LL, Maity AM, Evans TL, Stevenson JP, Langer CJ, Kucharczuk J et al. 2012. A phase I trial of the HIV protease inhibitor nelfinavir with concurrent chemoradiotherapy for unresectable stage IIIA/IIIB non-small cell lung cancer: a report of toxicities and clinical response. Journal of thoracic oncology : official publication of the International Association for the Study of Lung Cancer 7(4): 709-715.

Reyskens KM, Essop MF. 2014. HIV protease inhibitors and onset of cardiovascular diseases: A central role for oxidative stress and dysregulation of the ubiquitin-proteasome system. Biochimica et biophysica acta 1842(2): 256-268.

Riddle TM, Kuhel DG, Woollett LA, Fichtenbaum CJ, Hui DY. 2001. HIV protease inhibitor induces fatty acid and sterol biosynthesis in liver and adipose tissues due to the accumulation of activated sterol regulatory element-binding proteins in the nucleus. The Journal of biological chemistry 276(40): 37514-37519.

Ridnour LA, Oberley TD, Oberley LW. 2004. Tumor suppressive effects of MnSOD overexpression may involve imbalance in peroxide generation versus peroxide removal. Antioxidants & redox signaling 6(3): 501-512.

Rodriguez AM, Carrico PM, Mazurkiewicz JE, Melendez JA. 2000. Mitochondrial or cytosolic catalase reverses the MnSOD-dependent inhibition of proliferation by enhancing respiratory chain activity, net ATP production, and decreasing the steady state levels of H(2)O(2). Free radical biology & medicine 29(9): 801-813.

Rodriguez C, Mayo JC, Sainz RM, Antolin I, Herrera F, Martin V, Reiter RJ. 2004. Regulation of antioxidant enzymes: a significant role for melatonin. Journal of pineal research 36(1): 1-9.

Rojo AI, Salinas M, Martin D, Perona R, Cuadrado A. 2004. Regulation of Cu/Zn-superoxide dismutase expression via the phosphatidylinositol 3 kinase/Akt pathway and nuclear factor-kappaB. The Journal of neuroscience : the official journal of the Society for Neuroscience 24(33): 7324-7334.

Rubbo H, Radi R, Anselmi D, Kirk M, Barnes S, Butler J, Eiserich JP, Freeman

BA. 2000. Nitric oxide reaction with lipid peroxyl radicals spares alpha-tocopherol during lipid peroxidation. Greater oxidant protection from the pair nitric oxide/alpha-tocopherol than alpha-tocopherol/ascorbate. The Journal of biological chemistry 275(15): 10812-10818.

Rudich A, Ben-Romano R, Etzion S, Bashan N. 2005. Cellular mechanisms of insulin resistance, lipodystrophy and atherosclerosis induced by HIV protease inhibitors. Acta physiologica Scandinavica 183(1): 75-88.

Rudich A, Vanounou S, Riesenberg K, Porat M, Tirosh A, Harman-Boehm I, Greenberg AS, Schlaeffer F, Bashan N. 2001. The HIV protease inhibitor nelfinavir induces insulin resistance and increases basal lipolysis in 3T3-L1 adipocytes. Diabetes 50(6): 1425-1431.

Rusconi S, La Seta Catamancio S. 2002. HIV-1 protease inhibitors in development. Expert opinion on investigational drugs 11(3): 387-395.

Sablina AA, Budanov AV, Ilyinskaya GV, Agapova LS, Kravchenko JE, Chumakov PM. 2005. The antioxidant function of the p53 tumor suppressor. Nature medicine 11(12): 1306-1313.

Sarkar S, Dutta D, Samanta SK, Bhattacharya K, Pal BC, Li J, Datta K, Mandal C, Mandal C. 2013. Oxidative inhibition of Hsp90 disrupts the super-chaperone complex and attenuates pancreatic adenocarcinoma in vitro and in vivo. International journal of cancer Journal international du cancer 132(3): 695-706.

Sato S, Fujita N, Tsuruo T. 2000. Modulation of Akt kinase activity by binding to Hsp90. Proceedings of the National Academy of Sciences of the United States of America 97(20): 10832-10837.

Schroder M, Kaufman RJ. 2005. ER stress and the unfolded protein response. Mutation research 569(1-2): 29-63.

Sener DE, Gonenc A, Akinci M, Torun M. 2007. Lipid peroxidation and total antioxidant status in patients with breast cancer. Cell biochemistry and function 25(4): 377-382.

Senthil K, Aranganathan S, Nalini N. 2004. Evidence of oxidative stress in the circulation of ovarian cancer patients. Clinica chimica acta; international journal of clinical chemistry 339(1-2): 27-32.

Sgadari C, Monini P, Barillari G, Ensoli B. 2003. Use of HIV protease inhibitors to block Kaposi's sarcoma and tumour growth. The lancet oncology 4(9): 537-547.

Shim JS, Rao R, Beebe K, Neckers L, Han I, Nahta R, Liu JO. 2012. Selective inhibition of HER2-positive breast cancer cells by the HIV protease inhibitor nelfinavir. Journal of the National Cancer Institute 104(20): 1576-1590.

Shin SW, Seo CY, Han H, Han JY, Jeong JS, Kwak JY, Park JI. 2009. 15d-

PGJ2 induces apoptosis by reactive oxygen species-mediated inactivation of Akt in leukemia and colorectal cancer cells and shows in vivo antitumor activity. Clinical cancer research : an official journal of the American Association for Cancer Research 15(17): 5414-5425.

Shiota C, Woo JT, Lindner J, Shelton KD, Magnuson MA. 2006. Multiallelic disruption of the rictor gene in mice reveals that mTOR complex 2 is essential for fetal growth and viability. Developmental cell 11(4): 583-589.

Sinha RJ, Singh R, Mehrotra S, Singh RK. 2009. Implications of free radicals and antioxidant levels in carcinoma of the breast: a never-ending battle for survival. Indian journal of cancer 46(2): 146-150.

Sipe HJ, Jr., Jordan SJ, Hanna PM, Mason RP. 1994. The metabolism of 17 beta-estradiol by lactoperoxidase: a possible source of oxidative stress in breast cancer. Carcinogenesis 15(11): 2637-2643.

Sloand EM, Kumar PN, Kim S, Chaudhuri A, Weichold FF, Young NS. 1999. Human immunodeficiency virus type 1 protease inhibitor modulates activation of peripheral blood CD4(+) T cells and decreases their susceptibility to apoptosis in vitro and in vivo. Blood 94(3): 1021-1027.

Song G, Ouyang G, Bao S. 2005. The activation of Akt/PKB signaling pathway and cell survival. Journal of cellular and molecular medicine 9(1): 59-71.

Staal SP. 1987. Molecular cloning of the akt oncogene and its human homologues AKT1 and AKT2: amplification of AKT1 in a primary human gastric adenocarcinoma. Proceedings of the National Academy of Sciences of the United States of America 84(14): 5034-5037.

Stadtman ER, Levine RL. 2000. Protein oxidation. Annals of the New York Academy of Sciences 899: 191-208.

Stamler JS, Lamas S, Fang FC. 2001. Nitrosylation. the prototypic redox-based signaling mechanism. Cell 106(6): 675-683.

Stemke-Hale K, Gonzalez-Angulo AM, Lluch A, Neve RM, Kuo WL, Davies M, Carey M, Hu Z, Guan Y, Sahin A et al. 2008. An integrative genomic and proteomic analysis of PIK3CA, PTEN, and AKT mutations in breast cancer. Cancer research 68(15): 6084-6091.

Sullivan R, Graham CH. 2008. Chemosensitization of cancer by nitric oxide. Current pharmaceutical design 14(11): 1113-1123.

Sundaresan M, Yu ZX, Ferrans VJ, Sulciner DJ, Gutkind JS, Irani K, Goldschmidt-Clermont PJ, Finkel T. 1996. Regulation of reactive-oxygen-species generation in fibroblasts by Rac1. The Biochemical journal 318 (Pt 2): 379-382.

Tebas P, Powderly WG. 2000. Nelfinavir mesylate. Expert opinion on pharmacotherapy 1(7): 1429-1440.

Thannickal VJ, Fanburg BL. 2000. Reactive oxygen species in cell signaling. American journal of physiology Lung cellular and molecular physiology 279(6): L1005-1028.

Thomas S, Sharma N, Golden EB, Cho H, Agarwal P, Gaffney KJ, Petasis NA, Chen TC, Hofman FM, Louie SG et al. 2012. Preferential killing of triple-negative breast cancer cells in vitro and in vivo when pharmacological aggravators of endoplasmic reticulum stress are combined with autophagy inhibitors. Cancer letters 325(1): 63-71.

Toschi E, Sgadari C, Malavasi L, Bacigalupo I, Chiozzini C, Carlei D, Compagnoni D, Bellino S, Bugarini R, Falchi M et al. 2011. Human immunodeficiency virus protease inhibitors reduce the growth of human tumors via a proteasome-independent block of angiogenesis and matrix metalloproteinases. International journal of cancer Journal international du cancer 128(1): 82-93.

Touzet O, Philips A. 2010. Resveratrol protects against protease inhibitor-induced reactive oxygen species production, reticulum stress and lipid raft perturbation. Aids 24(10): 1437-1447.

Toyokuni S, Okamoto K, Yodoi J, Hiai H. 1995. Persistent oxidative stress in cancer. FEBS letters 358(1): 1-3.

Tsurutani J, Steinberg SM, Ballas M, Robertson M, LoPiccolo J, Soda H, Kohno S, Egilsson V, Dennis PA. 2007. Prognostic significance of clinical factors and Akt activation in patients with bronchioloalveolar carcinoma. Lung cancer 55(1): 115-121.

Vander Heiden MG, Plas DR, Rathmell JC, Fox CJ, Harris MH, Thompson CB. 2001. Growth factors can influence cell growth and survival through effects on glucose metabolism. Molecular and cellular biology 21(17): 5899-5912.

Veal EA, Day AM, Morgan BA. 2007. Hydrogen peroxide sensing and signaling. Molecular cell 26(1): 1-14.

Vincent S, Tourniaire F, El Yazidi CM, Compe E, Manches O, Plannels R, Roche R. 2004. Nelfinavir induces necrosis of 3T3F44-2A adipocytes by oxidative stress. Journal of acquired immune deficiency syndromes 37(5): 1556-1562.

Wang JM, Chao JR, Chen W, Kuo ML, Yen JJ, Yang-Yen HF. 1999. The antiapoptotic gene mcl-1 is up-regulated by the phosphatidylinositol 3-kinase/Akt signaling pathway through a transcription factor complex containing CREB. Molecular and cellular biology 19(9): 6195-6206.

Wang X, Mu H, Chai H, Liao D, Yao Q, Chen C. 2007. Human immunodeficiency virus protease inhibitor ritonavir inhibits cholesterol efflux from human macrophage-derived foam cells. The American journal of pathology 171(1): 304-314.

Weiss RA. 1993. How does HIV cause AIDS? Science 260(5112): 1273-1279.

Wlodawer A. 2002. Rational approach to AIDS drug design through structural biology. Annual review of medicine 53: 595-614.

Woo JH, Kim YH, Choi YJ, Kim DG, Lee KS, Bae JH, Min DS, Chang JS, Jeong YJ, Lee YH et al. 2003. Molecular mechanisms of curcumin-induced cytotoxicity: induction of apoptosis through generation of reactive oxygen species, down-regulation of Bcl-XL and IAP, the release of cytochrome c and inhibition of Akt. Carcinogenesis 24(7): 1199-1208.

Wood LD, Parsons DW, Jones S, Lin J, Sjoblom T, Leary RJ, Shen D, Boca SM, Barber T, Ptak J et al. 2007. The genomic landscapes of human breast and colorectal cancers. Science 318(5853): 1108-1113.

Wooster R, Weber BL. 2003. Breast and ovarian cancer. The New England journal of medicine 348(23): 2339-2347.

Xu C, Bailly-Maitre B, Reed JC. 2005. Endoplasmic reticulum stress: cell life and death decisions. The Journal of clinical investigation 115(10): 2656-2664.

Yager JD, Liehr JG. 1996. Molecular mechanisms of estrogen carcinogenesis. Annual review of pharmacology and toxicology 36: 203-232.

Yanchunas J, Jr., Langley DR, Tao L, Rose RE, Friborg J, Colonno RJ, Doyle ML. 2005. Molecular basis for increased susceptibility of isolates with atazanavir resistance-conferring substitution I50L to other protease inhibitors. Antimicrobial agents and chemotherapy 49(9): 3825-3832.

Yang Q, Inoki K, Ikenoue T, Guan KL. 2006a. Identification of Sin1 as an essential TORC2 component required for complex formation and kinase activity. Genes & development 20(20): 2820-2832.

Yang Y, Ikezoe T, Nishioka C, Bandobashi K, Takeuchi T, Adachi Y, Kobayashi M, Takeuchi S, Koeffler HP, Taguchi H. 2006b. NFV, an HIV-1 protease inhibitor, induces growth arrest, reduced Akt signalling, apoptosis and docetaxel sensitisation in NSCLC cell lines. British journal of cancer 95(12): 1653-1662.

Yasukawa T, Tokunaga E, Ota H, Sugita H, Martyn JA, Kaneki M. 2005. S-nitrosylation-dependent inactivation of Akt/protein kinase B in insulin resistance. The Journal of biological chemistry 280(9): 7511-7518.

Yerushalmi R, Hayes MM, Gelmon KA. 2009. Breast carcinoma--rare types: review of the literature. Annals of oncology : official journal of the European Society for Medical Oncology / ESMO 20(11): 1763-1770.

Yuan TL, Cantley LC. 2008. PI3K pathway alterations in cancer: variations on a theme. Oncogene 27(41): 5497-5510.

Zhang B, MacNaul K, Szalkowski D, Li Z, Berger J, Moller DE. 1999.

Inhibition of adipocyte differentiation by HIV protease inhibitors. The Journal of clinical endocrinology and metabolism 84(11): 4274-4277.

Zhong DS, Lu XH, Conklin BS, Lin PH, Lumsden AB, Yao Q, Chen C. 2002. HIV protease inhibitor ritonavir induces cytotoxicity of human endothelial cells. Arteriosclerosis, thrombosis, and vascular biology 22(10): 1560-1566.

Zhou BP, Liao Y, Xia W, Spohn B, Lee MH, Hung MC. 2001. Cytoplasmic localization of p21Cip1/WAF1 by Akt-induced phosphorylation in HER-2/neu-overexpressing cells. Nature cell biology 3(3): 245-252.

Zhou H, Gurley EC, Jarujaron S, Ding H, Fang Y, Xu Z, Pandak WM, Jr., Hylemon PB. 2006. HIV protease inhibitors activate the unfolded protein response and disrupt lipid metabolism in primary hepatocytes. American journal of physiology Gastrointestinal and liver physiology 291(6): G1071-1080.

Zhou H, Jarujaron S, Gurley EC, Chen L, Ding H, Studer E, Pandak WM, Jr., Hu W, Zou T, Wang JY et al. 2007. HIV protease inhibitors increase TNF-alpha and IL-6 expression in macrophages: involvement of the RNA-binding protein HuR. Atherosclerosis 195(1): e134-143.

Zhou L, Yang Q, Wang Y, Hu Y, Luo X, Bai D, Li S. 2008. Synthesis and biological evaluation of novel isopropanolamine derivatives as non-peptide human immunodeficiency virus protease inhibitors. Chemical & pharmaceutical bulletin 56(8): 1147-1152.

Zhou W, Ryan JJ, Zhou H. 2004. Global analyses of sumoylated proteins in Saccharomyces cerevisiae. Induction of protein sumoylation by cellular stresses. The Journal of biological chemistry 279(31): 32262-32268.

Zorov DB, Juhaszova M, Sollott SJ. 2006. Mitochondrial ROS-induced ROS release: an update and review. Biochimica et biophysica acta 1757(5-6): 509-517.

Zuehlke A, Johnson JL. 2010. Hsp90 and co-chaperones twist the functions of diverse client proteins. Biopolymers 93(3): 211-217.

Journal of Medicinal Chemistry

Article

pubs.acs.org/jmc

Synthesis, in Vitro, and in Cell Studies of a New Series of [Indoline-3,2′-thiazolidine]-Based p53 Modulators

Alessia Bertamino,[†] Maria Soprano,[‡] Simona Musella,[†] Maria Rosaria Rusciano,[‡] Marina Sala,[†] Ermelinda Vernieri,[†] Veronica Di Sarno,[†] Antonio Limatola,[§] Alfonso Carotenuto,[§] Sandro Cosconati,[∥] Paolo Grieco,[§] Ettore Novellino,[§] Maddalena Illario,[‡] Pietro Campiglia,*[,†] and Isabel Gomez-Monterrey*[,§]

[†]Department of Pharmacy, University of Salerno, 84084 Fisciano, Salerno, Italy

[‡]Department of Cellular and Molecular Biology and [§]Department of Pharmacy, University of Naples Federico II, 80131 Naples, Italy

[∥]DiSTABiF, Second University of Naples, 81100 Caserta, Italy

Supporting Information

ABSTRACT: Analogues of the previously described spiro-[imidazo[1,5-*c*]thiazole-3,3′-indoline]-2′,5,7(6*H*,7a*H*)-trione p53 modulators were prepared to explore new structural requirements at the thiazolidine domain for the antiproliferative activity and p53 modulation. In cell, antiproliferative activity was evaluated against two human tumor cell lines. Derivative 5-bromo-3′-(cyclohexane carbonyl)-1-methyl-2-oxospiro[indoline-3,2′-thiazolidine] (**4n**) emerged as the most potent compound of this series, inhibiting in vitro 30% of p53−MDM2 interaction at 5 μM and the cell growth of different human tumor cells at nanomolar concentrations. Docking studies confirmed the interactions of **4n** with the well-known Trp23 and Phe19 clefts, explaining the reasons for its binding affinity for MDM2. **4n** at 50 nM is capable of inducing the accumulation of p53 protein, inducing significant apoptotic cell death without affecting the cell cycle progression. Comparative studies using nutlin in the same cellular system confirm the potential of **4n** as a tool for increasing understanding of the process involved in the nontranscriptional proapoptotic activities of p53.

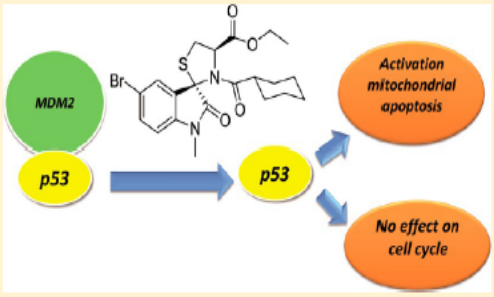

INTRODUCTION

p53 is the tumor suppressor protein that has been the most intensively studied for nearly 30 years.[1] p53 functions mainly as a transcription factor by binding to specific DNA sequences and by transactivating or repressing a large group of target genes.[2] Through these downstream targets, p53 pathway coordinates cell cycle arrest, DNA repair, apoptosis, and senescence to preserve genomic stability and prevent tumor formation in response to cellular insults, including DNA damage, hypoxia, and a deficiency of growth factors or nutrients.[1−4] Recently, novel functions of p53 in metabolism regulation and tumor motility, invasion, and metastasis have been unveiled.[5,6] p53 levels are tightly controlled in unstressed mammalian cells through a continuous cycle of ubiquitylation and degradation by the 26S proteasome, regulated primarily through the interaction of p53 with the ring-finger ubiquitin E3 ligase MDM2.[7] This protein controls the p53 levels through a direct binding interaction that neutralizes p53 transactivation activity, exports nuclear p53, and targets it for degradation via the ubiquitylation−proteasomal pathway.[8−10] Loss of p53 activity, by deletion, mutation, or MDM2 overexpression, is the most common event in the development and progression of cancer,[11,12] while the restoration of endogenous p53 function results in tumor regression in vivo.[1,13] In this context, the rescue of the impaired p53 activity and resensitization to apoptosis in cancer cells by disrupting the MDM2−p53 interaction offers an opportunity for anticancer therapeutics.[14] The tractability of the MDM2−p53 interaction as a drug target has been demonstrated, and a number of classes of potent small molecule inhibitors have been developed.[15] Vassilev et al.[16] identified the first group of molecules that target the MDM2−p53 interaction (Figure 1). These imidazoline derivatives, designated nutlins, specifically bind and dissociate MDM2 from p53, leading to extensive p53 activation and induction of a full-blown p53 response, which can trigger tumor shrinkage in experimental animals. The derivative nutlin-3 is currently undergoing phase I clinical evaluation against advanced solid tumors and hematological malignancies. The benzodiazepines[17] and the spirooxindole-based compounds[18] are other classes of small molecules that have been found to target the p53−MDM2 interaction. These results led to the preclinical development of TDP665759 and MI-319, which disrupt the binding of MDM2 to p53 in vitro and suppress the growth of

Received: February 28, 2013
Published: June 12, 2013

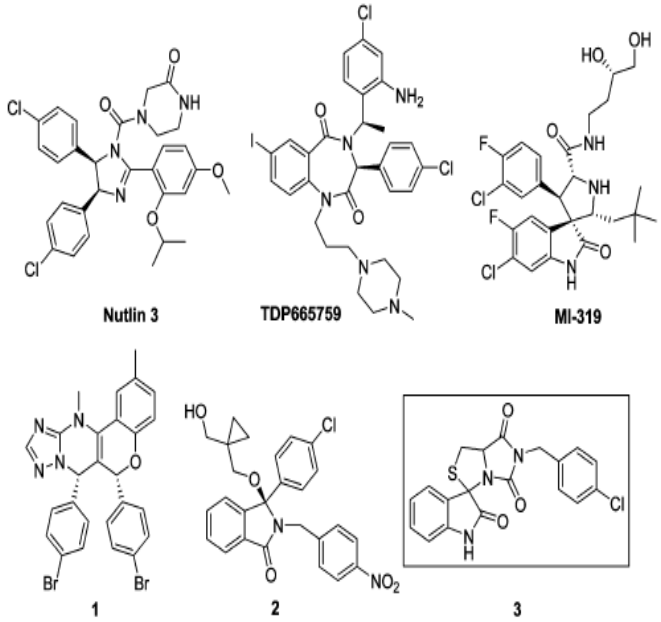

Figure 1. Structures of different inhibitors of p53–MDM2 interaction.

tumor cells both in vitro and in vivo. Both compounds limit tumor growth without causing major toxicity in the surrounding tissue. Although these products induce high levels of p53, these are not sufficient to activate the apoptotic cascade. Other small-molecule inhibitors include chromenotriazolopyrimidines (**1**)[19] and oxoindoles (**2**).[20]

Most of the inhibitors we have described above share a common design of a rigid heterocyclic scaffold highly functionalized with appropriate aryl/alkyl groups, which are supposed to mimic the critical p53 residues that bind MDM2. Different structural studies reveal that the p53–MDM2 protein interaction is mediated by the 15-residue α-helical transactivation domain of p53, which inserts into a hydrophobic cleft on the surface of MDM2.[21] Three residues within this domain, Phe19, Trp23, and Leu26, are essential for MDM2 binding, making this site an attractive target to design small molecules able to mimic the contacts and the orientations of these key amino acids.[22] Previously, we have reported a series of spiro(oxindole-3,3′-thiazolidine)-based derivatives potentially able to mimic at least two critical p53 residues that bind MDM2.[23] Compound **3** inhibited cell growth of different human tumor cells at submicromolar concentrations (IC_{50} in the range of 0.4–0.9 μM). This derivative induced apoptotic cell death after 24 h of treatment at cytotoxic concentrations but did not alter the normal course of cell cycle. However, **3** induced a time-dependent increment of p53 expression, indicating that the activity profiles of the compound might be regulated by this protein. More concretely, NMR studies performed on compound **3** demonstrated the ability of this compound to block p53–MDM2 interaction. In this paper, we describe the design, synthesis, and SAR studies of a more flexible series of spiro(oxindole-3,3′-thiazolidine) derivatives, leading to antiproliferative compounds with significantly improved potency and cellular activity over the parent compounds.

RESULTS AND DISCUSSION

Design. Compound **3** was designed starting from the known spirooxindole derivative MI-319 (Figure 1).[23] Its spiro(oxindole-3,3′-thiazolidine) scaffold allows interesting and efficient structural modifications. One of them, opening the imidazole ring, is described in this paper. In fact, we considered it of interest to manipulate the imidazo nucleus of compound **3** with the aim of altering its conformational properties. The opening of this ring would allow us to access more flexible structures (series **4** and **5**, Figure 2) with a potential third point of diversification through the 4′-carboxyl group of the thiazolidine moiety. This ring could allow the aromatic and/or alkyl side chains to assume more appropriate orientations to interact with the binding site. Accordingly, two small libraries of compounds were considered for synthesis. Both series retain the ester group at position C-4′, while the

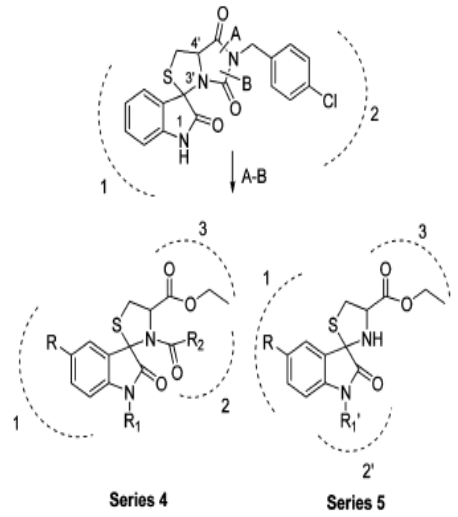

Figure 2. Design of new series **4** and **5**. Dashed lines define hypothetical interaction subsites.

dx.doi.org/10.1021/jm400311n | J. Med. Chem. 2013, 56, 5407–5421

Scheme 1. Synthesis of 2-Oxospiro[indoline-3,2′-thiazolidine]-4′-carboxylate Derivatives (Series 4 and 5)[a]

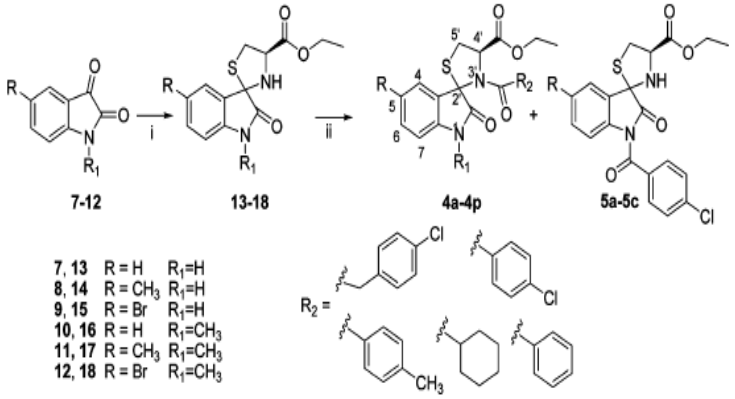

[a]Reagents and conditions: (i) Cys-OEt, $NaHCO_3$ in EtOH; (ii) R_2-COCl, TEA, THF, 2 h, room temp. See Table 1 for the correspondence between number of final products and substituent R, R_1, and R_2.

oxoindole moiety carries either a weak releasing (CH_3) or a withdrawing (Br) electron groups (R). Series **4** contains a substituted phenyl, benzyl, or a cyclohexyl side chains on the N-3′ (R_2), while these groups were positioned on N-1 in the series **5** (R_1).

Chemistry. The new (2′*R*,4′*R*)-ethyl 3′-substituted-2-oxospiro[indoline-3,2′-thiazolidine]-4′-carboxylate derivatives (**4a–f**, **4l–n**) were prepared applying the synthetic route shown in Scheme 1. Starting spirooxoindolethiazolidine skeletons (**13–18**) were constructed by condensation between the isatin derivatives (**7–12**) and cysteine ethyl ester in EtOH. These derivatives were obtained with 80–90% yields, as (2′*R*)/(2′*S*) epimeric mixtures ranging from 60/40 to 40/60 ratios as we previously described.[23,24] The 3′-acyl derivatives were obtained by reaction of compounds **13–18** with the corresponding 2-(4-chlorophenyl)acetyl, 4-chlorobenzoyl, 4-methylbenzoyl, benzoyl, or cyclohexanecarbonyl chlorides in THF using TEA as base.

In these conditions, all final products (**4a–f** and **4h–q**) were obtained as single diastereomers in 32–58% overall yields. These stereoselectivities in the acylation reactions of thiazolidine derivatives have been previously observed by us[24] and other authors[25] and can be explained by the fact that thiazolidines undergo facile ring opening and closure reactions. This favors the formation of thermodynamically more stable diastereoisomers. Moreover, the reaction of intermediates **13–15** (R_1 = H) with 4-Cl benzoyl chloride also gave the 1-substituted derivatives **5a–c** with 8–12% yields. In the synthesis of the 3-cyclohexylcarboxy derivatives **4n–q**, two isomers were obtained in a 11/1 to 6/1 ratio (estimated by ^{1}H NMR), which differs for the cis/trans configuration at the N3′-COC_6H_{11} amide bond. The major isomer (cis) in these mixtures was identified on the basis of the ROE observed in the ROESY spectrum of **4n** between the H-1″ of the cyclohexanecarbonyl group and the H-4′ of the thiazolidine (Figure 3 and Figure S1 in Supporting Information). Cis/trans isomerization about amide bond was evidenced by 2D NMR.[26] In fact, interconversion was demonstrated by an exchange cross-peak between the H-4′ hydrogen signals of the two isomers (Figure S1).

Changes in the condition of reactions that involve an increase of the reaction time (from 2 h to 12 or 24 h) do not significantly modify the above-described results, while increase of temperature resulted in a general decrease of reaction yields.

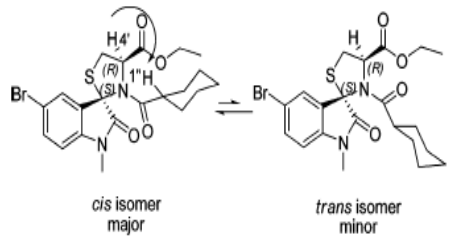

Figure 3. ROE interaction observed between H-4′ and H-1″ in the ROESY spectrum of compound **4n**.

However, with the use of microwave (Scheme 2), the reaction of intermediate **15** with 4-chlorobenzoyl chloride led to a mixture of two diastereoisomers (2′*S*,4′*R*)-**4f** and (2′*R*,4′*R*)-**4g** and the 1-substituted derivative **5c** in 33%, 15%, and 9% yields, respectively. In the same conditions and using cyclohexanecarbonyl chloride as acylation agent, we observed the formation of only a diastereoisomer (2′*S*,4′*R*)-**4q** (42%), the 1-cyclohexacarbonyl derivative **5d** (25%), and a minor product with structure of 2-oxo-5′*H*-spiro[indoline-3,2′-thiazole]-4′-ethyloxycarbonyl **6d** with a 15% yield.

The assignment of the relative configuration at the C-2′ asymmetric center as *R* was determined on the basis of a ROE enhancement between H-4′ and H-4 observed in the 2D ROESY spectra of **4g**. Absolute configurations were defined hypothesizing configuration retention at C-4′ according to structural determination achieved with the previous series.[23] In contrast, this ROE enhancement was not observed in any of the other derivatives, which were assigned to the *S* stereochemistry at C-2′.

The 1-(4-chlorobenzoyl)-2-oxospiro[indoline-3,2′-thiazolidine] derivatives (**5a–c**) were prepared using an alternative synthetic route as shown in Scheme 3. Treatment of isatins **7–9** with 4-chlorobenzoyl chloride in DCM and TEA gave the corresponding intermediates **19–21** which were condensed with cysteine ethyl ester in EtOH. In this condition, compounds **5a–c** were obtained as single (2′*S*,4′*R*) diastereoisomer in 60–63% yields according to their 1D and 2D NMR spectra. In addition, working with the 5-substituted intermediates **20** and **21**, we also observed the formation of thiazoline derivatives **6b** and **6c** with 11% and 8%, respectively. Moreover, the reaction of **7–9** with cyclohexanecarbonyl chloride did not lead to the desired 1-(cyclohexylcarbonyl)

dx.doi.org/10.1021/jm400311n | J. Med. Chem. 2013, 56, 5407–5421

Scheme 2. Reaction of Ethyl 5-Bromo-2-oxospiro[indoline-3,2′-thiazolidine]-4′-carboxylate with 4-Chlorobenzoyl and Cyclohexanecarbonyl Chlorides[a]

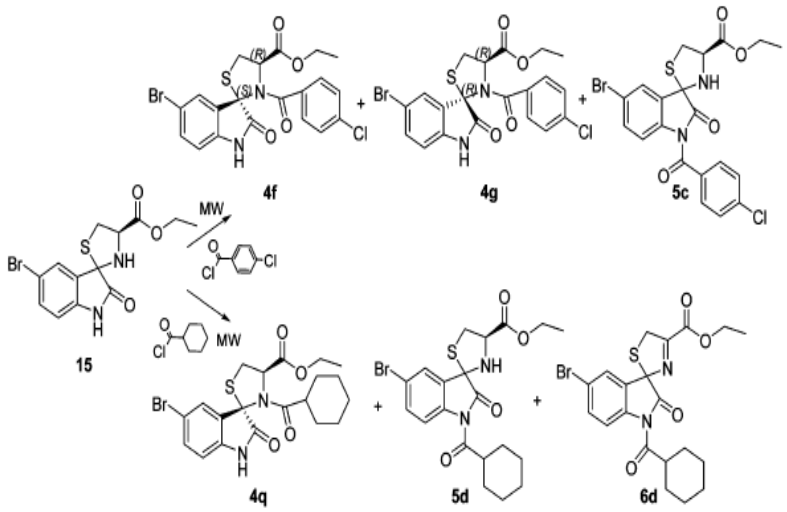

[a]Microwave, 10 min, 100 °C, 2 bar.

Scheme 3. Synthesis of (2′*S*,4′*R*)-Ethyl 2-Oxospiro[indoline-3,2′-thiazolidine]-4′-carboxylate Derivatives (5) and Ethyl 2-Oxo-5′*H*-spiro[indoline-3,2′-thiazole]-4′-carboxylate Derivatives (6)[a]

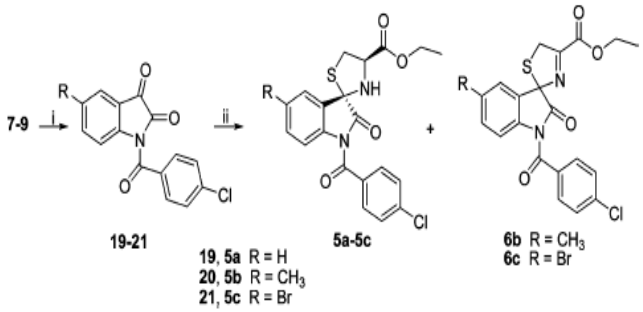

[a]Reagents and conditions: (i) 4-Cl-C_6H_4COCl, TEA, THF, 2 h, room temp; (ii) Cys-OEt, $NaHCO_3$ in EtOH.

derivative, recovering the starting materials. Poor reactivity of cyclohexane carbonyl chloride could be explained, if compared to 4-chlorobenzoyl chloride, by considering a higher steric hindrance of the first. Modifications of reaction conditions including changes of solvent, increase of temperature, or use of microwaves led to the same negative results.

Biological Effects. *Antiproliferative Activity.* The spirooxoindolethiazolidine derivatives were examined for antiproliferative activity against two tumor cell lines: the human breast adenocarcinoma MCF-7 and human colon carcinoma HT-29 at 24 h. The obtained IC_{50} values are summarized in Table 1.

Compound **3**, considered our hit compound, showed a similar micromolar antiproliferative activity against the two tumoral cell lines used in the assay. The opening derivatives **4a**, **4b**, and **4c** showed an elevated activity with IC_{50} values in the micromolar range against MCF-7 and submicromolar against HT29 cell lines. Exchange of the 4-chlorobenzyl group for 4-chlorophenyl gave compounds **4d–f**, more active against MCF-7 cells while **4f** was 6-fold more active against the HT29 cell line. The activity data for compounds **4a–f** and **4h–j** (IC_{50} from 0.08 to >4.0 μM) indicated that the nature of the substituents on the oxoindole moiety markedly affects the antiproliferative activity profile of these compounds. Contrary to what was observed in the precedent series (compound **3**),[23] the presence of an electron-withdrawing group, such as the bromide group, at position C-5 of the indole system caused an increase of the activity of the corresponding analogues **4c**, **4f**, and **4j** in both cell lines but particularly on HT29 cells. We observed that the configuration at the 2′ carbon has a notable influence on the cytotoxic activity on this cell line. In fact, (2′*R*,4′*R*)-**4g** was 18-fold less potent than its diastereoisomer (2′*S*,4′*R*)-**4f** on HT29 cells and 3-fold less potent on the MCF-7 cell line. The introduction of a methyl group at N-1 improved the activity of compounds **4h–j** compared to the non-methylated analogues (**4d–f**), especially on the colon cell line. The most potent compound of this subseries, **4j**, gave IC_{50} values of 520 and 80 nM in MCF-7 and HT29 cell lines, respectively. Modifications of **4j** at the N-3′ position produced different effects: the introduction of 4-Cl-benzyl group increased (2-fold) the antiproliferative activity of analogue **4k** on MCF-7 cells and reduced (4-fold) its activity on HT29 cells. A similar behavior was observed with compound **4l**, which contains a phenyl group at the N-3′ position. The introduction of a 4-CH_3-phenyl or a cyclohexyl group led to compounds **4m** and **4n**, which showed an antiproliferative activity in the nanomolar range (IC_{50} < 100 nM, for both cell lines). In particular, **4n** was 14-fold more potent than its analogue **4j** on MCF-7 cells. Further modifications of this compound involving

dx.doi.org/10.1021/jm400311n | J. Med. Chem. 2013, 56, 5407–5421

Table 1. Antiproliferative Activity of Spiro[indoline-3,2′-thiazolidine] (4 and 5) and Spiro[indoline-3,2′-thiazole] (6) Derivatives

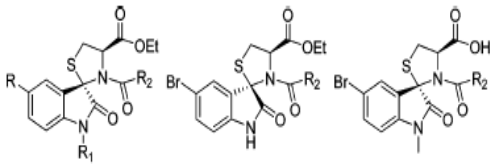

4a-f,4h-4q 4g 4r

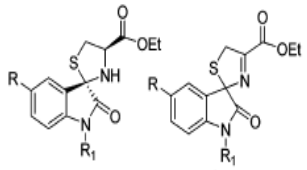

5 6

				$IC_{50} \pm SD$ (μM)[a]	
compd	R	R_1	R_2	MCF-7[b]	HT29[c]
3	H	H		1.21 ± 0.6	1.60 ± 0.4
4a	H	H	$CH_2C_6H_4$(4-Cl)	>5	1.00 ± 0.2
4b	CH_3	H	$CH_2C_6H_4$(4-Cl)	4.81 ± 1.0	0.78 ± 0.2
4c	Br	H	$CH_2C_6H_4$(4-Cl)	2.90 ± 0.8	0.66 ± 0.1
4d	H	H	C_6H_4(4-Cl)	2.15 ± 0.7	3.69 ± 0.9
4e	CH_3	H	C_6H_4(4-Cl)	2.12 ± 0.7	1.09 ± 0.6
4f	Br	H	C_6H_4(4-Cl)	0.90 ± 0.2	0.11 ± 0.09
4g	Br	H	C_6H_4(4-Cl)	3.00 ± 0.2	2.00 ± 0.8
4h	H	CH_3	C_6H_4(4-Cl)	4.52 ± 1.1	0.18 ± 0.09
4i	CH_3	CH_3	C_6H_4(4-Cl)	1.23 ± 0.4	0.12 ± 0.07
4j	Br	CH_3	C_6H_4(4-Cl)	0.52 ± 0.3	0.08 ± 0.01
4k	Br	CH_3	$CH_2C_6H_4$(4-Cl)	0.27 ± 0.1	0.36 ± 0.09
4l	Br	CH_3	C_6H_5	0.31 ± 0.1	0.21 ± 0.2
4m	Br	CH_3	C_6H_4(4-CH_3)	0.06 ± 0.05	0.09 ± 0.05
4n	Br	CH_3	cyclohexyl	0.04 ± 0.01	0.07 ± 0.01
4o	CH_3	CH_3	cyclohexyl	1.20 ± 0.6	1.10 ± 0.6
4p	H	CH_3	cyclohexyl	2.30 ± 0.8	1.90 ± 0.8
4q	Br	H	cyclohexyl	0.22 ± 0.1	0.56 ± 0.1
4r	Br	CH_3	cyclohexyl	2.01 ± 0.9	1.90 ± 0.7
5a	H	COC_6H_4(4-Cl)	H	1.01 ± 0.6	1.03 ± 0.8
5b	CH_3	COC_6H_4(4-Cl)	H	3.46 ± 0.9	0.23 ± 0.1
5c	Br	COC_6H_4(4-Cl)	H	0.15 ± 0.1	0.02 ± 0.01
5d	Br	cyclohexyl	H	2.08 ± 0.8	1.40 ± 0.8
6b	CH_3	COC_6H_4(4-Cl)		2.78 ± 0.9	0.21 ± 0.1
6c	Br	COC_6H_4(4-Cl)		0.86 ± 0.4	0.20 ± 0.1
6d	Br	cyclohexyl		1.63 ± 0.6	0.85 ± 0.4

[a]Data represent mean values (±SD) of three independent determinations. [b]Human breast adenocarcinoma cell line. [c]Human colon carcinoma cell line.

substitution or loss of the Br atom at the C5 (compounds **4o** and **4p**), lack of the CH_3 group at N1 (compound **4q**), and ethyl ester hydrolysis to carboxylic acid (**4r**) all resulted in a loss of activity in the resulting compounds. These derivatives were less potent than **4n** against MCF-7 (from 5- to 60-fold) and HT29 (from 8- to 28-fold) cell lines.

Furthermore, switching the 4-Cl-benzoyl or cyclohexylcarbonyl groups from position N3′ to position N1 led to contrasting results. 4-Chlorobenzoyl derivative **5c** showed cytotoxic activity in the nanomolar range on both cell lines (IC_{50} of 150 and 20 nM) and was ∼6-fold more potent than its regioisomer **4f**. Derivative **5a** was also 2- to 3-fold more potent than its regioisomer **4d**, while compound **5b** containing a CH_3 group at C-5 position showed a slight decrease of activity on MCF-7 cells compared to its analogue **4e**. In contrast, compound **5b** was 4-fold more potent than **4e** against HT29 cells. Surprisingly, the same change of the position for cyclohexyl carbonyl group (**4q** versus **5d**) led to a considerable decrease in activity. In fact, **5d** was 10-fold less potent than its regioisomer **4q** on MCF-7 cells. Finally, the presence of a more planar thiazoline ring in the structure produced different effects: derivative **6b** retained the cytotoxic activity of its thiazolidine analogue **5b**, while compound **6c** was 6- and 10-fold less active than **5c** on both cell lines. In contrast, compound **6d** showed a slight increase of activity (∼1.5-fold) on both cell lines compared to **5d**.

The antiproliferative activity of the most potent compound against both cell lines, **4n**, was also analyzed against a panel of human tumor cell lines, including PC3 (prostate), U937 (leukemia), Calu (lung), HEPG2 (liver), and C643 (anaplastic

dx.doi.org/10.1021/jm400311n | J. Med. Chem. 2013, 56, 5407−5421

Table 2. Antiproliferative Activity of 4n on Multiple Human Tumor Cell Lines and One Normal Cell Line

		$IC_{50} \pm SD$ (μM)[a]		
	cell line	4n	nutlin-3	Dox
origin tumor				
breast	MCF-7	0.04 ± 0.01	2.9 ± 0.31[27a]	0.02 ± 0.01
prostate	PC3	0.41 ± 0.21	30.3 ± 2.9[27b]	0.75 ± 0.10
leukemia	U937	0.07 ± 0.01	15.6 ± 1.9	0.12 ± 0.03
lung	Calu	0.10 ± 0.06	27.2 ± 5.3	1.81 ± 0.33
liver	HEPG2	0.14 ± 0.06	10.2 ± 5.1[27c]	0.08 ± 0.01
anaplastic thyroid	C643	0.55 ± 0.08	23 ± 11.2	0.07 ± 0.01
origin normal				
human gingival fibroblast	HGF	1.60 ± 0.15	1.40 ± 3.6	0.50 ± 0.15

[a]Data represent mean values (±SD) of three independent determinations at 24 h.

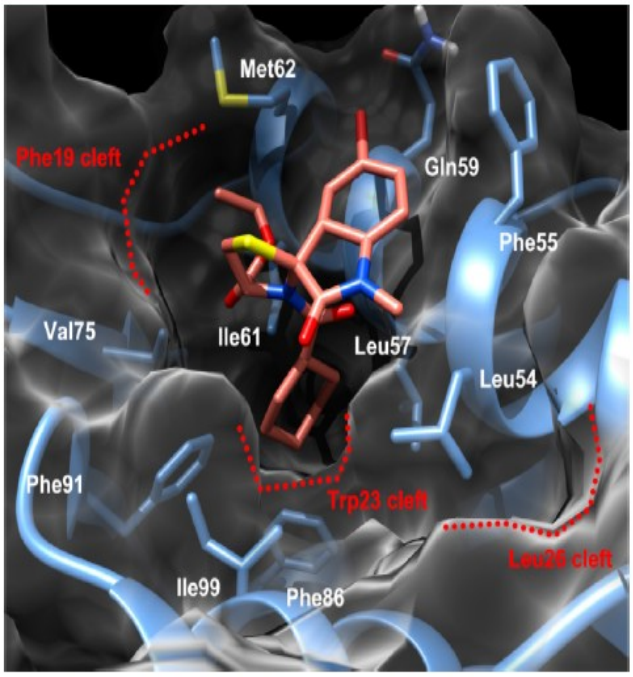

Figure 4. Predicted binding mode for compound 4n in the MDM2 binding site. The ligand is represented as pink stick, while the protein is represented as blue sticks and ribbons and transparent white surface.

thyroid) human cell lines (Table 2). Doxorubicin and nutlin-3 were used as reference cytotoxic agents. Data on the MCF-7 cell line are also reported in Table 2. In all tested cells lines, compound **4n** showed marked cytotoxic potency with IC_{50} in the range 0.07–0.55 μM, while nutlin-3 was much less effective in our panel, in accordance with some data found in the literature.[27] **4n** was 18-fold more potent than doxorubicin on the Calu cell line and was equipotent to doxorubicin in PC3 and U937 cell lines.

Table 2 also shows that **4n** inhibited the cellular growth of a human gingival fibroblast (HGF) normal cell line at low micromolar concentration. This cytotoxicity was similar to that shown by nutlin-3 on the same line and was 4 times less than that caused by doxorubicin. These data seem to indicate that **4n** has a good profile of cell selectivity.

In Vitro Modulation of p53–MDM2 Interaction. In order to test the ability of **4n** to inhibit p53–MDM2 interaction, we performed an in vitro binding assay using ImmunoSet p53/MDM2 complex ELISA (Figure S4). Nutlin-3 and compound **3** were also evaluated as references. In this assay and for all compounds, the minimum effective concentration was determined at 5 μM. At this concentration, the percentage inhibition was 19% for nutlin-3 and 25% for **3**, while compound **4n** has proved to be more effective inhibiting 30% of p53–MDM2 interaction.

Molecular Modeling Studies. To better rationalize the reasons behind the activity of our indoline-3,2′-thiazolidines, molecular docking studies were undertaken on **4n** which is the most potent antiproliferative agent in this series. To date, several X-ray structures are reported of the complex between MDM2 and different small molecules, and among these, we decided to choose the structure having PDB code 1LBL[28] in which MDM2 was solved at a very high resolution (1.60 Å) in complex with a spirooxindole derivative that is structurally related to the derivatives described herein. Therefore, this structure was used to dock, through the Autodock 4.2 (AD4) software,[29] compound **4n** and the cocrystal ligand. Docking of the latter compound confirmed the good performance of this software, which was able to predict the experimental binding pose with a root-mean-square deviation (rmsd) of 1.03 Å. For

dx.doi.org/10.1021/jm400311n | J. Med. Chem. 2013, 56, 5407–5421

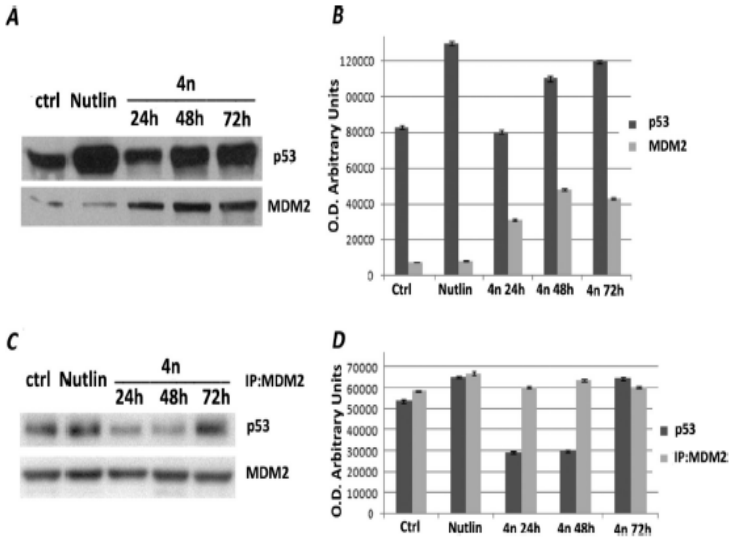

Figure 5. (A) MCF-7 cells were treated with 50 nM **4n** for 24, 48, and 72 h or 3 μM nutlin-3 for 24 h. Total cell lysates were analyzed by Western blotting for p53 and MDM2 with specific antibodies. (C) A similar experiment was performed for p53 after MDM2 immunoprecipitation. (B, D) Immunoblots were quantified by ImageQuant densitometric analysis. Protein expression levels were measured in arbitrary densitometric units, and data show the mean values ± SEM calculated from relative protein expression levels determined in three separate experiments.

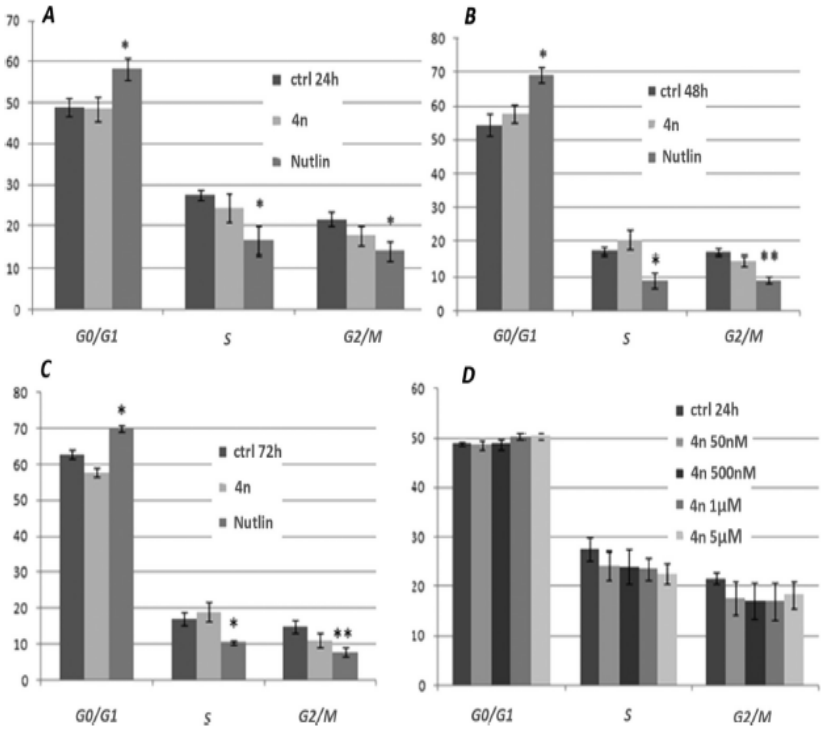

Figure 6. Effects of **4n** on cell cycle progression analyzed for DNA content by FACS in breast cancer MCF-7 cells untreated or treated with 50 nM **4n** or 3 μM nutlin-3 at (A) 24, (B) 48, and (C) 72 h and (D) MCF-7 cells untreated or treated with 50, 500, 1000, and 5000 nM **4n** at 24 h. The distribution and percentage of cells in G1, S, and G2/M phases of the cell cycle are indicated. Data points are mean values ± SEM. Significance is assumed at (*) $p < 0.05$, (**) $0.01 < p < 0.05$, (***) $p < 0.01$.

4n, the same calculations converged toward a single solution in which the lowest energy (ΔG_{AD4}) binding conformation was also belonging to the most populated cluster (f_{occ}). In particular, in the binding pose (ΔG_{AD4} = −8.32 kcal/mol, f_{occ} = 86/100) predicted for **4n** (Figure 4) the ligand is inserted into the MDM2 binding site so that the 3-cyclohexylcarboxy substituent is buried in the so-called Trp23 pocket, making favorable van der Waals contacts with Ile61, Val75, Phe86, Phe91, and Ile99 side chains. On the other hand, the MDM2 Phe19 subpocket is occupied by the ligand ethyl ester chain that is able to make direct contacts with Ile61 and Met62 side chains. The presence of this interaction could partially explain

dx.doi.org/10.1021/jm400311n | J. Med. Chem. 2013, 56, 5407−5421

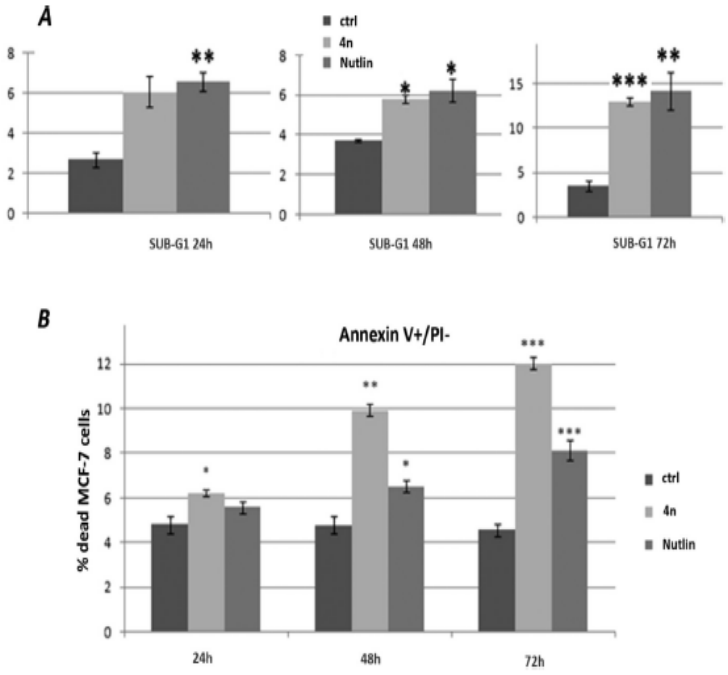

Figure 7. (A) Representative subG1 populations calculated from FACS histograms. MCF-7 cells were incubated with 50 nM **4n** or with 3 μM nutlin-3 for 24, 48, and 72 h. Data are expressed as the percentage of subG1 cells. (B) A similar experiment was performed, and the cells were analyzed by FACS for the occurrence of apoptosis (FITC-annexin binding). Values represent the mean ± SEM. Significance is assumed at (*) $p < 0.05$, (**) $0.01 < p < 0.05$, (***) $p < 0.01$.

why hydrolysis of the ethyl ester chain to the corresponding carboxylic acid results in the loss of activity. On the other hand, reduction of membrane penetration cannot be ruled out. Interestingly, the Leu26 cleft does not seem to be completely filled by the 5-bromo-2-oxoindoline nucleus that instead forms additional hydrophobic interactions with Leu54 through its N1-methyl substituent. This latter hydrophobic interaction could explain why **4d–f** are generally less active than their methylated analogues **4h–j**. In this position, edge–face π–π interaction with the Phe55 residue is also established in a shallow and rather liphophilic portion of the MDM2 protein in which the 5-bromine atom fills the crevice between Phe55, Met62, and Gln59. Indeed, the interaction with the Phe55 residue has already been detected through X-ray studies for other structurally unrelated ligands in a very recent work by Olson's group.[30] Interestingly, in the binding pose suggested by AD4 the ligand N3′-COC_6H_{11} amide bond adopts a cis configuration as already suggested by ROESY experiments.

Modulation of p53–MDM2 Interaction in Cell. To confirm in cell the ability of **4n** to inhibit the MDM2–p53 interaction, the expression levels of these two proteins were evaluated by Western blot after 24, 48, and 72 h of **4n** treatment and after 24 h with nutlin-3. Compound concentrations close to their IC_{50} on the MCF-7 cell line were used in this assay (i.e., 50 nM for **4n** and 3 μM for nutlin-3). In these conditions, **4n** induced the accumulation of p53 and MDM2 proteins, (Figure 5A and 5B). To determine whether **4n** was able to prevent MDM2–p53 interaction, p53 expression levels were measured after MDM2 immunoprecipitation (Figure 5C and Figure 5D). Cells were treated with **4n** for 24, 48, and 72 h or with nutlin-3 for 24 h. MDM2 was immunoprecipitated. The samples underwent Western blot to visualize p53 and to evaluate its association with MDM2. Treatment with **4n** reduced the MDM2–p53 interaction as evidenced by a significant decrease in the p53 levels bound to MDM2 at 24 and 48 h. Nutlin-3 seems to be inactive in this immunoprecipitation assay. We can hypothesize that nutlin acts more quickly than **4n**; its unresponsiveness to the test may be due to a recombination of p53 and MDM2 within 24 h. Interestingly, this recombination is also observed for **4n** after 72 h.

Cell-Cycle Progression. To investigate the effect in the reduction of tumor cell survival mediated by **4n**, MCF-7 cell cycle was analyzed after 24, 48, and 72 h of treatment. Again, nutlin-3 was used for comparison. Nutlin-3 (3 μM) induced cell cycle arrest, as shown by G0/G1 phase block and in accordance with literature data.[16] Compound **4n** (50 nM) did not significantly affect cell cycle. Indeed, **4n**-treated cells showed the same distribution in G1, S, and G2/M phases of untreated cell at 24, 48, and 72 h (Figure 6A, Figure 6B, and Figure 6C). When the same experiment was performed with increasing concentration of **4n** (500 nM, 1 μM, 5 μM), no difference in cell cycle effect was found compared to initial concentration (Figure 6 D).

Apoptotic Cell Death. Cell death was evaluated with preliminary, qualitative assessment of apoptosis by subG1 analysis. The treatment with **4n** (50 nM) showed a strong increase of the subG1 peak, which rose in a time dependent manner (Figure 7A). Nutlin-3 (3 μM) also induced a significant increase of cell death. However, the subG1 peak may consist of apoptotic and necrotic cells. To discriminate between the two possibilities, an annexin V binding assay was performed. **4n** and nutlin-3 induced a significant increase of cell fraction in early apoptosis (Figure 7B). In particular, the apoptotic cell percentage increased from 4% of untreated cells to 10% and 12% of cells after 48 and 72 h of **4n** treatment. Nutlin-3 determined a lower increase of early apoptosis compared to **4n**.

Although p53 plays a pivotal role in regulating cell cycle and apoptosis,[2,3] treatment of MCF-7 cells with **4n** or nutlin-3 has a

dx.doi.org/10.1021/jm400311n | J. Med. Chem. 2013, 56, 5407–5421

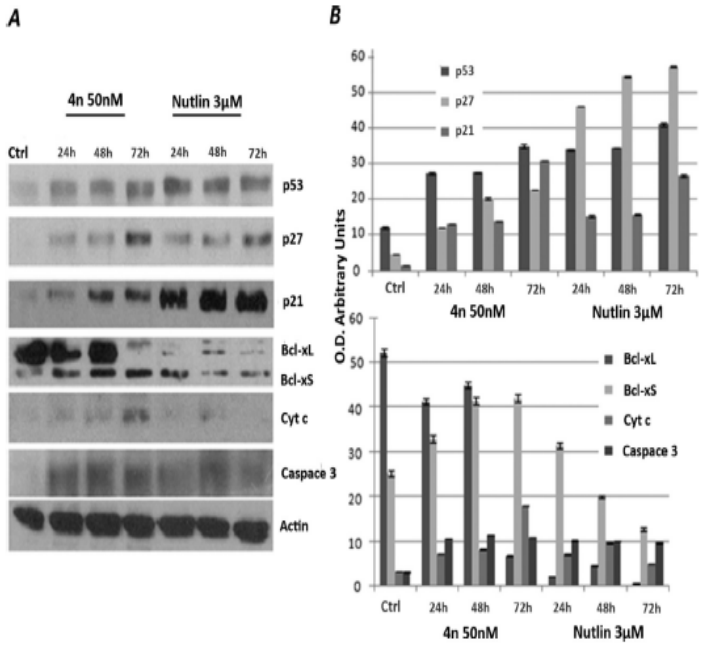

Figure 8. (A) MCF-7 cells were treated with 50 nM **4n** or 3 μM nutlin for the indicated time intervals. Total cell lysates were analyzed by Western blotting for phosphotyrosine p53, p21, p27, Bcl-xL/S, cytocrome *c*, and caspase-3 with specific antibodies. (B) Immunoblots were quantified by ImageQuant densitometric analysis. Protein expression levels were measured in arbitrary densitometric units, and data show the mean values ± SEM calculated from relative protein expression levels determined in three separate experiments: (*) $p < 0.05$ vs protein expression levels in untreated control cells.

different impact on both mechanisms. Indeed, whereas nutlin-3 determined a cell cycle arrest, **4n** induced apoptotic cell death. To investigate the cell death mechanism induced by **4n**, the p53 dependent apoptotic pathway was analyzed by Western blot. The analysis of the expression levels of p53 and p53 transcriptional targets, such as p21 and p27, showed a progressive increase of these proteins during the treatment with **4n** in a time dependent manner (Figure 8). However, these increases do not seem to be sufficient to induce cell cycle arrest. On the contrary, nutlin-3 showed a greater accumulation of p21 than **4n** at 24, 48, and 72 h, inducing cell cycle arrest (Figure 8A and Figure 8B). Cells committed to die via p53-dependent apoptosis typically follow the mitochondrial pathway, although p53 can also modulate cell death through death receptors.[31,32] p53 has been reported to trigger apoptosis by modulation of gene transcription of Bcl-2 family members and by physical interaction with these proteins.[31−33] Western blot results indicated that **4n** and nutlin regulate Bcl-2 members, reducing the antiapoptotic Bcl-xL protein and increasing the proapoptotic Bcl-xS protein, although the two drugs affect Bcl-xL/S expression at different times.

The induction of **4n**-mediated apoptosis was confirmed by the release of cytochrome *c* from mitochondria to the cytosol, which increased at various time intervals and became particularly evident at 72 h of drug treatment. Also nutlin-3 affects cytochrome *c* release at 48 h even if at lower levels compared to **4n**.[34,35] One of the final effectors of the apoptotic process is caspase-3, which is activated by extrinsic and intrinsic or mitochondrial pathways. The cleavage of caspase-3 is a clear indicator of apoptosis; hence, we analyzed the p53 fragment with a specific antibody. Western blot analysis revealed that both **4n** and nutlin-3 induced an accumulation of the cleavage product of caspase-3. All these findings suggest that in the MCF-7 breast cancer cell line, cell cycle arrest is the main molecular mechanism mediated by nutlin-3. On the contrary, 50 nM **4n** did not block cell cycle progression but rather it induced apoptosis.

■ CONCLUSIONS

Here we report the synthesis and biological evaluation of a series of new 2-oxospiro[indoline-3,2′-thiazolidine] derivatives, designed as inhibitors of p53−MDM2 protein−protein interaction, which exhibit activity against different tumor cell lines. In particular, compound **4n** showed high efficacy in MCF-7 (breast), HT29 (colon), calu (lung), and U937 (leukemia) human cell lines with IC_{50} values of 40, 70, 100, and 70 nM, respectively, with >10-fold selectivity against the HGF normal cell line. The well-known p53−MDM2 inhibitor, nutlin-3, was considerably less efficient in all tested cell lines and also in the in vitro p53−MDM2 binding inhibition assay. Docking studies allow us to predict binding mode for **4n** in the MDM2 binding site, in which our compound sets favorable van der Waals contacts with Ile61, Val75, Phe86, Phe91 and Ile99 side chains, direct contacts with Ile61 and Met62 side chains, and additional hydrophobic interactions with Leu54 and edge−face $\pi-\pi$ interaction with the Phe55 residue. In the MCF-7 cell line, **4n** induces a time-dependent increment in p53 expression, indicating that its activity profile, as in the case of nutlins, might be regulated by this protein. However, preliminary studies on the induction of apoptosis and cell cycle progression showed a different behavior for these compounds. Nutlin-3 markedly blocked the G0/G1 phase, causing a delay of cell cycle progression in responsive cells, while treatment with **4n** did not alter the normal course of cell cycle. Moreover, **4n** induces apoptotic cell death through the intrinsic apoptotic pathway. According to these findings, **4n** represents a new lead compound for the design of agents able to reactivate p53-

dx.doi.org/10.1021/jm400311n | J. Med. Chem. 2013, 56, 5407−5421

mediated apoptosis in cancer cells and provides a new tool for studying p53 signaling in the natural cellular context of tumors that retain wild-type p53. Further experiments aimed to identify more potent spirothiazolidin-based derivatives and to better understand the apoptotic mechanisms induced by this compound are underway.

EXPERIMENTAL SECTION

General. Reagents, starting materials, and solvents were purchased from commercial suppliers and used as received. Analytical TLC was performed on plates coated with a 0.25 mm layer of silica gel 60 F254 Merck and preparative TLC on 20 cm × 20 cm glass plates coated with a 0.5 mm layer of silica gel PF254 Merck. Silica gel 60 (300−400 mesh, Merck) was used for flash chromatography. Melting points were determined by a Kofler apparatus and are uncorrected. Optical rotations were measured on an Atago Polax 2-L polarimeter. ^{1}H NMR and ^{13}C NMR spectra were recorded with a Varian-400 spectrometer, operating at 400 and 100 MHz, respectively. Chemical shifts are reported in δ values (ppm) relative to internal Me_4Si, and J values are reported in hertz (Hz). ROESY[36] experiment was recorded at 25 °C in the phase-sensitive mode using the method from States.[37] Data block sizes were 2048 addresses in t2 and 512 equidistant t1 values. Before Fourier transformation, the time domain data matrices were multiplied by shifted sin 2 functions in both dimensions. A mixing time of 500 ms was used. ESIMS experiments were performed on an Applied Biosystem API 2000 triple-quadrupole spectrometer. Starting spiro(oxoindolethiazolidine) ethyl ester derivatives (**13**−**18**) were synthesized as described in refs 23 and 24. As an example, here we described the synthesis of (3*RS*,4′*R*)-ethyl 5-bromo-1-methyl-2-oxospiro[indoline-3,2′-thiazolidine]-4′-carboxylate (**18**). Combustion microanalyses were performed on a Carlo Erba CNH 1106 analyzer, and all reported values are within 0.4% of calculated values (Table 1S in Supporting Information). These elemental analyses confirmed >95% purity.

Synthesis of (3*RS*,4′*R*)-Ethyl 5-Bromo-1-methyl-2-oxospiro[indoline-3,2′-thiazolidine]-4′-carboxylate (18). $NaHCO_3$ (1.0 g, 12 mmol) and 5-bromo-1-methyl isatin (**12**, 2.4 g, 10 mmol) were added to a solution of L-Cys-OEt (2.3 g, 12 mmol) in ethanol (100 mL), and the suspension was stirred at room temperature for 12 h. Then the suspension was filtered, and the filtrate was concentrated. Spiro(oxoindolethiazolidine) ethyl ester residue was dissolved in DCM and washed with water (3 × 50 mL). The combined organic layer was dried over anhydrous sodium sulfate, filtered, and concentrated. A 5:1 diastereoisomeric mixture of the title's compound was obtained as an oil with 73% yield. ^{1}H NMR (400 MHz, $CDCl_3$) δ 1.36 (3H, m, CH_3), 3.10 and 3.12 (3H, s, CH_3), 3.31 and 3.43 (1H, m, H-5′a), 3.71 and 3.93 (1H, m, H-5′b), 4.25 (4H, m, CH_2), 4.46 and 4.66 (2H, m, H-4′), 6.69 and 6.75 (1H, d, J = 8.0 Hz, H-7), 7.48 (1H, d, H-6), 7.60 and 7.71 (1H, s, H-4). The compound was used in the next reaction without further purification.

General Procedure for the Synthesis of the (2′*R* or 2′*S*, 4′*R*)-Ethyl 3′-Substituted-2-Oxospiro[indoline-3,2′-thiazolidine]-4′-carboxylate Derivatives (4a−q). To a solution of (2′*R*,4′*R*)- and (2′*S*,4′*R*)-ethyl 2-oxospiro[indoline-3,2′-thiazolidine]-4′-carboxylate derivatives (**13**−**18**, 200 mg, 5 mmol) in dry THF (50 mL) was added a solution of corresponding 4-chlorobenzoyl or 4-methylbenzoyl or 4-chlorophenylacethyl or cyclohexanecarbonyl chlorides (5.5 mmol) in THF (10 mL) and TEA (10 mmol). The reaction mixture was stirred at room temperature for 2 h, and water was then added. The organic solution was washed with water (3 × 100 mL), dried over Na_2SO_4, and evaporated in vacuo. Flash chromatography on silica gel, using ethyl acetate/*n*-hexane as eluent, overall yielded the corresponding final derivatives as oil.

(2′*S*,4′*R*)-Ethyl 3′-(2-(4-Chlorophenylacetyl)-2-oxospiro[indoline-3,2′-thiazolidine]-4′-carboxylate (4a). Overall yield 43%. $[\alpha]^{25}_D$ −7.1 (*c* 0.1, MeOH). ^{1}H NMR (400 MHz, $CDCl_3$) δ 1.40 (t, 3H, CH_3); 3.44 (d, 1H, J = 12.0 Hz, H-5′a); 3.63 (s, 2H, CH_2); 3.95 (dd, 1H, J = 6.0 and 11.6 Hz, H-5′b); 4.39 (q, 2H, CH_2); 5.08 (d, 1H, J = 6.0, H-4′); 6.76 (d, 1H, J = 8.4 Hz, H-7); 7.04 (t, 1H, H-6); 7.15 (d, 2H, J = 8.0 Hz, aryl); 7.24 (t, 1H, J = 7.9 Hz, H-5); 7.28 (d, 2H, aryl); 7.43 (s, 1H, NH); 7.47 (d, 1H, H-4). ^{13}C NMR (100 MHz, $CDCl_3$) δ 14.5 (CH_3), 34.6 (C-5′), 41.4 (CH_2), 62.5 (CH_2), 64.3 (C-4′), 73.9 (C-2′), 109.3, 115.8, 123.5, 128.0, 128.9, 130.2, 134.4, 136.2, and 143.1 (aryl), 170.1, 173.9, and 178.0 (C═O). ESIMS m/z calcd for $C_{21}H_{19}ClN_2O_4S$, 430.08; found 430.16.

(2′*S*,4′*R*)-Ethyl 5-Methyl-3′-(2-(4-chlorophenyl)acetyl)-2-oxospiro[indoline-3,2′-thiazolidine]-4′-carboxylate (4b). Overall yield 39%.$[\alpha]^{25}_D$ −13.6 (*c* 0.25, MeOH). ^{1}H NMR (400 MHz, $CDCl_3$) δ 1.42 (t, 3H, CH_3); 2.04 (s, 3H, CH_3); 3.37 (d, 1H, J = 12.4 Hz, H-5′a); 3.61 (s, 2H, CH_2); 3.98 (dd, 1H, J = 6.0 and 11.6 Hz, H-5′b); 4.43 (q, 2H, CH_2); 5.04 (d, 1H, J = 6.0, H-4′); 6.70 (d, 1H, J = 8.0 Hz, H-7); 7.08 (d, 1H, H-6); 7.19 (d, 2H, J = 8.0 Hz, aryl); 7.31 (d, 2H, aryl); 7.40 (s, 1H, H-4); 7.79 (s, 1H, NH). ^{13}C NMR (100 MHz, $CDCl_3$) δ 14.2 (CH_3), 21.7 (CH_3), 34.8 (C-5′), 41.6 (CH_2), 62.3 (CH_2), 64.7 (C-4′), 74.2 (C-2′), 109.8, 123.2, 128.5, 129.6, 130.7, 133.0, 137.4, and 142.8 (aryl), 170.6, 173.4, and 178.3 (C═O). ESIMS m/z calcd for $C_{22}H_{21}ClN_2O_4S$, 444.09; found 444.15.

(2′*S*,4′*R*)-Ethyl 5-Bromo-3′-(2-(4-chlorophenyl)acetyl)-2-oxospiro[indoline-3,2′-thiazolidine]-4′-carboxylate (4c). Overall yield 37%. $[\alpha]^{25}_D$ −29.4° (*c* 0.4, MeOH). ^{1}H NMR (400 MHz, $CDCl_3$) δ 1.43 (t, 3H, CH_3); 3.42 (d, 1H, J = 12.6 Hz, H-5′a); 3.65 (s, 2H, CH_2); 4.01 (dd, 1H, J = 6.0 and 12.0 Hz, H-5′b); 4.45 (q, 2H, CH_2); 5.00 (d, 1H, J = 6.0, H-4′); 6.73 (d, 1H, J = 7.6 Hz, H-7); 7.23 (d, 2H, J = 8.0 Hz, aryl); 7.31 (d, 2H, aryl); 7.48 (d, 1H, H-6); 7.95 (s, 1H, H-4); 8.04 (s, 1H, NH). ^{13}C NMR (100 MHz, $CDCl_3$) δ 14.3 (CH_3), 21.9 (CH_3), 34.6 (C-5′), 41.5 (CH_2), 62.4 (CH_2), 64.9 (C-4′), 74.4 (C-2′), 109.5, 116.2, 123.4, 128.2, 129.0, 131.1, 132.5, 133.3, 137.2, and 143.2 (aryl), 170.2, 173.5, and 178.9 (C═O). ESIMS m/z calcd for $C_{21}H_{18}BrClN_2O_4S$, 507.99; found 508.04.

(2′*S*,4′*R*)-Ethyl 3′-(4-Chlorobenzoyl)-2-oxospiro[indoline-3,2′-thiazolidine]-4′-carboxylate (4d). Overall yield 49%. $[\alpha]^{25}_D$ −16.3 (*c* 0.25, MeOH). ^{1}H NMR (400 MHz, $CDCl_3$) δ 1.36 (t, 3H, CH_3); 3.40 (d, 1H, J = 11.6 Hz, H-5′a); 3.95 (dd, 1H, J = 6.0 and 11.6 Hz, H-5′b); 4.38 (q, 2H, CH_2); 4.87 (d, 1H, J = 6.0 Hz, H-4′); 6.77 (d, 1H, J = 8.0 Hz, H-7); 7.05 (t, 1H, J = 7.6 Hz, H-6); 7.20 (t, 1H, H-5); 7.33 (d, 2H, aryl, J = 7.6 Hz); 7.44 (d, 2H, aryl); 7.73 (d, 1H, H-4); 8.54 (s, 1H, NH). ^{13}C NMR (100 MHz, $CDCl_3$) δ 14.5 (CH_3), 34.5 (C-5′), 62.8 (CH_2), 66.8 (C-4′), 72.4 (C-2′), 110.7, 123.2, 125.5, 126,3, 128.4, 129.0, 130.3, 134.3, 137.1, and 141.2 (aryl), 168.4, 170.6, and 177.1 (C═O). ESIMS m/z calcd for $C_{20}H_{17}ClN_2O_4S$, 416.06; found, 416.14.

(2′*S*,4′*R*)-Ethyl 3′-(4-Chlorobenzoyl)-5-methyl-2-oxospiro[indoline-3,2′-thiazolidine]-4′-carboxylate (4e). Overall yield 58%.$[\alpha]^{25}_D$ −5.7 (*c* 0.1, MeOH). ^{1}H NMR (400 MHz, $CDCl_3$) δ 1.38 (t, 3H, CH_3); 2.34 (s, 3H, CH_3); 3.34 (d, 1H, J = 11.6 Hz, H-5′a); 3.98 (dd, 1H, J = 6.0 and 11.6 Hz, H-5′b); 4.38 (q, 2H, CH_2); 4.85 (d, 1H, J = 6.0 Hz, H-4′); 6.72 (d, 1H, J = 8.0 Hz, H-7); 7.03 (d, 1H, H-6); 7.33 (d, 2H, J = 8.0 Hz, aryl); 7.44 (d, 2H, aryl); 7.54 (s, 1H, H-4); 8.06 (s, 1H, NH). ^{13}C NMR (100 MHz, $CDCl_3$) δ: 14.5 (CH_3), 21.5 (CH_3), 34.5 (C-5′), 62.7 (CH_2), 66.7 (C-4′), 72.5 (C-2′), 110.2, 126.1, 128.4, 129.0, 130.8, 133.6, 136.2, and 138.4 (aryl), 167.6, 170.1, and 176.2 (C═O). ESIMS m/z calcd for $C_{21}H_{19}ClN_2O_4S$, 430.08; found, 430.08.

(2′*S*,4′*R*)-Ethyl 5-Bromo-3′-(4-chlorobenzoyl)-2-oxospiro[indoline-3,2′-thiazolidine]-4′-carboxylate (4f). Overall yield 46%. $[\alpha]^{25}_D$ −9.8 (*c* 0.24, MeOH). ^{1}H NMR (400 MHz, $CDCl_3$) δ 1.40 (t, 3H, CH_3); 3.35 (d, 1H, J = 12.0 Hz, H-5′a); 3.89 (dd, 1H, J = 6.0 and 11.8 Hz, H-5′b); 4.42 (q, 2H, CH_2); 4.84 (d, 1H, J = 6.0 Hz, H-4′); 7.36−7.50 (m, 5H, H-7, aryl); 7.78−7.81 (m, 2H, H-6, H-4); 8.04 (s, 1H, NH). ^{13}C NMR (100 MHz, $CDCl_3$) δ 14.5 (CH_3), 35.3 (C-5′), 63.1 (CH_2), 66.7 (C-4′), 72.3 (C-2′), 116.8, 118.8, 128.4, 128.6, 128.7, 129.2, 131.2, 139.3, and 140.9 (aryl), 168.7, 170.1, and 173.6 (C═O). ESIMS m/z calcd for $C_{20}H_{16}Br\,ClN_2O_4S$, 493.97; found, 494.09.

(2′*R*,4′*R*)-Ethyl 5-Bromo-3′-(4-chlorobenzoyl)-2-oxospiro[indoline-3,2′-thiazolidine]-4′-carboxylate (4g). Overall yield 15%. $[\alpha]^{25}_D$ −6.9 (*c* 0.11, MeOH). ^{1}H NMR (400 MHz, $CDCl_3$) δ 1.24 (t, 3H, CH_3); 3.61−3.62 (m, 2H, H-5′a, H-5′b); 4.25 (q, 2H, CH_2); 5.43 (t, 1H, J = 9.6 Hz, H-4′); 7.45 (d, 2H, J = 8.4 Hz, aryl);

dx.doi.org/10.1021/jm400311n | J. Med. Chem. 2013, 56, 5407−5421

7.61 (d, 1H, J = 9.2 Hz, H-7); 7.79 (s, 1H, H-4); 8.05 (d, 2H, aryl); 8.90 (d, 1H, H-6); 9.51 (s, 1H, NH). ^{13}C NMR (100 MHz, $CDCl_3$) δ 14.4 (CH_3), 34.0 (C-5′), 62.4 (CH_2), 66.9 (C-2′), 78.8 (C-4′), 115.2, 122.2, 129.1, 129.6, 133.4, 134.7, 135.9, and 138.5 (aryl), 165.4, 170.0, and 172.5 (C═O). ESIMS m/z calcd for $C_{20}H_{16}BrClN_2O_4S$, 493.97; found, 494.09.

(2′*S*,4′*R*)-Ethyl 3′-(4-Chlorobenzoyl)-1-methyl-2-oxospiro-[indoline-3,2′-thiazolidine]-4′-carboxylate (4h). Overall yield 56%. $[\alpha]^{25}_D$ −8.9 (c 0.2, MeOH). ^{1}H NMR (400 MHz, $CDCl_3$) δ 1.36 (t, 3H, CH_3); 3.29 (s, 3H, CH_3); 3.38 (d, 1H, J = 11.6 Hz, H-5′a); 3.97 (dd, 1H, J = 6.0 and 11.6 Hz, H-5′b); 4.38 (q, 2H, CH_2); 4.85 (d, 1H, J = 5.6 Hz, H-4′); 6.84 (d, 1H, J = 8.0 Hz, H-7); 7.10 (t, 1H, J = 8.0 Hz, H-6); 7.31−7.38 (m, 3H, H-5, aryl); 7.41 (d, 2H, aryl); 7.76 (d, 1H, J = 7.6 Hz, H-4); 8.51 (s, 1H, NH). ^{13}C NMR (100 MHz, $CDCl_3$) δ 14.5 (CH_3), 26.1 (CH_3), 34.5 (C-5′), 62.8 (CH_2), 66.7 (C-4′), 72.5 (C-2′), 108.5, 123.4, 125.2, 128.4, 129.0, 130.4, 134.1, 137.3, and 141.4 (aryl), 168.1, 170.7, and 177.2 (C═O). ESIMS m/z calcd for $C_{21}H_{19}ClN_2O_4S$, 430.08; found, 430.08.

(2′*S*,4′*R*)-Ethyl 3′-(4-Chlorobenzoyl)-1,5-dimethyl-2-oxospiro[indoline-3,2′-thiazolidine]-4′-carboxylate (4i). Overall yield 41%. $[\alpha]^{25}_D$ −15.2° (c 0.4, MeOH). ^{1}H NMR (400 MHz, $CDCl_3$) δ 1.37 (t, 3H, CH_3); 2.35 (s, 3H, CH_3); 3.33 (d, 1H, J = 12.0 Hz, H-5′a); 3.49 (s, 3H, CH_3); 4.00 (dd, 1H, J = 5.8 and 12.0 Hz, H-5′b); 4.38 (q, 2H, CH_2); 4.85 (d, 1H, J = 5.8 Hz, H-4′); 6.76 (d, 1H, J = 7.8 Hz, H-7); 7.12 (d, 1H, H-6); 7.33 (d, 2H, J = 7.6 Hz, aryl); 7.41 (d, 2H, aryl); 7.56 (s, 1H, H-4). ^{13}C NMR (100 MHz, $CDCl_3$) δ 14.5 (CH_3), 22.9 (CH_3), 29.8 (CH_3), 34.5 (C-5′), 62.8 (CH_2), 66.7 (C-4′), 72.5 (C-2′), 108.5, 123.4, 125.2, 128.4, 129.0, 130.4, 134.1, 137.3, and 141.4 (aryl), 168.1, 170.7, and 177.2 (C═O). ESIMS m/z calcd for $C_{22}H_{21}ClN_2O_4S$, 446.09; found, 446.11.

(2′*S*,4′*R*)-Ethyl 5-Bromo-3′-(4-chlorobenzoyl)-1-methyl-2-oxospiro[indoline-3,2′-thiazolidine]-4′-carboxylate (4j). Overall yield 54%. $[\alpha]^{25}_D$ −21.2° (c 0.4, MeOH). ^{1}H NMR (400 MHz, $CDCl_3$) δ 1.48 (t, 3H, CH_3); 3.32 (d, 1H, J = 12.4 Hz, H-5′a); 3.48 (s, 1H, CH_3); 3.94−3.99 (m, 1H, H-5′b); 4.40 (q, 2H, CH_2); 4.87 (d, 1H, J = 6.2 Hz, H-4′); 7.38−7.47 (m, 4H, aryl); 7.52 (d, 1H, J = 8.0 Hz, H-6); 7.79−7.83 (m, 2H, aryl). ^{13}C NMR (100 MHz, $CDCl_3$) δ 14.7 (CH_3), 25.1 (CH_3), 35.3 (C-5′), 63.2 (CH_2), 66.7 (C-4′), 72.8 (C-2′), 116.9, 128.7, 128.9, 129.0, 129.1, 131.4, 133.5, 137.9, 139.1 (aryl), 168.5, 169.4, and 175.4 (C═O). ESIMS m/z calcd for $C_{21}H_{18}BrClN_2O_4S$, 507.99; found, 508.04.

(2′*S*,4′*R*)-Ethyl 5-Bromo-3′-(2-(4-chlorophenyl)acetyl)-1-methyl-2-oxospiro[indoline-3,2′-thiazolidine]-4′-carboxylate (4k). Overall yield 38%. $[\alpha]^{25}_D$ −26.3° (c 0.11, MeOH). ^{1}H NMR (400 MHz, $CDCl_3$) δ 1.41 (t, 3H, CH_3); 3.20 (s, 3H, CH_3); 3.47 (d, 1H, J = 12.0 Hz, H-5′a); 3.63 (s, 2H, CH_2); 3.94 (dd, 1H, J = 6.0 and 11.6 Hz, H-5′b); 4.38 (q, 2H, CH_2); 5.06 (d, 1H, J = 6.0, H-4′); 6.66 (d, 1H, J = 8.4 Hz, H-7); 7.10 (d, 2H, J = 8.0 Hz, aryl); 7.27 (d, 2H, aryl); 7.39 (d, 1H, H-6); 7.60 (s, 1H, H-4). ^{13}C NMR (100 MHz, $CDCl_3$) δ 14.5 (CH_3), 27.0 (CH_3), 34.1 (C-5′), 41.7 (CH_2), 63.1 (CH_2), 64.5 (C-4′), 75.7 (C-2′), 110.1, 115.8, 127.8, 128.9, 129.2, 130.6, 132.9, 133.1, and 142.8 (aryl), 170.3, 174.3, and 177.8 (C═O). ESIMS m/z calcd for $C_{22}H_{20}BrClN_2O_4S$, 522.00; found 522.06.

(2′*S*,4′*R*)-Ethyl 5-Bromo-3′-benzoyl-1-methyl-2-oxospiro-[indoline-3,2′-thiazolidine]-4′-carboxylate (4l). Overall yield 32%. $[\alpha]^{25}_D$ −16.9° (c 0.5, MeOH). ^{1}H NMR (400 MHz, $CDCl_3$) δ 1.45 (t, 3H, CH_3); 3.29(s, 3H, CH_3); 3.36 (d, 1H, J = 12.4 Hz, H-5′a); 3.96−4.01 (m, 1H, H-5′b); 4.37 (q, 2H, CH_2); 4.91 (d, 1H, J = 6.2 Hz, H-4′); 6.73 (d, 1H, J = 8.0 Hz, H-7); 7.38−7.51 (m, 6H, H-6 and aryl); 7.91 (s, 1H, H-4). ^{13}C NMR (100 MHz, $CDCl_3$) δ 14.5 (CH_3), 25.6 (CH_3), 35.4 (C-5′), 63.1 (CH_2), 66.9 (C-4′), 73.1 (C-2′), 118.4, 127.5, 127.3, 128.2, 129.4, 133.5, 137.7, 139.2 (aryl), 168.8, 169.6, and 175.0 (C═O). ESIMS m/z calcd for $C_{20}H_{17}BrN_2O_4S$, 460.01; found, 460.09.

(2′*S*,4′*R*)-Ethyl 5-Bromo-1-methyl-3′-(4-methylbenzoyl)-2-oxospiro[indoline-3,2′-thiazolidine]-4′-carboxylate (4m). Overall yield 37%. $[\alpha]^{25}_D$ −14.2° (c 0.3, MeOH). ^{1}H NMR (400 MHz, $CDCl_3$) δ 1.40 (t, 3H, CH_3); 2.35 (s, 3H, CH_3); 3.28 (s, 3H, CH_3); 3.32 (d, 1H, J = 11.6 Hz, H-5′a); 3.95 (dd, 1H, J' = 6.0 and 11.6 Hz H-5′b); 4.39 (q, 2H, CH_2); 4.91 (d, 1H, J = 5.6 Hz, H-4′); 6.71 (d, 1H, J = 8.4 Hz, H-7); 7.14 (d, 2H, J = 7.6 Hz, aryl); 7.34 (d, 2H, aryl); 7.45 (d, 1H, H-6); 7.91 (s, 1H, H-4). ^{13}C NMR (100 MHz, $CDCl_3$) δ 14.5 (CH_3), 21.6 (CH_3), 27.0 (CH_2), 34.8 (C-5′), 62.8 (CH_2), 66.8 (C-4′), 72.5 (C-2′), 109.9, 115.9, 126.9, 128.3, 128.4, 129.4, 133.0, 141.3, and 143.0 (aryl), 169.4, 170.6, and 175.2 (C═O). ESIMS m/z calcd for $C_{22}H_{21}BrN_2O_4S$, 488.04; found, 488.11.

(2′*S*,4′*R*)-Ethyl 5-Bromo-3′-(cyclohexanecarbonyl)-1-methyl-2-oxospiro[indoline-3,2′-thiazolidine]-4′-carboxylate (4n). Overall yield 49%. $[\alpha]^{25}_D$ − 37.3° (c 0.8, MeOH). (A) ^{1}H NMR (400 MHz, $CDCl_3$) δ 1.15−1.22 (m, 4H, CH_2); 1.41 (t, 3H, CH_3); 1.64−1.78 (m, 6H, CH_2); 2.17 (t, 1H, CH); 3.20 (s, 3H, CH_3); 3.47 (d, 1H, J = 12.0 Hz, H-5′a); 3.97 (dd, 1H, J' = 6.0 and 11.6 Hz, H-5′b); 4.41 (q, 2H, CH_2); 5.13 (d, 1H, J = 5.6 Hz, H-4′); 6.67 (d, 1H, J = 8.4 Hz, H-7); 7.39 (d, 1H, H-6); 7.57 (s, 1H, H-4). ^{13}C NMR (100 MHz, $CDCl_3$) δ 14.4 (CH_3), 25.8 (CH_2), 26.7 (CH_3), 30.2 (CH_2), 34.1 (C-5′), 44.1 (CH), 62.9 (CH_2), 64.1 (C-4′), 75.7 (C-2′), 110.0, 115.8, 127.6, 128.9, and 132.7 (aryl); 170.3, 174.3, and 177.8 (C═O). (B) ^{1}H NMR (400 MHz, $CDCl_3$) δ 1.15−1.22 (m, 4H, CH_2); 1.41 (t, 3H, CH_3); 1.64−1.78 (m, 6H, CH_2); 2.17 (t, 1H, CH); 3.26 (s, 3H, CH_3); 3.34 (d, 1H, J = 12.0 Hz, H-5′a); 3.92 (dd, 1H, J' = 6.0 and 11.6 Hz, H-5′b); 4.37 (q, 2H, CH_2); 5.52 (d, 1H, J = 5.2 Hz, H-4′); 6.77 (d, 1H, J = 8.4 Hz, H-7); 7.49 (d, 1H, H-6); 7.56 (s, 1H, H-4). ^{13}C NMR (100 MHz, $CDCl_3$) δ 14.4 (CH_3), 25.8 (CH_2), 26.9 (CH_3), 29.3 (CH_2), 33.9 (C-5′), 43.8 (CH), 62.2 (CH_2), 64.7 (C-4′), 75.7 (C-2′), 110.2, 115.9, 127.9, 129.0, and 132.7 (aryl); 170.1, 174.5, and 177.6 (C═O). ESIMS m/z calcd for $C_{21}H_{25}BrN_2O_4S$, 480.07; found, 480.15.

(2′*S*,4′*R*)-Ethyl 5-Methyl-3′-(cyclohexanecarbonyl)-1-methyl-2-oxospiro[indoline-3,2′-thiazolidine]-4′-carboxylate (4o). Overall yield 47%. $[\alpha]^{25}_D$ −23.1° (c 0.5, MeOH). (A) ^{1}H NMR (400 MHz, $CDCl_3$) δ 1.15−1.26 (m, 4H, CH_2); 1.40 (t, 3H, CH_3); 1.63−1.73 (m, 6H, CH_2); 2.17 (t, 1H, CH); 2.30 (s, 3H, CH_3); 3.21 (s, 3H, CH_3); 3.45 (d, 1H, J = 12.0 Hz, H-5′a); 4.00 (dd, 1H, J' = 6.0 and 11.6 Hz, H-5′b); 4.40 (q, 2H, CH_2); 5.13 (d, 1H, J = 5.6 Hz, H-4′); 6.67 (d, 1H, J = 8.0 Hz, H-7); 7.06 (d, 1H, H-6); 7.26 (s, 1H, H-4). ^{13}C NMR (100 MHz, $CDCl_3$) δ 14.5 (CH_3), 21.4 (CH_3), 25.7 (CH_2), 26.9 (CH_3), 29.2 (CH_2), 33.8 (C-5′), 44.2 (CH), 62.7 (CH_2), 64.2 (C-4′), 75.7 (C-2′), 108.3, 125.0, 126.5, 130.3, 132.7, and 143.0 (aryl); 170.5, 174.2, and 177.8 (C═O). (B) ^{1}H NMR (400 MHz, $CDCl_3$) δ 1.15−1.26 (m, 4H, CH_2); 1.40 (t, 3H, CH_3); 1.63−1.73 (m, 6H, CH_2); 2.17 (t, 1H, CH); 2.35 (s, 3H, CH_3); 3.25 (s, 3H, CH_3); 3.30 (d, 1H, J = 12.0 Hz, H-5′a); 3.94 (dd, 1H, J' = 6.0 and 11.6 Hz, H-5′b); 4.36 (q, 2H, CH_2); 5.52 (d, 1H, J = 6.0 Hz, H-4′); 6.78 (d, 1H, J = 8.0 Hz, H-7); 7.18 (d, 1H, H-6); 7.64 (s, 1H, H-4). ^{13}C NMR (100 MHz, $CDCl_3$) δ 14.5 (CH_3), 21.1 (CH_3), 25.4 (CH_2), 25.8 (CH_3), 29.6 (CH_2), 32.2 (C-5′), 43.8 (CH), 62.0 (CH_2), 64.4 (C-4′), 75.8 (C-2′), 108.8, 126.4, 131.2, 132.9, and 143.2 (aryl); 170.7, 174.4, and 177.8 (C═O). ESIMS m/z calcd for $C_{22}H_{28}N_2O_4S$, 416.18; found, 416.24.

(2′*S*,4′*R*)-Ethyl 3′-(Cyclohexanecarbonyl)-1-methyl-2-oxospiro[indoline-3,2′-thiazolidine]-4′-carboxylate (4p). Overall yield 45%. $[\alpha]^{25}_D$ −20.0° (c 0.4, MeOH). (A) ^{1}H NMR (400 MHz, $CDCl_3$) δ 1.13−1.24 (m, 4H, CH_2); 1.39 (t, 3H, CH_3); 1.62−1.79 (m, 6H, CH_2); 2.19 (t, 1H, CH); 3.23 (s, 3H, CH_3); 3.45 (d, 1H, J = 12.0 Hz, H-5′a); 3.99 (dd, 1H, J' = 6.0 and 11.6 Hz, H-5′b); 4.38 (q, 2H, CH_2); 5.13 (d, 1H, J = 5.6 Hz, H-4′); 6.79 (d, 1H, J = 8.4 Hz, H-7); 7.02 (t, 1H, H-6); 7.27 (t, 1H, H-5); 7.46 (d, 1H, H-4). ^{13}C NMR (100 MHz, $CDCl_3$) δ 14.5 (CH_3), 25.7 (CH_2), 26.8 (CH_3), 29.2 (CH_2), 33.8 (C-5′), 44.1 (CH), 62.7 (CH_2), 64.2 (C-4′), 75.9 (C-2′), 108.5, 123.2, 124.2, 126.1, 129.9, 131.0, and 143.5 (aryl); 170.5, 174.2, and 177.8 (C═O). (B) ^{1}H NMR (400 MHz, $CDCl_3$) δ 1.13−1.24 (m, 4H, CH_2); 1.39 (t, 3H, CH_3); 1.62−1.79 (m, 6H, CH_2); 2.19 (t, 1H, CH); 3.28 (s, 3H, CH_3); 3.40 (d, 1H, J = 12.0 Hz, H-5′a); 3.95 (dd, 1H, J' = 6.0 and 11.6 Hz, H-5′b); 4.31 (q, 2H, CH_2); 5.51 (d, 1H, J = 6.4 Hz, H-4′); 6.89 (d, 1H, J = 8.4 Hz, H-7); 7.14 (t, 1H, H-6); 7.38 (t, 1H, H-5); 7.46 (d, 1H, H-4). ^{13}C NMR (100 MHz, $CDCl_3$) δ 14.5 (CH_3), 25.7 (CH_2), 27.0 (CH_3), 29.3 (CH_2), 32.1 (C-5′), 42.9 (CH), 62.1 (CH_2), 65.3 (C-4′), 75.9 (C-2′), 109.0, 122.8, 125.1, 127.2, 128.2, 131.0, and 143.7 (aryl); 170.6, 174.0, and 177.6 (C═O). ESIMS m/z calcd for $C_{21}H_{26}N_2O_4S$, 402.16; found, 402.20.

dx.doi.org/10.1021/jm400311n | J. Med. Chem. 2013, 56, 5407−5421

(2′*S*,4′*R*)-Ethyl 5-Bromo-3′-(cyclohexanecarbonyl)-2-oxospiro[indoline-3,2′-thiazolidine]-4′-carboxylate (4q). Overall yield 42%. $[\alpha]^{25}_{D}$ −27.1° (*c* 0.5, MeOH). ^{1}H NMR (400 MHz, $CDCl_3$) δ 1.15−1.22 (m, 4H, CH_2); 1.41 (t, 3H, CH_3); 1.64−1.78 (m, 6H, CH_2); 1.96 (t, 1H, CH); 3.43 (d, 1H, *J* = 12.0 Hz, H-5′a); 3.97 (dd, 1H, *J* = 6.0 and 11.6 Hz, H-5′b); 4.30 (q, 2H, CH_2); 4.63 (d, 1H, *J* = 6.0 Hz, H-4′,); 7.49 (d, 1H, *J* = 8.4 Hz, H-7′); 7.68 (s, 1H, H-4′); 8.10 (d, 1H, H-6′). ^{13}C NMR (100 MHz, $CDCl_3$) δ 14.4 (CH_3), 25.8 (CH_2), 29.3 (CH_2), 39.0 (C-1), 44.9 (CH), 62.6 (CH_2), 65.0 (C-2), 75.7 (C-4), 118.8, 127.3, 128.0, 134.1, and 139.4 (aryl), 172.0, 175.9, and 177.4 (C═O). ESIMS *m*/*z* calcd for $C_{20}H_{23}BrN_2O_4S$, 466.06; found, 466.12.

(2′*SR*,4′*R*)-5-Bromo-3′-(cyclohexanecarbonyl)-1-methyl-2-oxospiro[indoline-3,2′-thiazolidine]-4′-carboxylic Acid (4r). Overall yield 37%. ^{1}H NMR (400 MHz, $CDCl_3$) (*α*) δ 1.14−1.38 (m, 6H, CH_2); 1.58−1.79 (m, 4H, CH_2); 2.27 (t, 1H, CH); 3.19 (s, 3H, CH_3); 3.54 (t, 1H, H-5′a); 3.88−3.91 (m, 1H, H-5′b); 5.11 (d, 1H, *J* = 6.8 Hz, H-4′); 6.64 (d, 1H, *J* = 8.0 Hz, H-7); 7.34 (d, 1H, H-6); 7.65 (s, 1H, H-4). (*β*) δ 1.14−1.38 (m, 6H, CH_2); 1.58−1.79 (m, 4H, CH_2); 2.27 (t, 1H, CH); 3.22 (s, 3H, CH_3); 3.54 (t, 1H, H-5′a); 3.81−3.85 (m, 1H, H-5′b); 5.37 (d, 1H, *J* = 5.6 Hz, H-4′); 6.74 (d, 1H, *J* = 8.0 Hz, H-7); 7.47 (d, 1H, H-6); 8.00 (s, 1H, H-4). ^{13}C NMR (100 MHz, $CDCl_3$) (*α*) δ 25.6 (CH_2), 26.3 (CH_2), 27.1 (CH_2), 29.4 (CH_2), 34.5 (C-5′), 43.3 (CH), 64.9 (C-4′), 71.4 (C-2′), 109.9, 115.6, 127.7, 129.2, 132.5, and 142.6 (aryl); 174.7, 175.3, and 176.9 (C═O). (*β*) δ 25.9 (CH_2), 26.9 (CH_2), 28.9 (CH_2), 29.9 (CH_2), 32.6 (C-5′), 43.7 (CH), 58.7 (C-4′), 69.8 (C-2′), 110.4, 116.7, 129.5, 129.9, 133.6, and 141.2 (aryl); 174.5, 175.2, and 176.7 (C═O). ESIMS *m*/*z* calcd for $C_{18}H_{19}BrN_2O_4S$, 438.02; found, 438.10.

General Procedure for the Synthesis of the (2′*S*,4′*R*)-Ethyl 1-Substituted-2-Oxospiro[indoline-3,2′-thiazolidine]-4′-carboxylate Derivatives (5a−c). To a solution of indol-2,3-dione derivatives (**7**−**9**, 300 mg, 1.5 mmol) in dichloromethane was added 4-chlorobenzoyl chloride (1.8 mmol) and TEA (1.8 mmol). The reaction mixture was stirred at room temperature for 1 h, and water was then added. The organic solution was washed with water (3 × 100 mL), dried over Na_2SO_4, and evaporated in vacuo. Flash chromatography on silica gel, using ethyl acetate/*n*-hexane as eluent, overall yielded the corresponding derivatives **19**−**21**. 1-Substituted isatine **19**−**21** (150 mg, ∼0.5 mmol) derivatives were dissolved in ethanol, and cysteine ethyl ester and $NaHCO_3$ were added (0, 65 mmol). The mixture was stirred at room temperature for 12 h. Then ethanol was filtered and the surnatant was evaporated in vacuo. The crude was dissolved in dicholoromethane and washed with water (3 × 100 mL). The organic phase was dried over Na_2SO_4 and evaporated in vacuo. Flash chromatography on silica gel, using ethyl acetate/*n*-hexane as eluent, yielded the corresponding final derivatives **5a**−**c** as solid compounds.

(2′*S*,4′*R*)-Ethyl 1-(4-Chlorobenzoyl)-2-oxospiro[indoline-3,2′-thiazolidine]-4′-carboxylate (5a). Overall yield 32%. $[\alpha]^{25}_{D}$ +2.9° (*c* 0.4, MeOH). ^{1}H NMR (400 MHz, $CDCl_3$) δ 1.32 (t, 3H, CH_3); 3.34 (d, 2H, *J* = 5.6 Hz, H-5′); 4.27 (q, 2H, CH_2); 5.01 (dd, 1H, *J* = 5.5 and 13.0 Hz, H-4′); 7.08 (t, 1H, *J* = 7.6 Hz, H-6); 7.43 (d, 2H, *J* = 8.4 Hz, aryl); 7.59 (t, 1H, H-5); 7.81 (d, 1H, *J* = 7.6 Hz, H-7); 7.87 (d, 2H, aryl); 8.34 (d, 1H, *J* = 7.6 Hz, H-4). ^{13}C NMR (100 MHz, $CDCl_3$) δ 14.4 (CH_3), 40.8 (C-5′), 52.3 (C-4′), 62.8 (CH_2), 71.8 (C-2′), 120.9, 123.0, 129.1, 129.4, 131.7, 134.9, 137.5, 139.6, and 142.3 (aryl), 166.0, 172.1, and 190.6 (C═O). ESIMS *m*/*z* calcd for $C_{20}H_{17}ClN_2O_4S$, 416.06; found, 416.09.

(2′*S*,4′*R*)-Ethyl 1-(4-Chlorobenzoyl)-5-methyl-2-oxospiro[indoline-3,2′-thiazolidine]-4′-carboxylate (5b). Overall yield 28%. $[\alpha]^{25}_{D}$ +3.21° (*c* 0.5, MeOH). ^{1}H NMR (400 MHz, $CDCl_3$) δ 1.31 (t, 3H, CH_3); 2.27 (s, 3H, CH_3); 3.34 (d, 2H, *J* = 5.2 Hz, H-5′); 4.28 (q, 2H, CH_2); 5.02 (d, 1H, *J* = 6.0 Hz, H-4′); 7.36−7.44 (m, 3H, H-7, aryl); 7.72 (m, 3H, H-6, aryl); 8.11 (s, 1H, H-4). ^{13}C NMR (100 MHz, $CDCl_3$) δ 14.3 (CH_3), 21.0 (CH_3), 40.7 (C-5′), 52.8 (C-4′), 62.5 (CH_2), 72.3 (C-2′), 120.8, 128.8, 128.9, 129.1, 129.3, 131.7, 132.0, 134.8, 138.4, and 140.5 (aryl), 166.2, 169.3, and 190.2 (C═O). ESIMS *m*/*z* calcd for $C_{21}H_{19}ClN_2O_4S$, 430.08; found, 430.15

(2′*S*,4′*R*)-Ethyl 5-Bromo-1-(4-chlorobenzoyl)-2-oxospiro-[indoline-3,2′-thiazolidine]-4′-carboxylate (5c). Overall yield 36%. $[\alpha]^{25}_{D}$ +2.2 (*c* 0.4, MeOH). ^{1}H NMR (400 MHz, $CDCl_3$) δ 1.31 (t, 3H, CH_3); 3.68 (d, 2H, *J* = 5.2 Hz, H-5′); 4.25 (q, 2H, CH_2); 5.03 (dd, 1H, *J* = 5.2 and 12.0 Hz, H-4′); 7.12 (d, 1H, *J* = 7.6 Hz, NH); 7.37−7.43 (m, 3H, H-7, H-6, H4); 7.72 (d, 2H, *J* = 8.0 Hz, aryl); 7.86 (m, 2H, aryl). ^{13}C NMR (100 MHz, $CDCl_3$) δ 14.3 (CH_3), 30.9 (C-5′), 53.3 (C-4′), 62.5 (CH_2), 72.3 (C-2′), 128.8, 128.9, 129.1, 129.3, 131.7, 132.0, 134.8, 138.4, and 140.7 (aryl), 166.3, 170.3, and 190.2 (C═O). ESIMS *m*/*z* calcd for $C_{20}H_{16}BrClN_2O_4S$, 493.97; found, 494.05.

(2′*S*,4′*R*)-Ethyl 5-Bromo-1-(cyclohexanecarbonyl)-2-oxospiro[indoline-3,2′-thiazolidine]-4′-carboxylate (5d). Overall yield 25%.$[\alpha]^{25}_{D}$ −1.8 (*c* 0.1, MeOH). ^{1}H NMR (400 MHz, $CDCl_3$) δ 1.35 (t, 3H, CH_3); 1.39−1.48 (m, 4H, CH_2); 1.73−1.97 (m, 7H, CH_2 and CH); 3.23 (d, 1H, NH); 3.46 (dd, 1H, *J*′ = 5.2, *J*″ = 10.8 Hz, H-5′a); 3.93 (dd, 1H, *J*′ = 7.6, *J*″ = 10.8 Hz, H-5′b); 4.31 (q, 2H, CH_2); 4.63 (t, 1H, H-4′); 7.49 (d, 1H, *J* = 8.8 Hz, H-7); 7.67 (s, 1H, H-4); 8.10 (d, 1H, H-6). ^{13}C NMR (100 MHz, $CDCl_3$) δ 14.4 (CH_3), 25.8 (CH_2), 26.0 (CH_2), 29.2 (CH_2), 39.1 (C-5′), 45.0 (CH), 62.5 (CH_2), 65.0 (C-4′), 75.8 (C-2′), 118.8, 127.3, 128.0, 134.1, and 139.4 (aryl); 172.0, 175.9, and 177.4 (C═O). ESIMS *m*/*z* calcd for $C_{20}H_{23}BrN_2O_4S$, 466.06; found, 466.10.

Ethyl 1-(4-Chlorobenzoyl)-5-methyl-2-oxo-5′*H*-spiro-[indoline-3,2′-thiazole]-4′-carboxylate (6b). Overall yield 11%. ^{1}H NMR (400 MHz, $CDCl_3$) δ 1.36 (t, 3H, CH_3); 3.49 (s, 3H, CH_3); 4.39 (q, 2H, CH_2); 4.59 (dd, 2H, *J*′ = 16.4 Hz, *J*″ = 14.0 Hz, H-5); 7.26 (s, 1H, H-4); 7.32 (d, 1H, *J* = 8.0 Hz, H-7); 7.41−7.49 (m, 3H, aryl and H-6); 7.69 (d, 2H, *J* = 8.0 Hz, aryl). ^{13}C NMR (100 MHz, $CDCl_3$) δ 29.9 (CH_3), 45.5 (C-1), 53.8 (CH_3), 74.8 (C-2), 115.7, 126.3, 128.9, 130.3, 131.0, 131.6, and 155.4 (aryl), 172.7, 176.9, and 179.3 (C═O). ESIMS *m*/*z* calcd for $C_{21}H_{19}ClN_2O_4S$, 430.08; found, 430.12.

Ethyl 5-Bromo-1-(4-chlorobenzoyl)-2-oxo-5′*H*-spiro-[indoline-3,2′-thiazole]-4′-carboxylate (6c). Overall yield 8%. ^{1}H NMR (400 MHz, $CDCl_3$) δ 1.35 (t, 3H, CH_3); 4.29−4.36 (m, 4H, CH_2 and H-5); 7.47−7.53 (m, 3H, aryl and H-7′); 7.63−7.70 (m, 3H, aryl and H-4′); 8.14 (d, 1H, *J* = 8.0 Hz, H-6′). ^{13}C NMR (100 MHz, $CDCl_3$) δ 14.8 (CH_3), 44.8 (C-1), 62.9 (CH_2), 74.1 (C-2), 115.7, 119.3, 125.8, 127.7, 128.4, 129.9, 133.5, 139.3, and 156.6 (aryl), 173.1, 175.9, and 178.2 (C═O). ESIMS *m*/*z* calcd for $C_{20}H_{14}BrClN_2O_4S$, 491.95; found, 492.03.

Ethyl 5-Bromo-1-(cyclohexanecarbonyl)-2-oxo-5′*H*-spiro-[indoline-3,2′-thiazole]-4′-carboxylate (6d). Overall yield 12%. ^{1}H NMR (400 MHz, $CDCl_3$) δ 1.18−1.26 (m, 4H, CH_2); 1.39 (t, 3H, CH_3); 1.48−1.53 (m, 2H, CH_2); 1.62−1.70 (m, 4H, CH_2); 1.96 (t, 1H, CH); 4.42 (q, 2H, CH_2); 4.64 (dd, 2H, *J*′ = 12.0 Hz, *J*″ = 1 Hz, H-5); 7.52 (d, 1H, *J* = 8.0 Hz, H-7′); 7.58 (s, 1H, H-4′); 8.12 (d, 1H, H-6′). ^{13}C NMR (100 MHz, $CDCl_3$) δ 14.8 (CH_3), 25.6 (CH_2), 30.1 (CH_2), 44.4 (C-1), 45.6 (CH), 62.8 (CH_2), 74.4 (C-2), 118.2, 127.9, 128.6, 133.7, 139.5, and 156.3 (aryl), 172.6, 176.9, and 178.3 (C═O). ESIMS *m*/*z* calcd for $C_{20}H_{21}BrN_2O_4S$, 464.04; found, 464.11.

Biology. Dulbecco's modified Eagle medium (DMEM), fetal bovine serum (FBS), trypsin−EDTA solution (1×), penicillin and streptomycin, and phosphate buffered saline (PBS) were from Cambrex Biosciences. 3-(4,5-Dimethylthiazol-2-yl)-2,5-diphenyltetrazolium bromide (MTT), propidium iodide (PI), Triton X-100, sodium citrate, and formamide were purchased from Sigma (Milan, Italy). Rabbit polyclonal anti-caspase-3, anti-MDM2, anti-Bcl-xS/L, mouse monoclonal anti-actin, anti-p53, anti p21, anti p27, and anti cytochrome *c* were purchased from Santa Cruz Biotechnology (DBA; Milan, Italy). ECL reagent was obtained from Amersham Pharmacia Biotech, U.K.

Cell Culture. Human prostate cancer (PC 3), human histiocytic lymphoma (U937), human lung adenocarcinoma (Calu), human hepatoma (HepG2), human anaplastic thyroid carcinoma (C643), and human breast cancer (MCF-7) cell lines and human primary gingival fibroblasts were grown at 37 °C in Dulbecco's modified Eagle medium containing 10 mM glucose (DMEMHG) supplemented with 10% fetal calf serum and 100 units/mL each of penicillin and streptomycin and 2

mmol/L glutamine. In each experiment, cells were placed in fresh medium, cultured in the presence of synthesized compounds (from 0.1 to 25 mM), and followed for further analyses.

Cell Viability Assay. Cell viability was determined using the 3-[4,5- dimethylthiazol-2,5-diphenyl-2*H*-tetrazolium bromide (MTT) colorimetric assay. The test is based on the ability of mitochondrial dehydrogenase to convert, in viable cells, the yellow MTT reagent (Sigma Chemical Co., St. Louis, MO) into a soluble blue formazan dye. Cells were seeded into 96-well plates to a density of 10^5 cells/100 μL well. After 24 h of growth to allow attachment to the wells, compounds were added at various concentrations (from 0.1 to 25 mM). After 24 or 48 h of growth and after removal of the culture medium, 100 μL/well medium containing 1 mg/mL MTT was added. Microplates were further incubated at 37 °C for 2 h in the dark. The solution was then gently aspirated from each well, and the formazan crystals within the cells were dissolved with 100 μL of DMSO. Optical densities were read at 550 nm using a Multiskan Spectrum Thermo Electron Corporation reader. Results were expressed as percentage relative to vehicle-treated control (0.5% DMSO was added to untreated cells). IC_{50} (concentration eliciting 50% inhibition) values were determined by linear and polynomial regression. Experiments were performed in triplicate.

In Vitro Inhibition of p53−MDM2 Interaction Assay. We performed an in vitro binding assay using ImmunoSet p53/MDM2 complex ELISA set (Enzo Life Sciences). The assay was performed according to the manufacturer's directions . Briefly, 96-multiwell was coated with p53 capture antibody and left overnight at room temperature. Then coating solution was removed and an amount of 200 μL of blocking buffer was added to each wells. The plate was incubated for 1 h at room temperature. Blocking buffer was then removed, and an amount of 100 μL of p53/MDM2 standards was added to wells (except blank) in the presence of 5 μM indicated inhibitors. The plate was incubated for 1 h at room temperature on a plate shaker. Each well was washed 4 times with 200 μL of wash buffer, and an amount of 100 μL of MDM2 detection antibody was added to wells (except blank) for 1 h at room temperature. The plate was washed again, and an amount of 100 μL of SA-HRP conjugated antibody was added to the wells (except blank). The plate was incubated for 30 min at room temperature on a plate shaker. The wells were washed again, and an amount of 100 μL of TMB (3,3′,5,5′-tetramethylbenzidine) was added to each well for 30 min at room temperature. To stop reaction, an amount of 100 μL of 1 N HCl was added to the wells. After the plate reader was blanked against the substrate, optical density was read at 450 nm. Data were presented as % of inhibition referenced to control (only standards).

Cell Cycle Analysis. Cells (1×10^5) were harvested when subconfluent, fixed in 70% ethanol for 1 h at −20 °C, rehydrated in PBS, and the pellet was resuspended in 300 μL of PBS containing 250 μg/mL RNaseA and 10 μg/mL propidium iodide for 30 min in the dark. Samples were acquired with a CYAN flow cytometer (DAKO Corporation, San Jose, CA, U.S.). The cell cycle distribution, expressed as percentage of cells in the G0/G1, S, and G2/M phases, was calculated using SUMMIT software.

Annexin V Assay. Cells were plated at 1×10^6 in six-well plates and washed with 1× PBS and then with annexin V binding buffer. After centrifugation at 2000 rpm for 5 min, the cells were resuspended in 100 μL of annexin V binding buffer and incubated with 5 μL of FITC annexin V (BioLegend) and 2 μL of 500 μg/mL propidium iodide for 15 min at 25 °C in the dark. Finally, an amount of 400 μL of annexin V binding buffer was added to each test tube. Samples were acquired with a CYAN flow cytometer (DAKO Corporation, San Jose, CA, U.S.) and analyzed using SUMMIT software.

Western Blotting and Immunoprecipitation Analysis. MCF-7 cells were plated in Petri dishes (1×10^6 cells) in normal culture conditions and incubated with or without **4n** and nutlin. At the indicated times, cells were lysed using an ice cold lysis buffer (50 mM Tris, 150 mM NaCl, 10 mM EDTA, 1% Triton) supplemented with a mixture of protease inhibitors containing antipain, bestatin, chymostatin, leupeptin, pepstatin, phosphoramidon, Pefabloc, EDTA, and aprotinin (Boehringer, Mannheim, Germany). Equivalent amounts of protein were loaded on 8−12% sodium dodecyl sulfate (SDS)−polyacrylamide gels and electrophoresed followed by blotting onto nitrocellulose membranes (Bio-Rad, Germany). After blotting with 5% (w/v) fat-free milk powder and 0.1% Tween 20 in TBS, the membrane was incubated overnight at 4 °C with specific antibodies at the concentrations indicated by the manufacter's protocol (Santa Cruz Biotechnology). The antibody was diluted in Tris-buffered saline/Tween 20 and 5% milk powder. Following incubation with horseradish peroxidase conjugated secondary antibodies, bands were detected by enhanced chemiluminescence (ECL kit, Amersham, Germany). Each filter was then probed with mouse monoclonal anti-actin antibody. Level of expression of detected bands was quantified by NIH ImageJ 1.40 after normalization with β-actin. For immunoprecipitation, cells were lysed in immunoprecipitation buffer (0.05 mol/L Tris-HCl (pH 8.0), 0.005 mol/L EDTA, 0.15 mol/L NaCl, 1% Nonidet P-40, 0.5% sodium deoxycolate, 0.1% SDS, 0.01 mol/L NaF, 0.005 mol/L EGTA, 0.01 mol/L sodium pyrophosphate, and 0.001 mol/L phenylmethylsulfonyl fluoride). Rabbit polyclonal antibody reactive to MDM2 (Santa Cruz Biotechnology, Santa Cruz, CA, U.S.) and protein G plus/protein A agarose beads (Oncogene Science, Boston, MA, U.S.) were used to immunoprecipitate MDM2 from 1 mg total lysate. Mouse monoclonal antibodies to total p53 were from Santa Cruz Biotechnology.

Molecular Modeling Methods. The new version of the docking program AutoDock2 as implemented through the graphical user interface called AutoDockTools (ADT) was used to dock into the MDM2 structure **4n** and the cocrystal ligand. The MDM2 structure was retrieved from the Protein Data Bank (PDB code 1LBL),[28] and cocrystal waters and ligand were removed. **4n** was built using the builder in the Maestro package of the Schroedinger Suite 2007, and optimization using a version of MacroModel was also included. The constructed compounds and the receptor structure were converted to AD4 format files using ADT, automatically generating all other atom values. The docking area was centered around the putative binding site. Grids of 60 Å × 60 Å × 60 Å with 0.375 Å spacing were calculated around the docking area for the ligand atom types using AutoGrid4. For each ligand, 100 separate docking calculations were performed. Each docking calculation consisted of 10 million energy evaluations using the Lamarckian genetic algorithm local search (GALS) method. The GALS method evaluates a population of possible docking solutions and propagates the most successful individuals from each generation into the subsequent generation of possible solutions. A low-frequency local search according to the method of Solis and Wets is applied to docking trials to ensure that the final solution represents a local minimum. All dockings described in this paper were performed with a population size of 250, and 300 rounds of Solis and Wets local search were applied with a probability of 0.06. A mutation rate of 0.02 and a crossover rate of 0.8 were used to generate new docking trials for subsequent generations, and the best individual from each generation was propagated over the next generation. The docking results from each of the 100 calculations were clustered on the basis of root-mean-square deviation (rmsd) (solutions differing by less than 2.0 Å) between the Cartesian coordinates of the atoms and were ranked on the basis of free energy of binding (ΔG_{AD4}). Because AD4 does not perform any structural optimization and energy minimization of the complexes found, a molecular mechanics/energy minimization (MM/EM) approach was applied to refine the AD4 output. The computational protocol applied consisted of the application of 100 000 steps of the Polak−Ribiére conjugate gradients (PRCG) or until the derivative convergence was 0.05 kJ/mol. The **4n**/MDM2 complex picture was rendered employing the UCSF Chimera software.[38]

■ ASSOCIATED CONTENT

Supporting Information

Microanalytical data for all test compounds; ^{1}H NMR, ^{13}C NMR, and ROESY spectra of compound **4n**; in vitro p53/MDM2 binding assay results. This material is available free of charge via the Internet at http://pubs.acs.org.

AUTHOR INFORMATION

Corresponding Author

*For P.C.: e-mail, pcampiglia@unisa.it; phone, +39 089 96 9242. For I.G.-M.: e-mail, imgomez@unina.it; phone, +39 081 67 86 33.

Author Contributions

The manuscript was written through contributions of all authors. All authors have given approval to the final version of the manuscript.

Notes

The authors declare no competing financial interest.

ACKNOWLEDGMENTS

The ESIMS and NMR spectral data were provided by Centro di Ricerca Interdipartimentale di Analisi Strumentale, Università degli Studi di Napoli "Federico II", Italy. The assistance of the staff is gratefully appreciated. This work was supported by grants from Italian Ministero dell'Istruzione, Università e Ricerca (PRIN 20098SJX4F-002), Italy.

ABBREVIATIONS USED

MDM2, mouse double minute 2 homologue; EtOH, ethanol; THF, tetrahydrofuran; TEA, triethylamine; NOE, nuclear Overhauser effect; DCM, dichloromethane; $NaHCO_3$, sodium bicarbonate; SD, standard deviation; FACS, fuorescence activated cell sorting; SEM, standard error of the mean; TLC, thin-layer chromatography; MS, mass spectrometry; ESI, electrospray ionization; DMSO, dimethylsulfoxide; PBS, phosphate buffered saline; EDTA, ethylenediaminetetraacetic acid; TBS, Tris buffered saline

REFERENCES

(1) Levine, J.; Oren, M. The first 30 years of p53: Growing ever more complex. *Nat. Rev. Cancer* **2009**, *9*, 749−758.

(2) Vogelstein, B.; Lane, D.; Levine, A. J. Surfing the p53 network. *Nature* **2000**, *408*, 307−310.

(3) Vousden, K. H.; Prives, C. Blinded by the light: the growing complexity of p53. *Cell* **2009**, *137*, 413−431.

(4) Feng, Z.; Wu, R.; Lin, M.; Hu, W. Tumor suppressor p53: new functions of an old protein. *Front. Biol.* **2011**, *6*, 58−68.

(5) Maddocks, O. D. K.; Vousden, K. H. Metabolic regulation by p53. *J. Mol. Med.* **2011**, *89*, 237−245.

(6) Muller, P. A. J.; Vousden, K. H.; Norman, J. C. p53 and its mutants in tumor cell migration and invasion. *J. Cell Biol.* **2011**, *192*, 209−218 and references therein.

(7) Yang, Y.; Li, C. C.; Weissman, A. M. Regulating the p53 system through ubiquitination. *Oncogene* **2004**, *23*, 2096−2106.

(8) Momand, J.; Zambetti, G. P.; Olson, D. C.; George, D.; Levine, A. The mdm-2 oncogene product forms a complex with p53 protein and inhibits p53-mediated transactivation. *Cell* **1992**, *69*, 1237−1245.

(9) Geyer, R. K.; Yu, Z. K.; Maki, C. G. The MDM2 RING-finger domain is required to promote p53 nuclear export. *Nat. Cell Biol.* **2000**, *2*, 569−73.

(10) Haupt, Y.; Maya, R.; Kazaz, A.; Oren, M. Mdm2 promotes the rapid degradation of p53. *Nature* **1997**, *387*, 296−299.

(11) (a) Levine, A. p53, the cellular gatekeeper for growth and division. *Cell* **1997**, *88*, 323−331. (b) Greenblatt, M. S.; Bennett, W. P.; Hollstein, M.; Harris, C. C. Mutations in the p53 tumor suppressor gene: clues to cancer etiology and molecular pathogenesis. *Cancer Res.* **1994**, *54*, 4855−4878.

(12) (a) Fakharzadeh, S. S.; Trusko, S. P.; George, D. L. Tumorigenic potential associated with enhanced expression of a gene that is amplified in a mouse tumor cell line. *EMBO J.* **1991**, *10*, 1565−1569. (b) Oliner, J. D.; Kinzler, K. W.; Meltzer, P. S.; George, D. L.; Vogelstein, B. Amplification of a gene encoding a p53-associated protein in human sarcomas. *Nature* **1992**, *358*, 80−83. (c) Jones, S. N.; Hancock, A. R.; Vogel, H.; Donehower, L. A.; Bradley, A. Overexpression of Mdm2 in mice reveals a p53-independent role for Mdm2 in tumorigenesis. *Proc. Natl. Acad. Sci. U.S.A.* **1998**, *95*, 15608−15612.

(13) (a) Ventura, A.; Kirsch, D. G.; McLaughlin, M. E.; Tuveson, D. A.; Grimm, J.; Lintault, L.; Newman, J.; Reczek, E. E.; Weissleder, R.; Jacks, T. Restoration of p53 function leads to tumor regression in vivo. *Nature* **2007**, *445*, 661−665. (b) Xue, W.; Zender, L.; Miething, C.; Dickins, R. A.; Hernando, E.; Krizhanovsky, V.; Cordon-Cardo, C.; Lowe, S. W. Senescence and tumour clearance is triggered by p53 restoration in murine liver carcinomas. *Nature* **2007**, *445*, 656−660.

(14) (a) Brown, C. J.; Lain, S.; Verma, C. S.; Fersht, A. R.; Lane, D. P. Awakening guardian angels: drugging the p53 pathway. *Nat. Rev. Cancer* **2009**, *9*, 862−873. (b) Chene, P. Inhibiting the p53-MDM2 interaction: an important target for cancer therapy. *Nat. Rev. Cancer* **2003**, *3*, 102−109. (c) Hardcastle, I. R. Inhibitors of the MDM2-p53 interaction as anticancer drugs. *Drugs Future* **2007**, *32*, 883−896.

(15) (a) Fischer, P. Peptide, peptidomimetic, and small-molecule antagonists of the p53-HDM2 protein−protein interaction. *Int. J. Pept. Res. Ther.* **2006**, *12*, 3−19. (b) Shangary, S.; Wang, S. Small-molecule inhibitors of the MDM2-p53 protein−protein interaction to reactivate p53 function: a novel approach for cancer therapy. *Ann. Rev. Pharmacol. Toxicol* **2009**, *49*, 223−241.

(16) Vassilev, L. T.; Vu, B. T.; Graves, B.; Carvajal, D.; Podlaski, F.; Filipovic, Z.; Kong, N.; Kammlott, U.; Lukacs, C.; Klein, C.; Fotouhi, N.; Liu, E. A. In vivo activation of the p53 pathway by small-molecule antagonists of MDM2. *Science* **2004**, *303*, 844−848.

(17) (a) Grasberger, B. L.; Lu, T. B.; Schubert, C.; Parks, D. J.; Carver, T. E.; Koblish, H. K.; Cummings, M. D.; LaFrance, L. V.; Milkiewicz, K. L.; Calvo, R. R.; Maguire, D.; Lattanze, J.; Franks, C. F.; Zhao, S. Y.; Ramachandren, K.; Bylebyl, G. R.; Zhang, M.; Manthey, C. L.; Petrella, E. C.; Pantoliano, M. W.; Deckman, I. C.; Spurlino, J. C.; Maroney, A. C.; Tomczuk, B. E.; Molloy, C. J.; Bone, R. F. Discovery and cocrystal structure of benzodiazepinedione HDM2 antagonists that activate p53 in cells. *J. Med. Chem.* **2005**, *48*, 909−912. (b) Koblish, H. K.; Zhao, S. Y.; Franks, C. F.; Donatelli, R. R.; Tominovich, R. M.; LaFrance, L. V.; Leonard, K. A.; Gushue, J. M.; Parks, D. J.; Calvo, R. R.; Milkiewicz, K. L.; Marugan, J. J.; Raboisson, P.; Cummings, M. D.; Grasberger, B. L.; Johnson, D. L.; Lu, T. B.; Molloy, C. J.; Maroney, A. C. Benzodiazepinedione inhibitors of the Hdm2: p53 complex suppress human tumor cell proliferation in vitro and sensitize tumors to doxorubicin in vivo. *Mol. Cancer Ther.* **2006**, *5*, 160−169.

(18) (a) Ding, K.; Lu, Y.; Nikolovska-Coleska, Z.; Qui, S.; Ding, Y.; Gao, W.; Stuckey, J.; Krajewski, K.; Roller, P. P.; Tomita, Y.; Parrish, D. A.; Deschamps, J. R.; Wang, S. Structure-based design of potent non-peptide MDM2 inhibitors. *J. Am. Chem. Soc.* **2005**, *127*, 10130−10131. (b) Yu, S.; Qin, D.; Shangary, S.; Chen, J.; Wang, G.; Ding, K.; McEachern, D.; Qiu, S.; Nikolovska-Coleska, Z.; Miller, R.; Kang, S.; Yang, D.; Wang, S. Potent and orally active small-molecule inhibitors of the MDM2-p53 interaction. *J. Med. Chem.* **2009**, *52*, 7970−7973.

(19) Allen, J. G.; Bourbeau, M. P.; Wohlhieter, G. E.; Bartberger, M. D.; Michelsen, K.; Hungate, R.; Gadwood, R. C.; Gaston, R. D.; Evans, B.; Mann, L. W.; Matison, M. E.; Schneider, S.; Huang, X.; Yu, D.; Andrews, P. S.; Reichelt, A.; Long, A. M.; Yakowec, P.; Yang, E. Y.; Lee, T. A.; Oliner, J. D. Discovery and optimization of chromeno-triazolopyrimidines as potent inhibitors of the mouse double minute 2-tumor protein 53 protein−protein interaction. *J. Med. Chem.* **2009**, *52*, 7044−7053.

(20) (a) Hardcastle, I. R.; Ahmed, S. U.; Atkins, H.; Farnie, G.; Golding, B. T.; Griffin, R. J.; Guyenne, S.; Hutton, C.; Kallblad, P.; Kemp, S. J.; Kitching, M. S.; Newell, D. R.; Norbedo, S.; Northen, J. S.; Reid, R. J.; Saravanan, K.; Willems, H. M. G.; Lunec, J. Small-molecule inhibitors of the MDM2-p53 protein−protein interaction based on an isoindolinone scaffold. *J. Med. Chem.* **2006**, *49*, 6209−6221. (b) Hardcastle, I. R.; Junfeng Liu, J.; Valeur, E.; Watson, A.; Ahmed, S. U.; Blackburn, T. J.; Bennaceur, K.; Clegg, W.; Drummond, C.; Endicott, J. A.; Golding, B. T.; Griffin, R. J.; Gruber, J.; Haggerty, K.;

Harrington, R. W.; Hutton, C.; Kemp, S.; Lu, X.; McDonnell, J. M.; Newell, D. R.; Noble, M. E. M.; Payne, S. L.; Revill, C. H.; Riedinger, C.; Xu, Q.; Lunec, J. Isoindolinone inhibitors of the murine double minute 2 (MDM2)-p53 protein−protein interaction: structure−activity studies leading to improved potency. *J. Med. Chem.* **2011**, *54*, 1233−1243.

(21) (a) Kussie, P. H.; Gorina, S.; Marechal, V.; Elenbaas, B.; Moreau, J.; Levine, A. J.; Pavletich, N. P. Structure of the MDM2 oncoprotein bound to the p53 tumor suppressor transactivation domain. *Science* **1996**, *274*, 948−953. (b) Lee, H.; Mok, K. H.; Muhandiram, R.; Park, K. H.; Suk, J. E.; Kim, D. H.; Chang, J.; Sung, Y. C.; Choi, K. Y.; Han, K. H. Local structural elements in the mostly unstructured transcriptional activation domain of human p53. *J. Biol. Chem.* **2000**, *275*, 29426−29432.

(22) (a) Murray, J. K.; Gellman, S. H. Targeting protein−protein interactions: lessons from p53/MDM2. *Biopolymers* **2007**, *88*, 657−686. (b) Shangary, S.; Wang, S. Small-molecule inhibitors of the MDM2-p53 protein−protein interaction to reactivate p53 function: a novel approach for cancer therapy. *Annu. Rev. Pharmacol. Toxicol.* **2009**, *49*, 223−241.

(23) Gomez-Monterrey, I.; Bertamino, A.; Porta, A.; Carotenuto, A.; Musella, S.; Aquino, C.; Granata, I.; Sala, M.; Brancaccio, D.; Picone, D.; Ercole, C.; Stiuso, P.; Campiglia, P.; Grieco, P.; Ianelli, P.; Maresca, B.; Novellino, E. Identification of the spiro(oxindole-3,3′-thiazolidine)-based derivatives as potential p53 activity modulators. *J. Med. Chem.* **2010**, *53*, 8319−8329.

(24) Bertamino, A.; Aquino, C.; Sala, M.; de Simone, N.; Mattia, C. A.; Erra, L.; Musella, S.; Iannelli, P.; Carotenuto, A.; Grieco, P.; Novellino, E.; Campiglia, P.; Gomez- Monterrey, I. Design and synthesis of spirotryprostatin-inspired diketopiperazine systems from prolyl spirooxoindolethiazolidine derivatives. *Bioorg. Med. Chem.* **2010**, *18*, 4328−4337.

(25) (a) Szilagyi, L.; Gyorgydeak, Z. Comments on the putative stereoselectivity in cysteine-aldehyde reactions. Selective C(2) inversion and C(4) epimerization in thiazolidine-4-carboxylic acids. *J. Am. Chem. Soc.* **1979**, *101*, 427−432. (b) Deroose, F. D; De Clercq, J. Novel enantioselective syntheses of (+)-biotin. *J. Org. Chem.* **1995**, *60*, 321−330.

(26) Neuhaus, D.; Williamson, M. P. *The Nuclear Overhauser Effect in Structural and Conformational Analysis*; Wiley-VCH: New York, 2000.

(27) (a) Arva, N. C.; Talbott, K. E.; Okoro, D. R.; Brekman, A.; Qiu, W. G.; Bargonetti, J. Disruption of the p53-Mdm2 complex by nutlin-3 reveals different cancer cell phenotypes. *Ethnicity Dis.* **2008**, *18* (S2), 1−8. (b) Supiot, S.; Hill, R. P.; Bristow, R. G. Nutlin-3 radiosensitizes hypoxic prostate cancer cells independent of p53. *Mol. Cancer Ther.* **2008**, *7*, 993−999. (c) Zheng, T.; Jiabei Wang, J.; Song, X.; Meng, X.; Pan, S.; Jiang, H.; Liu, L. Nutlin-3 cooperates with doxorubicin to induce apoptosis of human hepatocellular carcinoma cells through p53 or p73 signaling pathways. *J. Cancer Res. Clin. Oncol.* **2010**, *136*, 1597−1604.

(28) Popowicz, G. M.; Czarna, A.; Wolf, S.; Wang, K.; Wang, W.; Dömling, A.; Holak, T. A. Structures of low molecular weight inhibitors bound to MDMX and MDM2 reveal new approaches for p53-MDMX/MDM2 antagonist drug discovery. *Cell Cycle* **2010**, *9*, 1104−1111.

(29) (a) Huey, R.; Morris, G. M.; Olson, A. J.; Goodsell, D. S. A semiempirical free energy force field with charge-based desolvation. *J. Comput. Chem.* **2007**, *28*, 1145−1152. (b) Cosconati, S.; Forli, S.; Perryman, A. L.; Harris, R.; Goodsell, D. S.; Olson, A. J. Virtual screening with AutoDock: theory and practice. *Expert Opin. Drug Discovery* **2010**, *5*, 597−607.

(30) Gonzalez-Lopez de Turiso, F.; Sun, D.; Rew, Y.; Bartberger, M. D.; Beck, H. P.; Canon, J.; Chen, A.; Chow, D.; Correll, T. L.; Huang, X.; Julian, L. D.; Kayser, F.; Lo, M. C.; Long, A. M.; McMinn, D.; Oliner, J. D.; Osgood, T.; Powers, J. P.; Saiki, A. Y.; Schneider, S.; Shaffer, P.; Xiao, S. H.; Yakowec, P.; Yan, X.; Ye, Q.; Yu, D.; Zhao, X.; Zhou, J.; Medina, J. C.; Olson, S. H. Rational design and binding mode duality of MDM2−p53 inhibitors. *J. Med. Chem.* **2013**, in press.

(31) Vousden, K. H.; Xin, Lu, X. Live or let die: the cell's response to p53. *Nat. Rev. Cancer* **2002**, *2*, 594−604.

(32) Haupt, S.; Berger, M.; Goldberg, Z.; Haupt, Y. Apoptosis—the p53 network. *J. Cell Sci.* **2003**, *116*, 4077−4085.

(33) Pietsch, E. C.; Sykes, S. M.; McMahon, S. B.; Murphy, M. E. The p53 family and programmed cell death. *Oncogene* **2008**, *27*, 6507−6521.

(34) Hori, T.; Kondo, T.; Kanamori, M.; Tabuchi, Y.; Ogawa, R.; Zhao, Q.-L.; Ahmed, K.; Yasuda, T.; Seki, S.; Suzuki, K.; Kimura, T. Nutlin-3 enhances tumor necrosis factor-related apoptosis-inducing ligand (TRAIL)-induced apoptosis through up-regulation of death receptor 5 (DR5) in human sarcoma HOS cells and human colon cancer HCT116 cells. *Cancer Lett.* **2010**, *287*, 98−108.

(35) Tseng, H.-Y.; Jiang, C. C.; Croft, A.; Tay, K. H.; Thorne, R. F.; Fan Yang, F.; Liu, H.; Hersey, P.; Zhang, X. D. Contrasting effects of nutlin-3 on TRAIL- and docetaxel-induced apoptosis due to upregulation of TRAIL-R2 and Mcl-1 in human melanoma cells. *Mol. Cancer Ther.* **2010**, *9*, 3363−3374.

(36) Bax, A.; Davis, D. G. 2D ROESY with cw spinlock for mixing phase sensitive using States-TPPI method. *J. Magn. Reson.* **1985**, *63*, 207−213.

(37) States, D. J.; Haberkorn, R. A.; Ruben, D. J. A two-dimensional nuclear Overhauser experiment with pure absorption phase four quadrants. *J. Magn. Reson.* **1982**, *48*, 286−292.

(38) Pettersen, E. F.; Goddard, T. D.; Huang, C. C.; Couch, G. S.; Greenblatt, D. M.; Meng, E. C.; Ferrin, T. E. UCSF Chimera—a visualization system for exploratory research and analysis. *J. Comput. Chem.* **2004**, *25*, 1605−1612.